

Dissertation zur Erlangung des Doktorgrades
der Fakultät für Chemie und Pharmazie
der Ludwig-Maximilians-Universität München

**Application of Many-Body Perturbation
Theory to the Description of Correlated Metals**

Stanislav Chadov

aus

Kiew, Ukraine

2007

Erklärung

Diese Dissertation wurde im Sinne von §13 Abs. 3 der Promotionsordnung vom 29. Jan 1998 von Prof. Dr. H. Ebert betreut.

Ehrenwörtliche Versicherung

Diese Dissertation wurde selbstständig, ohne unerlaubte Hilfe erarbeitet.

München, am 20.12.2007

Stanislav Chadov

Dissertation eingereicht am 20.12.2007

1. Gutachter: Prof. Dr. H. Ebert
2. Gutachter: Prof. Dr. A. Lichtenstein
/Institut für Theor. Physik, Uni Hamburg/

Mündlichen Prüfung am 22.02.2008

Contents

1	Introduction	7
2	The Hubbard model	13
2.1	The Hubbard Hamiltonian	13
2.2	The strong interaction limit	17
2.3	The weak interaction limit	18
3	Perturbational description	23
3.1	The Baym-Kadanoff theory	23
3.2	The T -matrix approximation	27
3.3	T -matrix formulation for real energies	32
4	The mean-field approximations	35
5	The energy functional description	39
5.1	Density functional theory	41
5.2	The local density approximation	44
5.3	The LDA+ U method	47
5.3.1	The Coulomb interaction matrix	48
5.3.2	The double-counting term	51
5.4	Spectral density functional theory	53
5.5	The dynamical-mean field approximation	58
5.6	LDA+DMFT	61
6	Numerical implementation	65
6.1	DMFT within the KKR method	65
6.1.1	Solution of the Kohn-Sham equations	65

6.1.2	Common features and comparison of the DMFT solvers	72
6.2	Application to ground-state properties	77
6.2.1	Orbital magnetic moments	77
6.2.2	Calculation of the total energy	83
6.2.3	Summary	85
6.3	Applications to photoemission	86
6.3.1	Introduction	86
6.3.2	Theoretical framework	88
6.3.3	Fano-effect in the VB-XPS of Fe and Co	93
6.3.4	High-energy angle-resolved VB-XPS of Ni	95
6.3.5	High-energy angle-integrated VB-XPS of NiMnSb	96
7	Application to linear response theory	99
7.1	Time-dependent perturbation theory	99
7.2	Optical conductivity	103
7.3	Green's function within the variational basis formalism: implementation in the LMTO method	105
7.4	Accounting for localized correlations	108
7.5	Applications to 3 <i>d</i> -transition metal systems	111
7.6	Application to heavy-fermion systems	114
8	Summary	119
	Bibliography	123
	Acknowledgements	137
	Curriculum vitae – Lebenslauf	139
	List of Publications (2002-2007)	141

Chapter 1

Introduction

Electron systems with strong interaction received strong theoretical and experimental interest for several decades. This interest has been intensified with the discovery of heavy-fermion and related non-Fermi-liquid systems and high- T_C superconductors. An extensive and continuous effort in theoretical field is devoted to the investigation of the most extensively used nowadays prototype for an exactly solvable model of many-electron systems - the so-called *Hubbard* model [1]. Being relatively simple, the Hubbard model contains a great manifold of phenomena which up to now is far from being fully investigated, as well as the rich possibilities for testing various physical ideas and methods. It was successfully applied to describe the set of new electronic phenomena where electronic correlations are significant: such as metal insulator transition [2], itinerant magnetism [3], spin-density waves [4] and local pair formation [5, 6] which plays a key role in the explanation of the high- T_C superconductivity and the superconductivity in the heavy-fermion systems.

However, it is very difficult to solve the Hubbard model in general, except of the few tractable limits. One is the so-called weak-coupling limit which leads to the non-interacting electron gas which is well-understood. However, even for a weak coupling there is an exceptional situation occurring at the half-filling. Namely, even the infinitesimally small Coulomb repulsion drives the system through metal-insulator transition, which cannot be described by the free-electron picture [7]. Much less clear is the limit of strong interaction. At a half filling the model turns to the Heisenberg antiferromagnetic insulator

[7]. However, if the occupation is away from half-filling the behavior of the system becomes a complete mystery.

During the last 40 years of investigations numerous approaches have been suggested: decoupling of the Green's functions [1], the variational approach [8], linearization of the equations of motion [9], the self-consistent moments method [10], the composite operators approach (COM) [11] and many others. However none of them can be considered as universal. One of the approaches dealing with the simplest extension of the Hubbard model, which adequately accounts for a situation in solid, namely, the strongly interacting dilute electron gas in the one-particle scalar potential, is the so-called *Baym-Kadanoff* theory [12]. However, the complexity of the crystals containing many different atoms per unit cell, interactions between electronic and lattice degrees of freedom demands a very detailed investigation of the band structure in such systems and do not allow to apply the Baym-Kadanoff approach in a straightforward way for the real solid.

The only general *ab-initio* approach which accounts for the specific features in real compounds is based on the so-called Density Functional Theory (DFT) developed by Hohenberg, Kohn and Sham [13–15]. The majority of practical nowadays DFT applications to magnetic solids are based on the local mean-field description provided by the so-called Local Spin Density Approximation (LSDA) which treats the exchange-correlation part of an effective single-particle DFT potential as a density-dependent exchange-correlation potential treated on the basis of the results for the homogeneous electron gas. There are a lot of successes of LSDA, however, there are also some failures related to the fact that in case when some portion of the electronic structure could be better described by the atomic-like orbitals, the homogeneous gas is not a suitable starting point.

Thus, a reasonable strategy in this situation would be to have a simple and accurate approach that could describe the most important features of the realistic electron structure and at the same time takes the most important correlation effects into account.

One of the first successful steps in this direction was the so-called GW approximation (GWA) for quasiparticle spectra in solids [16, 17] which delivers the one-particle Green's function accounting for the non-local self-energy calculated to the lowest order in the screened non-local

Coulomb interaction (W). Being applied for strongly correlated systems like NiO, the GWA gives a rather good description of the size of the band gap and also improves the description of the O p -band compared to the LSDA. However, the application to more complex systems has not been feasible up to now due to large computational efforts.

Another approach accounting for correlation effects in localized d - and f -shells is the so-called LSDA+U method [18, 19]. The method separates the localized d - (or f)-electron subsystem from the rest and introduces the additional Coulomb repulsion U in the form of a Hubbard model term. The rest consisting of the delocalized conduction electrons is described by the orbital-independent one-particle LSDA potential. This approach gives a more reliable description of the electronic structure within the same charge, spin and orbital ordering than does the plain LSDA. However, due to the single energy scale it does not describe the most interesting correlation effects which are connected with the energy (or time) dependence of the self-energy: the renormalization of the quasiparticle spectra and mass enhancement.

The real breakthrough in this field was made few years later with the development of the Dynamical Mean-Field Theory (DMFT) [20–23]. This approach distinguishes the localized interacting electronic subsystem from the rest and provides the conditions required by the Baym-Kadanoff description by treating the coupling of the interacting subsystem with its environment as a local mean-field. Thus the many-body problem becomes equivalent to the well-known *Anderson* model [24] and can be solved by the corresponding impurity solvers based on various approximating techniques or applying the so-called Quantum Monte Carlo method (QMC) [25]. The combination of LSDA and DMFT gains several advantages by using the partially non-local description of electron correlations. First of all, it is able to deal with both ground-state and the excitation properties of solids. Second, the method gives access to finite temperatures (using the Matsubara formalism for the Green's function), thus the critical temperatures of phase transitions are accessible. In general, the method reproduces the correct quasiparticle behavior as well as the LSDA and LSDA+U results in the limits where these methods are valid. Among all the extensions of the LSDA only the LSDA+DMFT approach is presently able to describe the strongly correlated paramagnetic metals with lower and

upper Hubbard bands and a narrow quasiparticle peak at the Fermi level [21, 26]. Since the implementation of the LSDA+DMFT scheme and its applications is the subject of this thesis, more details about the assessment and the advantages of the DMFT are given in the following chapters.

The theoretical background providing a basis for the LSDA+DMFT scheme used in the present work has the following structure.

Chapter 2 discusses the main concepts of the Hubbard model which then is used in the construction of the Baym-Kadanoff formalism outlined in Chapter 3. In Chapter 4 we consider the formal structure of the mean-field approximation which allows to build the practically manageable approaches to the functional theories, such as the LSDA to the DFT and the DMFT to the more general Spectral Density Functional Theory (SDFT). The functional theories and the corresponding mean-field approximations is the subject of Chapter 5.

Several aspects will be of a particular interest in this thesis.

First of all, this is the development and implementation of the single-site impurity solver as an extended version of the so-called T -matrix approximation for the real energies based on work of Drchal *et al.* [27]. The extended version delivers the localized single-site dynamical self-energy in a form of a full matrix including the spin-flip terms. Being the perturbational approach, the T -matrix approximation is the logical continuation of the Baym-Kadanoff theory. For this reason the formal mathematical description of the solver is given in the Section 3.3 which is included in the theoretical framework.

Chapter 6 is devoted to the implementation of the impurity solver in the fully self-consistent (both in charge and in self-energy) LSDA+DMFT scheme within the Korringa-Kohn-Rostoker Green's function method. The self-energy is explicitly added as a non-local energy-dependent potential to the corresponding Kohn-Sham equation. The latter allows to account for the localized dynamical correlation not only in the Green's function but in all the matrix elements as well as in the self-consistent effective one-particle potential. This gives access to the various spectroscopies as well as for a better treatment of the ground-state properties. In particular, applications to the description of photoemission spectra and the Fano-effect are presented. In addition, the influence of dynamical and static correlations on the ground-state

properties (spin and orbital magnetic moments, the total energy) is separately analyzed.

the double-counting of interaction part corresponding LSDA part is adequately approach.

In Chapter 7 the application of the LSDA+DMFT scheme to the linear response theory is considered. The formulation of the linear response coefficients, namely of the optical conductivity in the framework of time-dependent perturbation theory is given in terms of the one-particle Green's function. Alternatively to the previous LSDA+DMFT implementation, the present scheme is based on the Linearized Muffin-Tin Orbitals (LMTO) method (Sec. 7.3 and 7.4). The choice of the variational basis formalism and neglecting the charge self-consistency is motivated by the speed of the calculations. On the other hand, the account of the localized correlations within the Green's function only, turns out to be sufficient to describe the most important features of optical and magneto-optical spectra in $3d$ -transition metals which are not given by the plain LSDA.

In order to probe the applicability of the LMTO+DMFT scheme to the description of strongly-correlated metallic systems, the optical and magneto-optical spectra for the heavy-fermion US compound are calculated in addition. In particular with respect to the magneto-optical properties a noticeable improvement in comparison to the LSDA+U results is obtained.

Chapter 2

The Hubbard model

Here we will consider the main concepts and the most important properties of the Hubbard model with respect to correlated systems. In particular we will consider two cases, the strong and the weak interaction limits and the specific mathematical techniques used in their description.

2.1 The Hubbard Hamiltonian

The Hubbard model we use describes the valence-band electrons interacting via the two-body repulsive Coulomb potential V . It can be represented by the following Hamiltonian:

$$\begin{aligned} H(t) = & \int d^3r c^\dagger(\mathbf{r}, t) H^0(\mathbf{r}) c(\mathbf{r}, t) \\ & + \frac{1}{2} \int d^3r \int d^3r' c^\dagger(\mathbf{r}, t) c^\dagger(\mathbf{r}', t) V(\mathbf{r}, \mathbf{r}', t) c(\mathbf{r}', t) c(\mathbf{r}, t). \end{aligned} \quad (2.1)$$

Here $c^\dagger(\mathbf{r}, t), c(\mathbf{r}, t)$ are the operators of electron creation and annihilation in the space-time point (\mathbf{r}, t) ; the one-particle Hamiltonian $H^0(\mathbf{r}) = K(\mathbf{r}) + V_{\text{ext}}(\mathbf{r})$ is the sum of kinetic energy operator K and the some effective local potential V_{eff} ; the non-local potential V represents the electron-electron interaction.

Introducing the arbitrary complete basis set $\{\phi_\mu(\mathbf{r})\}$ we turn the

expression (2.1) into the following form:

$$H = \sum_{\mu\mu'} H_{\mu\mu'}^0 (c_{\mu}^{\dagger} c_{\mu'} + \text{h.c.}) + \frac{1}{2} \sum_{\mu\mu'\nu\nu'} V_{\mu\mu'\nu\nu'} c_{\mu}^{\dagger} c_{\mu'}^{\dagger} c_{\nu} c_{\nu'}, \quad (2.2)$$

with the index μ denoting the unit cell \mathbf{R} , orbital lm and spin σ quantum numbers. If more than one atom per cell is present a full index denoting the particular atomic site within the unit cell is used. The matrix elements of the non-interacting Hamiltonian and the Coulomb interaction are defined as:

$$H_{\mu\mu'}^0 = \int d^3r \phi_{\mu}^*(\mathbf{r}) H^0(\mathbf{r}) \phi_{\mu'}(\mathbf{r}), \quad (2.3)$$

$$V_{\mu\mu'\nu\nu'} = \int d^3r \int d^3r' \phi_{\mu}^*(\mathbf{r}) \phi_{\mu'}^*(\mathbf{r}') V(\mathbf{r}, \mathbf{r}') \phi_{\nu}(\mathbf{r}') \phi_{\nu'}(\mathbf{r}). \quad (2.4)$$

The fermionic operators $c_{\mu}^{\dagger}, c_{\mu}$ are represented explicitly as

$$c^{\dagger}(\mathbf{r}, t) = \sum_{\mu} \phi_{\mu}^*(\mathbf{r}) c_{\mu}^{\dagger}(t), \quad c(\mathbf{r}, t) = \sum_{\mu} \phi_{\mu}(\mathbf{r}) c_{\mu}(t). \quad (2.5)$$

Taking into account the anticommutative relations of the fermionic operators

$$\begin{aligned} [c(\mathbf{r}, t), c(\mathbf{r}', t)]_{+} &= [c^{\dagger}(\mathbf{r}, t), c^{\dagger}(\mathbf{r}', t)]_{+} = 0, \\ [c(\mathbf{r}, t), c^{\dagger}(\mathbf{r}', t)]_{+} &= \delta(\mathbf{r} - \mathbf{r}') \end{aligned} \quad (2.6)$$

together with the general equation of motion for any operator $X(t)$ within the Heisenberg picture:

$$i \frac{\partial}{\partial t} X(t) = [X(t), H(t)], \quad (2.7)$$

and implying that the interaction V is instantaneous, the following differential equation for c and c^{\dagger} is obtained:

$$\left[i \frac{\partial}{\partial t} - H^0(\mathbf{r}) \right] c(\mathbf{r}, t) = \left[\int d^3r' V(\mathbf{r}, \mathbf{r}') c^{\dagger}(\mathbf{r}', t) c(\mathbf{r}', t) \right] c(\mathbf{r}, t). \quad (2.8)$$

As we are interested in properties of crystals we consider Hamiltonians with periodic potentials $V_{\text{ext}}(\mathbf{r}) = V_{\text{ext}}(\mathbf{r} + \mathbf{R})$.

If the interaction V is switched off, the solution of Eq. (2.8) can be represented by the Bloch waves:

$$\phi_{\mathbf{k}\mu}(\mathbf{r}) = e^{i\mathbf{k}\cdot\mathbf{r}} u_{\mathbf{k}\mu}(\mathbf{r}), \quad (2.9)$$

where \mathbf{k} is the electron crystal momentum and the functions $u_{\mathbf{k}\mu}(\mathbf{r})$ are lattice-periodic.

There are two particular classes of materials where the Bloch waves can be substantially simplified.

For some of the metals in the groups I-IV of the periodic table electrons behave as if they were nearly free. The prime reason for this behavior is the high mobility of valence electrons which provides a good screening of the ionic background potential. For the nearly free electrons the complete neglect of the screened lattice potential is rather good approximation. In this case we are allowed to set $u = 1$ and consider the eigenstates (2.9) as plane waves. In particular for applications within low temperature condensed matter physics the solution of the full Hamiltonian for such systems is constructed by using the ground state as a reference system. Such delocalized or itinerant electron systems are characterized by broad energy bands, therefore, most of the information about their electron properties can be derived from their band structure.

The second class consists of materials with insulating behavior, in which the lattice potential confining the electrons is strong and they are “tightly-bound” to the lattice sites. In this case it is convenient to develop a theoretical description by using the site-centered *Wannier* functions [28, 29] orthogonal for different sites. The latter can be constructed as linear combination of all the Bloch states (2.9) for a given band μ :

$$W_{\mathbf{R}\mu}(\mathbf{r}) = \frac{1}{\sqrt{N}} \sum_{\mathbf{k}} e^{i\mathbf{k}\cdot(\mathbf{r}-\mathbf{R})} u_{\mathbf{k}\mu}(\mathbf{r}). \quad (2.10)$$

Since the energy bands for localized electron systems are rather narrow, the standard band picture fails and we have to consider the electronic structure in real space.

A variety of properties in both itinerant and localized electron systems are substantially dependent on the Coulomb repulsion which in

turn reflects the corresponding behavior - either itinerant or localized. Here we will briefly review the basic properties of the Hubbard model which occur due to the presence of localized electron interaction.

As the overlaps of Wannier functions (2.10) decrease exponentially, the corresponding matrix element $V_{\mu\mathbf{R}\mu'\mathbf{R}'\mu''\mathbf{R}''\mu'''\mathbf{R}'''}$ rapidly decreases with $|\mathbf{R}-\mathbf{R}'|$ and the most contributing ones will be the on-site elements $V_{\mu\mathbf{R}\mu'\mathbf{R}'\mu''\mathbf{R}''\mu'''\mathbf{R}'''} = U_{\mu\mu'\nu\nu'} = U$. For simplicity we will consider the single band case: $U_{\mu\mu'\nu\nu'} = U$. We simplify the expression (2.2) by taking into account electron hopping only between the nearest neighbors:

$$\int d^3r W_{\mathbf{R}}^*(\mathbf{r})H^0(\mathbf{r})W_{\mathbf{R}'}(\mathbf{r}) = -t_{\mathbf{R}\mathbf{R}'} = \begin{cases} -t, & \text{if } \mathbf{R}, \mathbf{R}' - \text{n. n.} \\ 0, & \text{else} \end{cases} \quad (2.11)$$

The resulting Hamiltonian is known as the one-band Hubbard model:

$$H = -t \sum_{\{\mathbf{R},\mathbf{R}'\},\sigma} c_{\mathbf{R}\sigma}^\dagger c_{\mathbf{R}'\sigma} + U \sum_{\mathbf{R}} n_{\mathbf{R}\uparrow} n_{\mathbf{R}\downarrow}. \quad (2.12)$$

Here the summation in the kinetic term is done over the pairs of the nearest neighbors. We introduced the occupation number operator

$$n_{\mathbf{R}\sigma} = c_{\mathbf{R}\sigma}^\dagger c_{\mathbf{R}\sigma}, \quad (2.13)$$

which has a possible eigenvalues 0, 1, or $n_\sigma^2 = n_\sigma$ on each site. We also define the charge operator on site \mathbf{R}

$$n_{\mathbf{R}} = \sum_{\sigma} n_{\mathbf{R}\sigma} = \sum_{\sigma} c_{\mathbf{R}\sigma}^\dagger c_{\mathbf{R}\sigma}, \quad (2.14)$$

and the local spin operator

$$\vec{S}_{\mathbf{R}} = \frac{\hbar}{2} \sum_{\sigma\sigma'} c_{\mathbf{R}\sigma}^\dagger \vec{\sigma}_{\sigma\sigma'} c_{\sigma'\mathbf{R}}, \quad (2.15)$$

where $\sigma_{\sigma\sigma'}^i$ are the Pauli matrices.

As the axis of the spin quantization can be chosen arbitrarily, the Hubbard Hamiltonian should not change under the rotation of the spin direction. Indeed, taking into account definitions (2.13)-(2.15) one can express the sum of squares of the on-site spins as

$$\sum_{\mathbf{R}} \vec{S}_{\mathbf{R}}^2 = \sum_{\mathbf{R}} \left(\frac{1}{4} n_{\mathbf{R}} - \frac{3}{2} n_{\mathbf{R}\uparrow} n_{\mathbf{R}\downarrow} \right), \quad (2.16)$$

which leads to the following representation for Hamiltonian (2.12):

$$H = -t \sum_{\{\mathbf{R}, \mathbf{R}'\}, \sigma} c_{\mathbf{R}\sigma}^\dagger c_{\mathbf{R}'\sigma} - \frac{2}{3} U \sum_{\mathbf{R}} \vec{S}_{\mathbf{R}}^2 + \frac{U}{6} \sum_{\mathbf{R}} n_{\mathbf{R}}. \quad (2.17)$$

This expression is invariant with respect to the rotation of the spin direction. The important property which can be seen immediately is that for positive repulsive potential U the spin on each site should be maximized.

2.2 The strong interaction limit

For large values of Coulomb repulsion ($U \gg t$) an important parameter of the Hubbard model is the filling factor n of the electrons. Values of $n = 0$ and $n = 2$ correspond to the totally empty and totally occupied band. In both cases this indicates the presence of an insulating state. For an intermediate values of n the system exhibits metallic properties. However, there is the special case $n = 1$, when only half of the band is filled, which corresponds to the so-called *Mott* insulator [2] which has the excitation spectrum as illustrated on Fig. (2.1). We will consider the

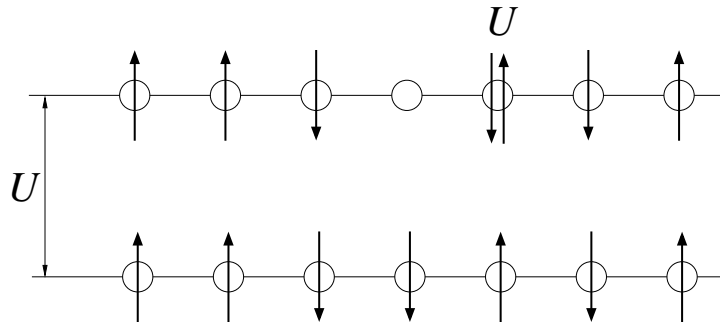


Fig. 2.1. The energy spectrum of a Mott insulator consists of two spin configurations corresponding to the ground state and a virtual state which differs by the number of the double-occupied sites. In the ground state each site is occupied by one electron.

effects caused by the hopping term t in (2.17) as a small perturbation, taking t^2/U as the relevant order parameter.

As the spin on each site is maximized by the Coulomb repulsion, the ground state of the system will represent the manifold of all pos-

sible configurations where one electron sits at each site. Thus different ground-state functions are orthogonal. For an N -atomic system the ground state will be 2^N times degenerate. The perturbed levels caused by the small hopping effects are determined by the number of the double-occupied sites characterized by the on-site Coulomb repulsion U . Following the *Brillouin-Wigner* perturbation theory [30, 31] and keeping the terms up to the second order in t^2/U one can represent the system to be described by the Hamiltonian

$$H = \frac{2t^2}{|U|} \sum_{\{\mathbf{R}, \mathbf{R}'\}} \left(\vec{S}_{\mathbf{R}} \vec{S}_{\mathbf{R}'} - \frac{1}{4} \right), \quad (2.18)$$

which demonstrate that the total energy could be lowered if the neighboring spins possess antiparallel alignment. Thus, for a large U and the case of a half-filling we obtain the so-called Heisenberg antiferromagnet.

If the occupation number is not fixed to be one, the restricted Hilbert space will split into configurations of empty holes, and up and down spins. The corresponding Hamiltonian possesses the form which is known as the so-called t - J -model

$$H = -t \sum_{\{\mathbf{R}, \mathbf{R}'\}, \sigma} c_{\mathbf{R}\sigma}^\dagger c_{\mathbf{R}'\sigma} + J \sum_{\{\mathbf{R}, \mathbf{R}'\}} \left(\vec{S}_{\mathbf{R}} \vec{S}_{\mathbf{R}'} - \frac{1}{4} n_{\mathbf{R}} n_{\mathbf{R}'} \right). \quad (2.19)$$

Due to the hopping term the holes are able to move. They transfer charge but without carrying spin. The movement of holes can induce spin-flip events and the long range order spin configurations may get destroyed. Therefore, this situation requires the quasiparticle treatment in order to describe correlation dynamics. The quasiparticles are objects corresponding to single particles whose motions are modified by interactions with the other particles in the system. In the present context this is equivalent to the lowest-lying excited states of the many-body system.

2.3 The weak interaction limit

For small values of the Coulomb repulsion ($U \ll t$) we can consider the interaction term as a small perturbation. In this case the electronic

states are close to those of the non-interacting electron gas. The non-interacting electron Hamiltonian reduces to the kinetic term of (2.12) which is conveniently treated in momentum space by making a Fourier transform of the kinetic part.

One of the early attempts to describe the effects of weak fermionic interactions was made by *Landau* who proposed the theory of the so-called *Fermi liquid* [32, 33]. It is based on the assumption that *the weak excitation spectrum is built according to the same principle as weak excitations for the non-interacting electron gas*. The essential postulate is that the quantity k_F (the reciprocal vector corresponding to the occupied state with the highest energy) is connected to the particle density n in the same way as in the non-interacting electron gas, $k_F = (3\pi^2 n)^{1/3}$. Like in the non-interacting electron gas the number of excited electrons is equal to the number of holes left below the Fermi energy ϵ_F (the energy of the highest occupied state). The circumstances which correspond to this assumption can easily be obtained by considering the density dependence of the kinetic energy for the non-interacting electron gas $\epsilon_{\text{kin}} \sim k_F^2 \sim n^{2/3}$. Taking into account that the typical interaction energy of particles with a mean distance $\langle r \rangle$ will be $\epsilon_{\text{pot}} \approx e^2 / \langle r \rangle \sim n^{1/3}$, we find that

$$\frac{\epsilon_{\text{pot}}}{\epsilon_{\text{kin}}} \sim n^{-1/3}, \quad (2.20)$$

which means that *in the system of interacting particles the kinetic term becomes the dominant energy contribution at high densities*. Despite of some similarity with the non-interacting electron gas, there exists a big difference arising from the fact that the excitations in a Fermi liquid interact with each other. Some of the well-known consequences of this interaction are the superconductivity and superfluidity phenomena.

By means of a perturbation theory the excitation of a Fermi liquid caused by Coulomb interaction V can be expressed as

$$\Delta E = \langle \text{GS} | V | \text{GS} \rangle + \sum_{|\nu\rangle \neq |\text{GS}\rangle} \frac{\langle \text{GS} | V | \nu \rangle \langle \nu | V | \text{GS} \rangle}{\epsilon^{(0)} - \epsilon_\nu} + \dots \quad (2.21)$$

Here $|\text{GS}\rangle$ is the ground-state many-body wave function of the Fermi liquid. The analysis of perturbation series shows that in the 1st order

only those processes will contribute in which both final and initial states belong to the ground state (often called the *Fermi sea*). This results in two possibilities: direct interaction and exchange interaction (Fig. 2.2):

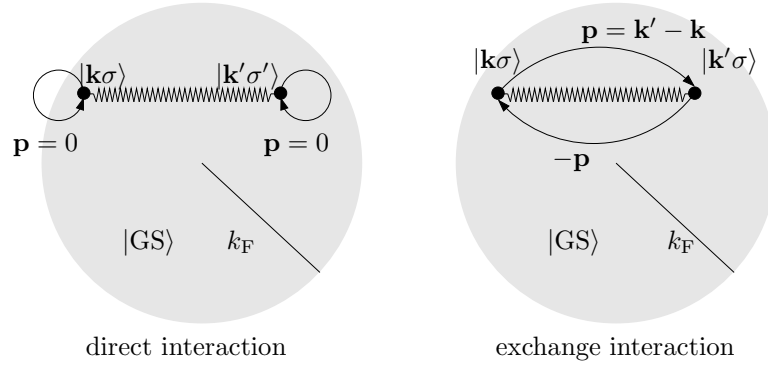


Fig. 2.2. The two possible processes occurring in the 1st-order perturbation theory. The interacting particles are characterized by momentum k and spin σ . The wave-line represents Coulomb interaction which is characterized by momentum p . The figure is taken from Ref. [34].

The 1st-order contribution is finite that ensuring the stability of the Fermi liquid for relatively small amplitudes of particle-particle interaction. The 2nd-order correction involves the interaction between the excited states $|\nu\rangle$. The possible processes again can be classified as “direct”- and “exchange”-type (Fig. 2.3). However, due to the singular behavior of the square of the interaction matrix element in the momentum space, the 2nd-order direct term diverges. Similar, the higher-order corrections also will diverge. Accordingly, it is necessary to account for the complete perturbation series. The corresponding technique based on the Green’s function formalism (which we will briefly consider later) is maturely developed, although its actual *ab-initio* applications in the calculations are rather limited, mainly due to the limitation in the computational resources.

For the weak limit of interaction the structure of elementary excitations can be defined analytically and explicitly used in the construction of realistic spectra. Elementary excitations can occur only in the vicinity of k_F . It is reasonable to consider only those which have relatively long lifetime or small attenuation probability. The attenuation magnitude is determined either by splitting of one excitation into several

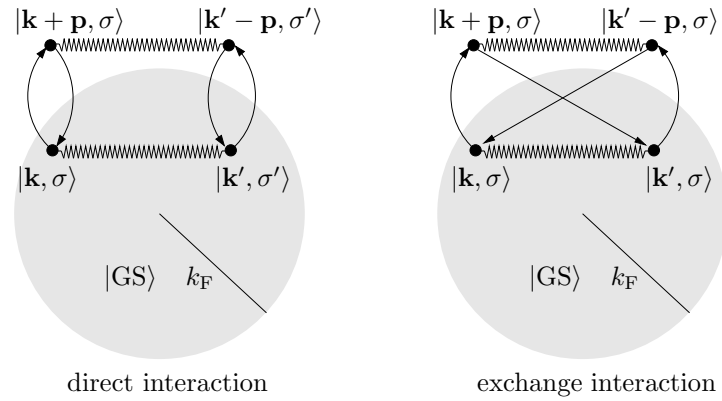


Fig. 2.3. The two possible processes occurring in the 2nd-order perturbation theory. The figure is taken from Ref. [34].

others, or by collisions between them. If the energy of excitation is high enough compared to the temperature, the splitting processes will be dominant and the attenuation probability is proportional to the probability of the splitting. Considering the corresponding diagram in

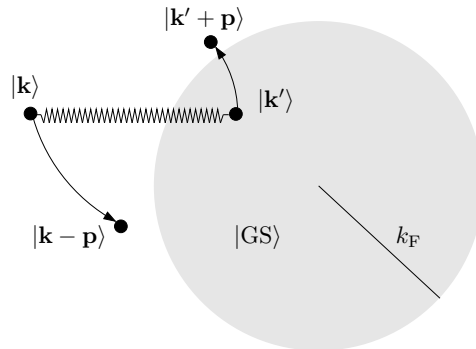


Fig. 2.4. The relaxation of the excitation due to the splitting process: Coulomb interaction with particle $|k'\rangle$ splits the excitation $|k\rangle$ into two excitations $|k - p\rangle$ and $|k' + p\rangle$ which have lower energies, and the hole left by particle $|k'\rangle$ in the Fermi sea.

Fig. 2.4 one can show that the splitting probability is proportional to p^2 , where p is the momentum connected with the corresponding Coulomb matrix element. On other hand, the use of quadratic dependence of the electron energy on momentum leads to the linear dependence of the excitation on p . From here it is clear that the attenuation will be relatively small only for the excitations with moments close to k_F . Considering the finite temperatures, similar speculations show that the

elementary excitation description of the Fermi liquid is applicable only for the temperatures.

Chapter 3

Perturbational description

3.1 The Baym-Kadanoff theory

The suitable instrument for the description of physical properties is the one-particle propagator or one-particle Green's function $G(1, 1')$ which describes the propagation of disturbances which appear when a single particle is removed at time-space coordinate $1' = (\mathbf{r}_{1'}, t_{1'})$ and added at coordinate $1 = (\mathbf{r}_1, t_1)$ in a many-particle equilibrium system. We consider the one-particle propagator defined within the interaction picture

$$G(1, 1'; U) = \frac{1}{i} \frac{\langle \text{T} [S c(1) c^+(1')] \rangle}{\langle \text{T} [S] \rangle}. \quad (3.1)$$

where $U = U(1)$ is the local scalar potential included in the Hamiltonian as $\int U(\mathbf{r}, t) n(\mathbf{r}, t) d\mathbf{r}$. The average occurring in Eq. (3.1) is taken over the grand-canonical ensemble:

$$\langle X \rangle = \frac{\text{Tr} \{ \exp \{ -\beta(H - \mu N) \} X \}}{\text{Tr} \{ \exp \{ -\beta(H - \mu N) \} \}} \quad (3.2)$$

where H is the full Hamiltonian of the system, N is the operator of total number of particles. Both operators are time-independent. $\beta = 1/(k_B T)$; μ is the chemical potential. T is the *time-ordering* operator:

$$\text{T} [A_1(t_1) \dots A_N(t_N)] = (-1)^P A_{i_1}(t_{i_1}) \dots A_{i_N}(t_{i_N}), t_{i_1} > \dots > t_{i_N} \quad (3.3)$$

where P is the parity of permutation needed to order the operators A_i chronologically.

In the interaction picture all the U dependence of the Green's function is encapsulated in the S term:

$$S = \exp \left\{ -i \int U(2)n(2)d2 \right\}, \quad (3.4)$$

where $n(2) = c(2)c^\dagger(2)$ is the occupation number operator. The operators c and c^\dagger obey the relationships (2.6) and (2.8). The integration with respect to time is performed along the imaginary axis from 0 to $-i\beta$, where β is the inverse temperature. The zero temperature case, $\beta = 1/(k_B T) = \infty$ which corresponds to the ground state of the system, is included into the considerations on equal footing.

The calculation of the one-particle Green's function for the system with pair interaction implies the necessity to introduce the two-particle propagator. Indeed, the equation of motion for the one-particle Green's function can be derived from Eq. (2.8) applying the operator $\frac{1}{i}\langle \text{Tr} \{ S \{ \cdot \} c^\dagger(1') \} \rangle$ (acting as $\frac{1}{i}\langle \text{Tr} \{ S \{ \cdot \} c^\dagger(1') \} \rangle A = \frac{1}{i}\langle \text{Tr} \{ S \{ A \} c^\dagger(1') \} \rangle$) to both sides.

Expressing the time derivative in the sense of a generalized function

$$\text{T} \left[\frac{\partial}{\partial t_1} c(1)c^\dagger(1') \right] = \frac{\partial}{\partial t_1} \text{T} [c(1)c^\dagger(1')] - \delta(1 - 1') \quad (3.5)$$

and using the definition (3.1), the equation of motion for $G(1, 1'; U)$ is obtained from Eq. (2.8) as

$$\left[i \frac{\partial}{\partial t_1} - H_0(1) \right] G(1, 1'; U) = \delta(1 - 1') - i \int d2 V(1, 2) G_2(12, 1'2'^+; U) \Big|_{t_2=t_1}. \quad (3.6)$$

The superscript “+” means that the time-argument 2 has to be taken infinitesimally larger than exactly 2 to obey the time-ordering. The two-particle propagator is defined as

$$G_2(12, 1'2'; U) = \left(\frac{1}{i} \right)^2 \frac{\langle \text{T} [S c(1)c(2)c^\dagger(2')c^\dagger(1')] \rangle}{\langle \text{T} [S] \rangle}. \quad (3.7)$$

The latter can be reexpressed in terms of the one-particle propagator by variation of $G(1, 1'; U)$ with respect to the scalar potential U :

$$G_2(12, 1'2'^+; U) \Big|_{t_2=t_1} = G(2, 2^+; U)G(1, 1'; U) + \frac{\delta G(1, 1'; U)}{\delta U(2^+)}. \quad (3.8)$$

Thus the equation of motion (3.6) can be rewritten in terms of one-particle propagator and its functional derivative:

$$\left\{ i \frac{\partial}{\partial t_1} - H_0(1) + i \int d2V(1, 2) [G(2, 2^+; U) + \frac{\delta}{\delta U(2^+)}] \right\} G(1, 1'; U) = \delta(1 - 1'). \quad (3.9)$$

There are no techniques available to solve this equation directly, but it can be used to generate approximate equations.

It is convenient to introduce the inverse Green's function G^{-1} as

$$\int d\bar{1} G^{-1}(1, \bar{1})G(\bar{1}, 1') = \int d\bar{1} G(1, \bar{1})G^{-1}(\bar{1}, 1') = \delta(1 - 1'). \quad (3.10)$$

Applying it from the right-hand side to Eq. (3.9) we obtain the well-known *Dyson* equation connecting non-interacting and interacting one-particle Green's functions:

$$G^{-1}(1, 1'; U) = G_0^{-1}(1, 1'; U) + \Sigma(1, 1'; U). \quad (3.11)$$

Here G_0 is the resolvent of the one-particle Hamiltonian H_0 , which describes a single particle propagation in the scalar potential U :

$$\left[i \frac{\partial}{\partial t_1} - H_0(1) \right] G_0(1, 1'; U) = \delta(1 - 1'). \quad (3.12)$$

Using the last two expressions we can write the equation of motion (3.6) as

$$\left[i \frac{\partial}{\partial t_1} - H_0(1) \right] G(1, 1') = \delta(1 - 1') + \int d\bar{1} \Sigma(1, \bar{1})G(\bar{1}, 1'). \quad (3.13)$$

The central quantity of Eq. (3.11) is the Σ term called the *self-energy*, which contains the interactions of a certain particle with its environment via a two-body potential V :

$$\begin{aligned} \Sigma(1, 1'; U) = & -i \int d\bar{2} V(1, \bar{2})G(\bar{2}, \bar{2}^+; U)\delta(1 - 1') + \\ & +i \int d\bar{2}d\bar{1} V(1, \bar{2}) \left[\frac{\delta G(1, \bar{1}; U)}{\delta U(\bar{2})} \right] G^{-1}(\bar{1}, 1'; U) \end{aligned} \quad (3.14)$$

This implies the important property of the self-energy - *it is a functional of the one-particle Green's function only.*

Taking into account that

$$\begin{aligned}
& \frac{\delta G(1, \bar{1})}{\delta U(\bar{2})} G^{-1}(\bar{1}, 1') \\
&= -\frac{\delta G^{-1}(1, \bar{1})}{\delta U(\bar{2})} G(\bar{1}, 1') \\
&= \frac{\delta [G_0^{-1}(1, \bar{1}) - \Sigma(1, \bar{1})]}{\delta U(\bar{2})} G(\bar{1}, 1') \\
&= \delta(1 - \bar{1})\delta(1 - \bar{2})G(\bar{1}, 1') - \frac{\delta \Sigma(1, \bar{1})}{\delta U(\bar{2})} G(\bar{1}, 1'), \quad (3.15)
\end{aligned}$$

and inserting it in Eq. (3.14) leads to the important relation which can be used to derive approximate expressions for the self-energy:

$$\begin{aligned}
\Sigma(1, 1'; U) &= iV(1, 1')G(1, 1'; U) - \\
&- i\delta(1 - 1') \int d\bar{2} V(1, \bar{2})G(\bar{2}, \bar{2}^+; U) \\
&+ i \int d\bar{1}d\bar{2} V(1, \bar{2})G(1, \bar{1}; U) \frac{\delta \Sigma(\bar{1}, 1'; U)}{\delta U(\bar{2})}. \quad (3.16)
\end{aligned}$$

For example, neglecting $\delta \Sigma / \delta U$ one derives the famous Hartree-Fock approximation. The next orders can be obtained by varying the Hartree-Fock self-energy and reinserting it in (3.16).

It is more convenient to analyze these perturbation series by using Feynman diagrams (for review see e.g. [35–37]). The summation of diagrams is a rather complicated problem as one has to account for an infinite number of terms. The numerical techniques based on the so-called *quantum Monte-Carlo* (QMC) method [38, 39] perform the full summation, but since they are time consuming their applications are rather limited. On other hand, not all the microscopic physical processes should be necessarily included in the perturbation expansion. Indeed, one can try to choose the infinite subset of diagrams describing a certain type of interaction and derive the analytical expression for it. Thus, identifying a certain approximate self-energy becomes an important issue to describe the proper physical nature of the system.

The general constrain is based on the derivations made above. It was formulated by *Baym* and *Kadanoff* who have shown that an arbitrary choice of self-energy does not guarantee the fulfillment of microscopic conservation laws of particle number and energy [40, 41]. To avoid this, the self-energy should obey the following properties:

- It must be a functional derivative of the *Luttinger-Ward* potential [42] which is a functional of the one-particle interacting Green's function and the bare Coulomb interaction.
- The self-energy and the interacting one-particle Green's function should self-consistently satisfy the Dyson equation (3.11).

The necessity of these requirements was first confirmed in both delocalized and localized correlation descriptions by model GW calculations [43].

Although the Baym-Kadanoff theory gives a recipe to find the exact self-energy for the effective one-particle problem, its application to solid state physics requires further assumptions and approximations in the theory itself as well as the development of the *ab-initio* methods which it could be combined with. The latter concerns first of all, the modification of the approaches based on the well-known density functional theory within the local density approximation as being the most successful *ab-initio* approach in the description of the ground-state properties of weakly-correlated systems. This will be the subject of the following chapters. At present we will consider the derivation of practically manageable approximate expression for the self-energy which by construction satisfies the Baym-Kadanoff conditions in order to obey the conservation laws.

3.2 The T -matrix approximation

In the present work the account of correlations is based on the so-called *T-matrix approximation* [12] which fulfills the conservation requirements mentioned above. The T -matrix is introduced as a kind of

an effective interaction:

$$\begin{aligned} T(12; 1'2') = & \\ & V(1, 2)\delta(1 - 1')\delta(2 - 2') \\ & + i \int d\bar{1} d\bar{2} T(12; \bar{1}\bar{2})G(\bar{1}, 1')G(\bar{2}, 2')V(1', 2'). \end{aligned} \quad (3.17)$$

Applying the Born expansion for the two-particle Green's function,

$$\begin{aligned} G_2(12; 1'2') \approx & \\ & G(1, 1')G(2, 2') - G(1, 2')G(2, 1') \\ & + i \int d\bar{1} d\bar{2} G(1, \bar{1})G(2, \bar{2})V(\bar{1}, \bar{2})G_2(\bar{1}\bar{2}; 1'2'), \end{aligned} \quad (3.18)$$

one can re-express it in terms of the T -matrix as

$$\begin{aligned} V(1, 2)G_2(12; 1'2') = & \\ & \int d\bar{1}d\bar{2} T(12; \bar{1}\bar{2}) \\ & \times [G(\bar{1}, 1')G(\bar{2}, 2') - G(\bar{1}, 2')G(\bar{2}, 1')]. \end{aligned} \quad (3.19)$$

Substituting it into the equation of motion (3.6) and comparing the result with Eq. (3.13) we can express the self-energy via the T -matrix:

$$\Sigma(1, 1') = -i \int d2d\bar{2} [T(12; 1'\bar{2}) - T(12; \bar{2}1')] G(\bar{2}, 2). \quad (3.20)$$

The precision of this approach is restricted only by reliance on the Born approximation (3.18) which is valid for a dilute gas of particles. However, it has the advantage that even for rather big magnitudes of the Coulomb interaction the effective interaction represented by the T -matrix remains finite.

Taking into account the instantaneity and homogeneity of the Coulomb interaction, i.e. $V(1, 1') = V(1 - 1') = V(\mathbf{r}_1 - \mathbf{r}_{1'})\delta(t_1 - t_{1'})$, it follows from Eq. (3.17), that the T -matrix has the following structure:

$$T(12; 1'2') = \delta(t_1 - t_2)\delta(t_{1'} - t_{2'}) \langle \mathbf{r}_1, \mathbf{r}_2 | T(t_1 - t_{1'}) | \mathbf{r}_{1'}, \mathbf{r}_{2'} \rangle. \quad (3.21)$$

The homogeneity of the electron gas also allows to express the product of the Green's functions in EQeq:T-matrix-def as

$$\begin{aligned} iG(1, 1')G(2, 2') &= iG(\mathbf{r}_1 - \mathbf{r}_{1'}, t_1 - t_{1'})G(\mathbf{r}_2 - \mathbf{r}_{2'}, t_2 - t_{2'}) \\ &= \langle \mathbf{r}_1, \mathbf{r}_2 | \Phi(t_1 - t_{1'}) | \mathbf{r}_{1'}, \mathbf{r}_{2'} \rangle. \end{aligned} \quad (3.22)$$

Inserting these quantities into Eq. (3.17) and making a Fourier transformation with respect to $t_1 - t_{1'}$ we obtain the following saddle equation for the T -matrix:

$$\begin{aligned} \langle \mathbf{r}_1, \mathbf{r}_2 | T(\epsilon) | \mathbf{r}_{1'}, \mathbf{r}_{2'} \rangle = & \\ & \delta(\mathbf{r}_1 - \mathbf{r}_{1'}) \delta(\mathbf{r}_2 - \mathbf{r}_{2'}) V(\mathbf{r}_{1'} - \mathbf{r}_{2'}) \\ & + V(\mathbf{r}_{1'} - \mathbf{r}_{2'}) \int d\bar{\mathbf{r}}_1 d\bar{\mathbf{r}}_2 \langle \mathbf{r}_1, \mathbf{r}_2 | T(\epsilon) | \bar{\mathbf{r}}_1, \bar{\mathbf{r}}_2 \rangle \langle \bar{\mathbf{r}}_1, \bar{\mathbf{r}}_2 | \Phi(\epsilon) | \mathbf{r}_{1'}, \mathbf{r}_{2'} \rangle. \end{aligned} \quad (3.23)$$

Considering the Green's function and all related quantities within a certain energy-independent basis set $\{\phi_i(\mathbf{r})\}$ in order to find the T -matrix we have to solve a simple matrix equation at each energy point ϵ :

$$T_{1234}(\epsilon) = V_{1234} + \sum' V_{121'2'} \Phi_{1'2'3'4'}(\epsilon) T_{3'4'34}(\epsilon), \quad (3.24)$$

where the quantity Φ , known as electron-electron correlation function, is defined as the convolution of two Green's functions:

$$\Phi_{1234}(\epsilon) = i \int \frac{d\epsilon'}{2\pi} G_{13}(\epsilon - \epsilon') G_{24}(\epsilon'). \quad (3.25)$$

Applying analogous considerations to Eq. (3.20) it is transformed to the matrix integral form:

$$\Sigma_{12}(\epsilon) = \frac{1}{i} \int \frac{d\epsilon'}{2\pi} [T_{121'2'}(\epsilon' + \epsilon) - T_{211'2'}(\epsilon' + \epsilon)] G_{2'1'}(\epsilon'). \quad (3.26)$$

Fulfilling Eqs. (3.24)-(3.26) by a corresponding transformation of Eq. (3.11)

$$G^{-1}(\epsilon) = G_0^{-1}(\epsilon) + \Sigma(\epsilon), \quad (3.27)$$

we obtain a closed set of equations from where both the interacting Green's function and the corresponding self-energy can be found in a self-consistent way.

If we consider the finite temperature case, the corresponding integration represents the summation over the so-called *Matsubara* poles, $\epsilon_n = i(2n - 1)\pi\hbar/\beta$, $n = 1, 2, \dots$ which are the poles of the finite-temperature Green's function. For the zero-temperature case the integration is performed from $-\infty$ to $+\infty$ along the real axis.

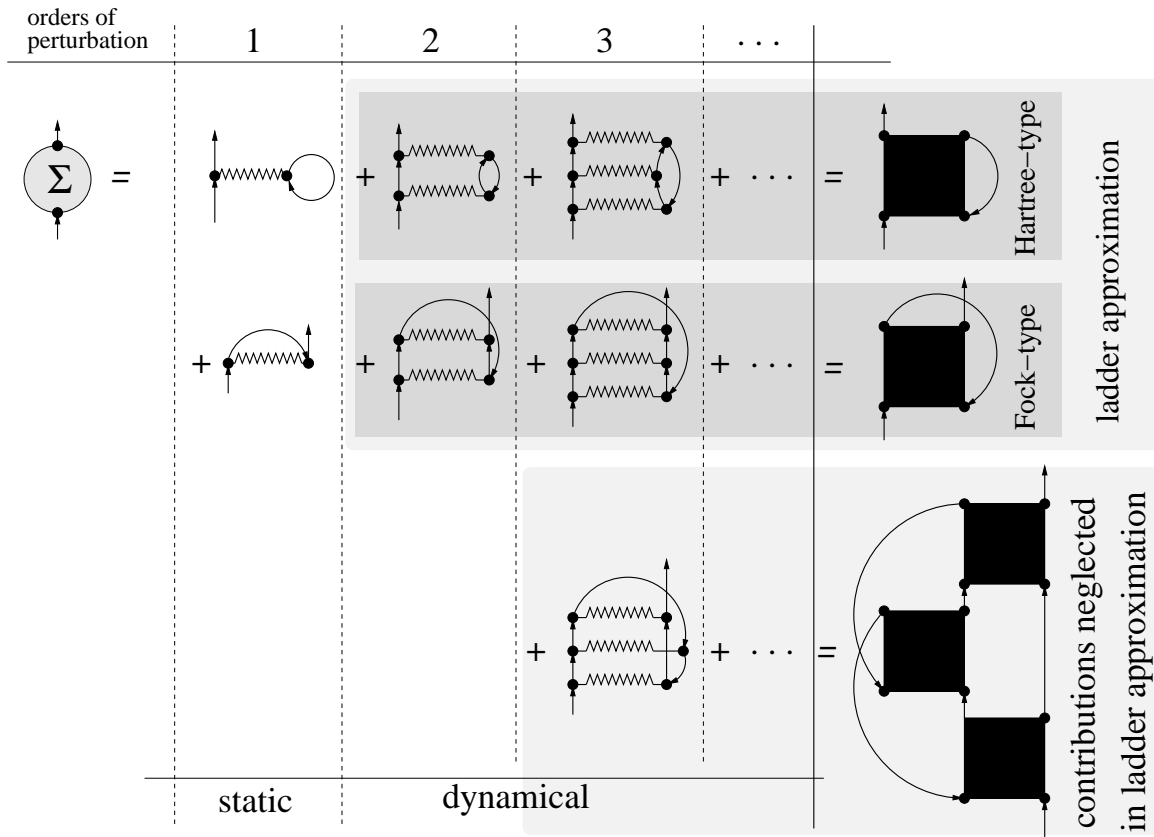


Fig. 3.1. Diagrammatic structure of the self-energy Σ . The shaded regions contain time-dependent diagrams which represent fluctuation dynamics. The black box represents the T -matrix and the wavy line - bare Coulomb interaction. Two dark-shaded channels of Hartree- and Fock-types contain full account of dynamical effects in the 2nd order. Any other channel starts at least from the 3rd-order diagrams.

The T -matrix approximation to the self-energy can be expressed by so-called *ladder* diagrams which split into two subsets classified according to their construction as *Hartree*- and *Fock*-channels. The corresponding diagrammatic scheme is illustrated in Fig. 3.1. One can see, that the 1st-order diagrams represent the conventional Hartree-Fock approximation. Using the subsequent insertions of the bare Coulomb potential V denoted by zigzag line we arrive at the simple representation of the final sum which has the same structure as the corresponding 1st-order diagrams. However, the bare potential is now changed to the effective renormalized or screened potential, which is now represented by the T -matrix. The construction of the T -matrix according to the Eq. (3.17) or (3.24) can also be represented by Feynman diagrams as

sketched in Fig. 3.2.

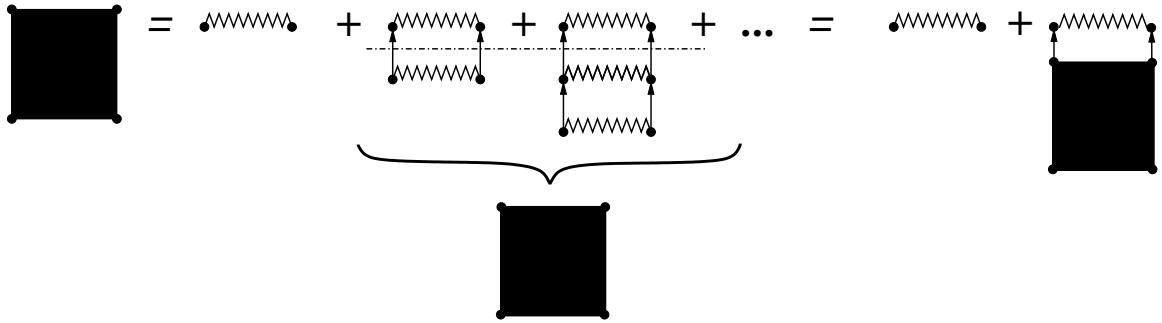


Fig. 3.2. Renormalization of the bare potential. Cutting the additional infinite set of the diagrams along the dashed line leads to the Bethe-Salpeter equation (3.17) for the T -matrix.

In 2nd-order perturbation theory the ladder approximation accounts for all possible dynamical interactions. Any other dynamical process will involve at least three distinct collisions. The static part of the self-energy contained in the 1st-order diagrams should be subtracted from the final expression if one is interested only in dynamical effects. Of course one is not restricted to the Hartree-Fock only and can construct the channels of higher orders. For example, having once calculated the T -matrix for Hartree- and Fock-channel one can still make use of it by creating new contributions as shown in the bottom of Fig. 3.1. This way one goes beyond the standard T -matrix approximation as represented by Eq. (3.17) and (3.26). However, at least for moderately-correlated materials the most important dynamics is usually accounted for by the ladder approximation and the magnitude of the subsequent channels falls down fast with increasing order. Taking this into account together with the growing complexity and computational effort in the calculation of higher-order channels they are often neglected.

For the electron-electron interaction the insertions of the bare potential are connected by the propagator lines having the same direction (electron-electron correlation function). The channels based on this type of diagrams are classified as particle-particle (PP) type. In complete analogy one can consider the interaction between the electron and the hole, which can be represented by connecting the bare potential by antiparallel lines. This kind of channels is called particle-hole (PH) type. Building particle-hole interaction in terms of ladder diagrams it

is easy to see that the 1st- and the 2nd-order diagrams will be the same as for the PP-channel. After subtraction of these double-counted terms the PH-channel starts from the third order and can be added to the PP-channel.

Combining the PP- and PH-channels provides the basis for the so-called *T-matrix Plus Fluctuation Exchange* (FLEX) scheme which is often used in the present work. Originally it follows from the work of Bickers and Scalapino [44]. The extension of the scheme to the multiorbital case and first self-consistent implementation was made by Lichtenstein and Katsnelson [45, 46]. Later on, the derivation of the FLEX equations for real-energies corresponding to the zero-temperature limit was made by Drchal, Janis and Kudrnovskyy [27]. Recently Pourovskyy, Katsnelson and Lichtenstein have proposed a further extension of the FLEX finite-temperature scheme [47] by taking into account relativistic effects.

3.3 *T*-matrix formulation for real energies

Here we will derive the TMA equations within the real-energy formalism following the work of Drchal *et al.* [27], which is extended here to the full matrix formulation with respect to the spin-orbital basis set. As we mentioned above, this formalism corresponds to the zero-temperature limit usually implied when using band structure methods.

The original formulation (3.24)-(3.26) of TMA was given in terms of *causal* quantities. However, it is more convenient to work with their *retarded* equivalents which possess analytical properties substantially simplifying the infinite integration on the real axis. We indicate the causal quantities with a superscript “c” and relate them to the retarded ones by:

$$G^{(c)}(\epsilon) = \Re G(\epsilon) + i \operatorname{sgn}(\epsilon - \mu) \Im G(\epsilon). \quad (3.28)$$

Here μ is the chemical potential, $\Re G$ and $\Im G$ are *hermitian* and *antihermitian* components of the Green’s function matrix G :

$$\begin{aligned} \Re G_{\Lambda\Lambda'} &= \frac{1}{2} (G_{\Lambda\Lambda'} + G_{\Lambda'\Lambda}^*) , \\ \Im G_{\Lambda\Lambda'} &= \frac{1}{2i} (G_{\Lambda\Lambda'} - G_{\Lambda'\Lambda}^*) , \end{aligned} \quad (3.29)$$

where G^* is the complex conjugate of G . In practice, the matrix G is derived in a symmetric form, thus right-hand sides of Eqs. (3.29) are purely real.

Using Eq. (3.28) we derive the expression for the two-particle propagator Φ in Eq. (3.25) in terms of the retarded Green's function. For simplicity we group the pair of the Green's function matrix indices in a single index Λ , which numbers the appropriate basis functions:

$$\begin{aligned}
\Im \Phi_{\Lambda\Lambda'}^{(c)}(\epsilon) &= \\
&= \int_{-\infty}^{\infty} \frac{d\omega'}{2\pi} \left[\Re G_{\Lambda}^{(c)}(\epsilon - \epsilon') \Re G_{\Lambda'}^{(c)}(\epsilon') - \Im G_{\Lambda}^{(c)}(\epsilon - \epsilon') \Im G_{\Lambda'}^{(c)}(\epsilon') \right] \\
&= \int_{-\infty}^{\infty} \frac{d\omega'}{2\pi} \left[\Re G_{\Lambda}(\epsilon - \epsilon') \Re G_{\Lambda'}(\epsilon') \right. \\
&\quad \left. - \operatorname{sgn}(\epsilon - \epsilon' - \mu) \operatorname{sgn}(\epsilon' - \mu) \Im G_{\Lambda}(\epsilon - \epsilon') \Im G_{\Lambda'}(\epsilon') \right]. \quad (3.30)
\end{aligned}$$

Taking into account the analytical properties of the retarded functions that imply the integral relation:

$$\int_{-\infty}^{\infty} d\epsilon' \left[\Re G_{\Lambda}(\epsilon - \epsilon') \Re G_{\Lambda'}(\epsilon') + \Im G_{\Lambda}(\epsilon - \epsilon') \Im G_{\Lambda'}(\epsilon') \right] = 0, \quad (3.31)$$

one can simplify the calculation of the pair-correlation function:

$$\begin{aligned}
\Im \Phi_{\Lambda\Lambda'}^{(c)}(\epsilon) &= \\
&- \int_{-\infty}^{\infty} \frac{d\omega'}{2\pi} \left[1 + \operatorname{sgn}(\epsilon - \epsilon' - \mu) \operatorname{sgn}(\epsilon' - \mu) \right] \Im G_{\Lambda}(\epsilon - \epsilon') \Im G_{\Lambda'}(\epsilon') \\
&= \operatorname{sgn}(\epsilon - 2\mu) \int_{\mu}^{\epsilon - \mu} \frac{d\epsilon'}{\pi} \Im G_{\Lambda}(\epsilon - \epsilon') \Im G_{\Lambda'}(\epsilon'). \quad (3.32)
\end{aligned}$$

A corresponding procedure we apply to the calculation of the self-energies given by Eq. (3.26). The infinite integration is now expressed

as

$$\begin{aligned}
& \int_{-\infty}^{\infty} \frac{d\omega'}{2\pi} G^{(c)}(\epsilon') T^{(c)}(\epsilon' + \epsilon) = \\
& - \int_{-\infty}^{\infty} \frac{d\omega'}{2\pi} [1 + \operatorname{sgn}(\epsilon' - \mu) \operatorname{sgn}(\epsilon' + \epsilon - \mu)] \Im G(\epsilon') \Im T(\epsilon' + \epsilon) \\
& = \operatorname{sgn}(\epsilon) \int_{\mu-\epsilon}^{\mu} \frac{d\epsilon'}{\pi} \Im G(\epsilon') \Im T(\epsilon' + \epsilon). \tag{3.33}
\end{aligned}$$

The advantage of the expressions given by Eqs. (3.32) and (3.33) is that the integration involves only antihermitian/imaginary components which decay very fast with an energy argument going to infinity. For practical calculation the range of the \Im -components of Φ , T and Σ can be taken to be finite (roughly within 1 Ry).

The hermitian/real counterparts are related to antihermitian/imaginary by means of the so-called *Hilbert* transformation based on Cauchy's integral theorem (see e.g. Ref. [48]):

$$f(z_0) = \frac{1}{2\pi} \int_{-\infty}^{\infty} dx \frac{\operatorname{Im} f(x)}{x - z_0}, \tag{3.34}$$

where z_0 is an arbitrary complex argument taken in the area of analyticity of the complex function f . The requirement of analyticity is not critical for the real axis as long as f is just finite (integrable). On the real axis the Hilbert transform (3.34) is reduced to the so-called *Kramers-Kronig* relations:

$$\begin{aligned}
\Re f(x_0) &= \frac{1}{\pi} \int_{-\infty}^{\infty} dx \frac{\Im f(x)}{x - x_0}, \\
\Im f(x_0) &= -\frac{1}{\pi} \int_{-\infty}^{\infty} dx \frac{\Re f(x)}{x - x_0}. \tag{3.35}
\end{aligned}$$

The result of the Kramers-Kronig relations is determined up to an arbitrary additive constant. For the situation considered here this constant is fixed by requiring a Fermi liquid behavior of the dynamical self-energy near the Fermi level, i.e. $\Sigma(\epsilon_F) = 0$.

Chapter 4

The mean-field approximations

Before considering the next class of the many-body theories based on total energy functionals, namely the Density Functional Theory (DFT) [13] and the recently developed Spectral Density Functional Theory (SDFT) [49], it is instructive to give some overview for the approximations which allow to develop practical numerical schemes for the corresponding functional theories. The features of these approximations are very similar and can be unified into a single theoretical approach referred as the mean-field approximation discussed in the following.

Despite of the complexity of the many-body problem discussed above for a wide range of systems a rather crude treatment, without full inclusion of correlations could be applied. This is the case when the correlations could be included on the average, by considering a certain particle moving in an effective *mean* field, which does not depend on the coordinates of other particles.

The formal structure of any mean-field theory can be illustrated by taking as a starting point the interaction part of the Hubbard Hamiltonian:

$$H_{\text{int}} = \frac{1}{2} \sum_{\mu\nu\nu'\mu'} V_{\mu\nu\nu'\mu'} c_{\mu}^{\dagger} c_{\nu}^{\dagger} c_{\nu'} c_{\mu'}. \quad (4.1)$$

Considering only the direct interaction and introducing the density operator $n_{\mu\mu'} = c_{\mu}^{\dagger} c_{\mu'}$ we can rewrite Eq. (4.1) as

$$H_{\text{int}} = \frac{1}{2} \sum_{\mu\mu'\nu\nu'} V_{\mu\nu\nu'\mu'} n_{\mu\mu'} n_{\nu\nu'}. \quad (4.2)$$

The mean-field approximation is based on the assumption that the deviation of the $n_{\mu\mu'}$ operator from its average $\langle n_{\mu\mu'} \rangle - n_{\mu\mu'}$ is small. This leads to the following approximation for the averaged product $\langle n_{\mu\mu'} n_{\nu\nu'} \rangle$ and the corresponding effective mean-field Hamiltonian:

$$H_{\text{MF}} = \frac{1}{2} \sum_{\mu\mu'\nu\nu'} V_{\mu\nu\nu'\mu'} \langle n_{\mu\mu'} n_{\nu\nu'} \rangle,$$

$$\langle n_{\mu\mu'} n_{\nu\nu'} \rangle \approx n_{\mu\mu'} \langle n_{\nu\nu'} \rangle + \langle n_{\mu\mu'} \rangle n_{\nu\nu'} - \langle n_{\mu\mu'} \rangle \langle n_{\nu\nu'} \rangle. \quad (4.3)$$

One can view the product $n_{\mu\mu'} \langle n_{\nu\nu'} \rangle$ as the interaction of the operator $n_{\mu\mu'}$ with some effective mean-field $\langle n_{\nu\nu'} \rangle$. The averages $\langle n_{\mu\mu'} \rangle$ can be determined from the condition of stationarity of the effective system by minimizing its free energy F_{MF} :

$$F_{\text{MF}} = -\frac{1}{\beta} \ln \text{Tr} \{ e^{-\beta H_{\text{MF}}} \}, \quad (4.4)$$

with $\beta = 1/k_{\text{B}}T$, k_{B} the Boltzmann constant and T the temperature.

$$\begin{aligned} & \frac{d}{d\langle n_{\nu\nu'} \rangle} F_{\text{MF}} \\ &= \frac{\text{Tr} \left\{ e^{-\beta H_{\text{MF}}} \frac{dH_{\text{MF}}}{d\langle n_{\nu\nu'} \rangle} \right\}}{\text{Tr} \{ e^{-\beta H_{\text{MF}}} \}} \\ &= \frac{1}{\text{Tr} \{ e^{-\beta H_{\text{MF}}} \}} \text{Tr} \left\{ e^{-\beta H_{\text{MF}}} \sum_{\mu\mu'} V_{\mu\nu\nu'\mu'} (n_{\mu\mu'} - \langle n_{\mu\mu'} \rangle) \right\} \\ &= \sum_{\mu\mu'} V_{\mu\nu\nu'\mu'} (\langle n_{\mu\mu'} \rangle_{\text{MF}} - \langle n_{\mu\mu'} \rangle) \\ &= 0. \end{aligned} \quad (4.5)$$

Thus we arrive at a closed set of the mean-field equations. This approach provides a physically sensible method to study interacting systems where the correlations are weakly deviating from their average values. The question is under which conditions this criterion is satisfied. As we are starting from the point where we don't know the exact averages $\langle n_{\mu\mu'} \rangle$ one has to do some guess. For localized systems as a natural choice for such a guess the spatial average $\langle n_{\mu\mu'} \rangle_{\text{spatial}}$ over the

nearest neighbors can serve. The proximity of the $\langle n_{\mu\mu'} \rangle_{\text{spatial}}$ to the exact thermodynamic average $\langle n_{\mu\mu'} \rangle$ is determined by the *central limit theorem* stating that the fluctuations around the expectation value become smaller by the order of $N^{-1/2}$, where N is the number of nearest neighbors. This means that the *mean-field theory is exact in the limit of the infinite coordination number*. In systems with translational invariance this corresponds to the infinite spatial dimensionality. The reliability of a mean-field description via dimensionality was investigated by Metzner and Vollhardt [50] and later by Potthoff and Nolting [51].

The mean-field framework provides common concepts underlying different theories dealing with interacting systems, as the Weiss molecular field theory for a classical magnet, density functional theory for the inhomogeneous electron gas and the spectral density functional theory for strongly-correlated electron systems [49]. All mentioned approaches differ by the choice of the particular local or localized quantity for which the corresponding mean-field free-energy functional is constructed. For example in Weiss theory it is the on-site magnetization, in density functional theory it is the local electron density, in spectral density functional theory - the localized Green's function. A detailed overview of the mean-field representations can be found in the work of Georges [52].

Chapter 5

The energy functional description

The description of the equilibrium many-body system is in principle always connected with the problem of minimization its total free energy. Thus, all the existing many-body theories can be viewed as based on the free energy functional which for a system at equilibrium has to be minimized. The minimization is performed with respect to some suitable variable (or set of variables) which should contain all necessary information about the system. Thus, the goal of theory is to construct the proper free-energy functional of the corresponding variable and to prove the existence of its global minimum which can then be found by solving the corresponding variational equation. Since the different constructions of the free energy (or total energy) functional ($E[\rho]$, $E[G]$, ...) describe the same many-body system, with respect to their minima they all should coincide. Mathematically this is equivalent to the possibility to link them by the so-called Legendre transformation.

Another, less strict requirement is that the corresponding variable should be as simple as possible, or by other words, physically tractable. From this point of view, the variable of the Baym-Kadanoff theory, namely the actual Green's function of the whole many-body system is too complex. Of course, it contains all the necessary and unnecessary information. However, the way in which it is derived (the perturbational description discussed in Chapter 3) is rather complicated and completely unmanageable for realistic systems. Here we will consider let's say the "minimal variable set" functional theory which utilizes only one variable - the local electron density. Due to its simplicity the theory affords to provide a corresponding "minimal input set", or alternatively,

the “*ab-initio*” way to solve the equilibrium many-body problem. This theory is naturally called Density Functional Theory (DFT) and it will be the subject of the first section of the present chapter (Sec. 5.1).

As mentioned above, the main goal of any energy functional theory is to choose a proper variable and to prove the existence of the global minimum for the corresponding functional. However, these conditions are not yet sufficient to derive a practically manageable approach. Indeed, the functional itself (or at least, its derivative) still has to be found. The construction of the energy functional in terms of the chosen variable is nothing else as the mean-field approximation which was discussed in Chapter 4. For the local density as a variable this procedure is called the Local Density Approximation (LDA).

On the other hand, the insufficient knowledge of the nature of electronic interactions does not allow to complete this construction at least in terms of the local density. We can only describe its most obvious part and try to guess the unknown one. In many cases when the unknown part is small this description is sufficient. However sometimes, namely in case of the strongly-correlated systems the unknown part of the functional becomes significant and the LDA approach fails. The possible direction to deal with this problem is to simplify the corresponding energy functional. However, the cost for that is the complication of the corresponding variable. Thus, the goal is to find a way which still remains simple but at the same time sufficient to capture the important part of the unknown interaction. As one of such compromises, specific for locally-correlated systems the so-called LDA+DMFT (Dynamical Mean-Field Theory) have appeared, which has to be seen much less “*ab-initio*” than pure LDA. It utilizes the advantageous features of both approaches - the Baym-Kadanoff theory for the localized correlated electrons and the local-density description for the rest of the system. However before considering the DMFT method it will be instructive first to make a functional link between LDA and DMFT. This will be discussed in the Sec. 5.4. In the following Sec. 5.5 the description of the DMFT which is the central aspect of this thesis finally will be given.

5.1 Density functional theory

Density functional theory (DFT) is a general many-body theory supplying the framework which enables one to determine the ground state energy of any system, in particular solids, consisting of electrons in an external potential. By applying DFT with various boundary conditions one can calculate energy differences which, in turn, are directly related to physical observables.

Originally developed by Hohenberg, Kohn and Sham [13–15] in the mid-sixties, DFT uses the idea of *Thomas-Fermi* theory meant to circumvent the technical difficulties implied by the use of many-body techniques – e.g. Hartree-Fock theory – introducing the electron density as a basic variable rather than the many-electron wave function. As it will be shown in the following, this way one arrives at a one-particle problem that is much easier to solve than the corresponding many-body problem. An appealing feature of the theory is that, unlike the Hartree-Fock method, it takes the exchange *and* correlation of the electrons simultaneously into account. The corresponding term, known as exchange–correlation energy, is the only one requiring a suitable approximation within DFT.

The theory is based on the two theorems of Hohenberg and Kohn [13]. The first one states that *the total ground state of a system with N electrons and hence all ground-state properties are functionals of the local density $\rho(\mathbf{r})$* . This allows DFT to define the energy of the system as a functional of the local density $\rho(\mathbf{r})$:

$$E_{\text{tot}}[\rho] = \int d^3r \rho(\mathbf{r})V_{\text{ext}}(\mathbf{r}) + \Delta[\rho], \quad (5.1)$$

where $\Delta[\rho] = K[\rho] + E_{\text{H}}[\rho] + E_{\text{xc}}[\rho]$ is the sum of the kinetic, Hartree and exchange–correlation energies [15]. This quantity does not depend on any external fields reflecting the fact that different many-electron systems differ only by the local external potential $V_{\text{ext}}(\mathbf{r})$ felt by the electrons. The energy functional $\Delta[\rho(\mathbf{r})]$ is nothing else but the internal energy of the electron gas and it is universal in the sense that it refers to any system, independent on the number of particles and/or the external potential.

The second theorem of DFT [13] states that *the ground state energy*

functional associated with a given external potential is a minimum over densities corresponding to a given total electron number N . The density yielding the minimum total energy is the ground state density. Thus, the ground state can be found from the stationarity condition (4.5) minimizing the total energy by means of a functional derivative

$$\left. \frac{\delta E_{\text{tot}}[\rho]}{\delta \rho(\mathbf{r})} \right|_{\rho=\rho_{\text{GS}}(\mathbf{r})} = 0, \quad (5.2)$$

where ρ_{GS} is the ground-state electron density. The electron density is defined as

$$\rho(\mathbf{r}) = -\frac{1}{\pi} \text{Im} \int^{\epsilon_{\text{F}}} d\epsilon G(\mathbf{r}, \mathbf{r}, \epsilon), \quad (5.3)$$

where $G(\mathbf{r}, \mathbf{r}', \epsilon)$ is the so-called Kohn-Sham Green's function defined as a resolvent of the effective one-particle Hamiltonian entering the corresponding Schrödinger (Kohn-Sham) equation obtained from the variation of the total energy:

$$[\epsilon + \nabla_{\mathbf{r}}^2 - V_{\text{eff}}(\mathbf{r})] G(\mathbf{r}, \mathbf{r}', \epsilon) = \delta(\mathbf{r} - \mathbf{r}'), \quad (5.4)$$

with $-\nabla_{\mathbf{r}}^2$ being the operator of the kinetic energy, and ϵ Lagrange multipliers. The eigenvalues of the effective one-particle problem $\{\epsilon_i\}$ will correspond to the poles of the Green's function. The following expressions are used for the effective one-particle potential V_{eff} :

$$V_{\text{eff}}(\mathbf{r}) = V_{\text{ext}}(\mathbf{r}) + V_{\text{H}}(\mathbf{r}) + V_{\text{xc}}(\mathbf{r}), \quad (5.5)$$

the external potential created by ionic charges $Z_{\mathbf{R}}$ sitting on the lattice sites \mathbf{R} :

$$V_{\text{ext}}(\mathbf{r}) = \sum_{\mathbf{R}} \frac{Z_{\mathbf{R}}}{|\mathbf{r} - \mathbf{R}|}, \quad (5.6)$$

the Hartree potential:

$$V_{\text{H}}(\mathbf{r}) = \int d^3r' \frac{\rho(\mathbf{r}')}{|\mathbf{r} - \mathbf{r}'|}, \quad (5.7)$$

and the so-called exchange-correlation potential:

$$V_{\text{xc}}(\mathbf{r}) = \frac{\delta E_{\text{xc}}[\rho]}{\delta \rho(\mathbf{r})}. \quad (5.8)$$

Taking the imaginary part of the expression (5.4) in the limit $\mathbf{r}' = \mathbf{r}$ and performing an integration over the space and the energy one obtains the so-called band energy E_{band} :

$$\begin{aligned} E_{\text{band}} &= -\frac{1}{\pi} \text{Im} \int d\epsilon \cdot \epsilon \int d^3r G(\mathbf{r}, \mathbf{r}, \epsilon) \\ &= K[\rho] + \int d^3r V_{\text{eff}}(\mathbf{r})\rho(\mathbf{r}) \\ &= K[\rho] + \int d^3r V_{\text{ext}}(\mathbf{r})\rho(\mathbf{r}) + \int d^3r V_{\text{H}}(\mathbf{r})\rho(\mathbf{r}) + \int d^3r V_{\text{xc}}(\mathbf{r})\rho(\mathbf{r}). \end{aligned} \quad (5.9)$$

Using it, one can eliminate the kinetic energy term arriving at the following expression for the total energy which is easily manageable:

$$\begin{aligned} E_{\text{tot}}[\rho] &= -\frac{1}{\pi} \text{Im} \int d\epsilon \cdot \epsilon \int d^3r G(\mathbf{r}, \mathbf{r}, \epsilon) \\ &\quad - E_{\text{H}}[\rho] + \int d^3r V_{\text{xc}}(\mathbf{r})\rho(\mathbf{r}) + E_{\text{xc}}[\rho]. \end{aligned} \quad (5.10)$$

The Hartree energy E_{H} can be written explicitly as

$$\begin{aligned} E_{\text{H}}[\rho] &= \frac{1}{2} \int d^3r \rho(\mathbf{r}) \int d^3r' \frac{\rho(\mathbf{r}')}{|\mathbf{r} - \mathbf{r}'|} \\ &= \frac{1}{2} \int d^3r V_{\text{H}}(\mathbf{r})\rho(\mathbf{r}). \end{aligned} \quad (5.11)$$

Combining Eqs. (5.3)-(5.8) we can find the local density $\rho(\mathbf{r})$ and the total energy of the ground state. As the system of equations is closed it has to be solved in a self-consistent manner.

Although this approach is rigorously applicable to the ground state only, it is substantially simplified due to the reduction of the many-body problem to the single-particle problem with the effective local potential being varied in such a way that the resulting density mimics the true density of the system.

The system of Eqs. (5.3)-(5.8) is exact provided the exact is the form of the exchange-correlation functional $E_{\text{xc}}[\rho]$ is known. For the inhomogeneous electron gas the exact expression for E_{xc} can be given in a form of the Coulomb interaction between the electron and its surrounding exchange-correlation hole described by the density distribution function $\rho_{\text{xc}}(\mathbf{r}, \mathbf{r}' - \mathbf{r})$:

$$E_{\text{xc}}[\rho] = \frac{1}{2} \int d^3r \rho(\mathbf{r}) \int d^3r' \frac{\rho_{\text{xc}}(\mathbf{r}, \mathbf{r}' - \mathbf{r})}{|\mathbf{r} - \mathbf{r}'|}. \quad (5.12)$$

The exchange-correlation hole density is defined as

$$\rho_{\text{xc}}(\mathbf{r}, \mathbf{r}' - \mathbf{r}) = \rho(\mathbf{r}') \int_0^1 d\lambda (g_\lambda(\mathbf{r}, \mathbf{r}') - 1), \quad (5.13)$$

where $g_\lambda(\mathbf{r}, \mathbf{r}')$ is the so-called pair correlation function, λ is the coupling constant. The important property of $E_{\text{xc}}[\rho]$ is its independence of the actual form of the exchange-correlation hole. This can be shown by making the substitution $\mathbf{r} - \mathbf{r}' = \mathbf{r}''$ [53] bringing the expression of exchange-correlation functional to the form

$$E_{\text{xc}}[\rho] = \int d^3r \rho(\mathbf{r}) \int dr'' r''^2 \int d\Omega'' \rho_{\text{xc}}(\mathbf{r}, \mathbf{r}''), \quad (5.14)$$

which depends only on the average over the spherical angle Ω'' . Thus, $E_{\text{xc}}[\rho]$ depends only on the distance but not on the direction of the Coulomb interaction. Integrating the exchange-correlation density leads to the sum rule [53]:

$$4\pi \int dr' r'^2 \int d\Omega \rho_{\text{xc}}(\mathbf{r}, \mathbf{r}') = -1, \quad (5.15)$$

ensuring that the exchange-correlation hole corresponds to a unity charge around the electron.

5.2 The local density approximation

An expression for the exchange-correlation functional $E_{\text{xc}}[\rho]$ that is widely used is based on the so-called *local density approximation* (LDA) which is being relatively simple and at the same time is most successful.

It uses the same expression for ρ_{xc} as in the homogeneous electron gas, but for each spatial point utilizes the local value of the charge density $\rho(\mathbf{r})$:

$$\rho_{xc}^{\text{LDA}}(\mathbf{r}, \mathbf{r}' - \mathbf{r}) = \rho(\mathbf{r}') \int_0^1 d\lambda [g_\lambda^h(|\mathbf{r} - \mathbf{r}'|, \rho(\mathbf{r})) - 1], \quad (5.16)$$

where g_λ^h is the pair correlation function for the homogeneous electron gas. The advantage of this expression is that it satisfies the sum rule (5.15). Applying it to the Eq. 5.12 we arrive at the local density approximation [14]

$$E_{xc}^{\text{LDA}}[\rho] = \int d^3r \rho(\mathbf{r}) \varepsilon_{xc}^h(\rho(\mathbf{r})), \quad (5.17)$$

where $\varepsilon_{xc}^h(\rho)$ is the exchange-correlation energy for the homogeneous electron gas with the density ρ . For the exchange component of the energy the relation is simple [54, 55]

$$\varepsilon_x^h(\rho) = -\frac{3e^2}{4} \left(\frac{3}{\pi}\right)^{1/3} \rho^{4/3}. \quad (5.18)$$

However, the correlation component $\varepsilon_c^h(\rho)$ on the other hand is not known exactly. In fact the determination of the correlation energy in a homogeneous interacting electron system is already a complicated many-body problem. Early approximate expressions for $\varepsilon_c^h(\rho)$ were provided by perturbation theory [56, 57] and later became outdated by highly precise Quantum Monte-Carlo (QMC) calculations for the Fermi liquid [58]. Modern expressions for $\varepsilon_c^h(\rho)$ [59–61] are the parameterizations of these calculations. The approximation (5.17) has proved to be amazingly successful, even when applied to the systems that are quite different from the electron gas.

Extending the LDA to spin-polarized systems the additional degree of freedom is introduced by splitting the local density into spin-up and spin-down channels [15, 56] resulting into the local spin-density approximation (LSDA):

$$E_{xc}^{\text{LSDA}}[\rho_\uparrow, \rho_\downarrow] = \int d^3r \rho(\mathbf{r}) \varepsilon_{xc}^h(\rho_\uparrow(\mathbf{r}), \rho_\downarrow(\mathbf{r})), \quad (5.19)$$

where $\varepsilon_{xc}^h(\rho_{\uparrow}(\mathbf{r}), \rho_{\downarrow}(\mathbf{r}))$ is the exchange-correlation energy density for the homogeneous electron gas where the densities for up and down spins $\rho_{\uparrow}(\mathbf{r})$ and $\rho_{\downarrow}(\mathbf{r})$ are introduced.

The LSDA approach is *ab-initio* since it does not contain any additional input parameters. On other hand, the analysis of the accuracy of a particular form used for the exchange-correlation potential could be validated mostly by the agreement between calculated and experimental data.

The applicability of LSDA is mostly restricted to macroscopic systems where the local effects which occur on the scale of N^{-1} and N^{-3} (with N being the number of particles) are rather small. On the other hand, single atoms and cluster systems do not allow to neglect these effects. A well known example is the hydrogen atom where the LSDA orbital energy is -0.54 Ry instead of -1 Ry, while the total energy calculated within LSDA is rather good: -0.976 Ry instead of -1 Ry [62]. The incorrect asymptotic behavior of the LSDA potential on far distances results in the overestimation of the total energy and the reduction of the binding energy and strong overestimation of the removal energy as well. This leads to the failure of the LSDA to describe the existence of negative ions [60], that are found to be stable experimentally.

To overcome these difficulties a lot of techniques were devised, such as semi-local functionals which include the gradient corrections of local density (GGA) [63, 64], orbital functionals which utilize the exact expression for the exchange energy (OPM) [65–69], the self-interaction correction method (SIC) [60, 70–73] which is intended to compensate the incomplete vanishing of self-interaction in LSDA, non-local functionals (in the sense that the functional depends on the integral of $\rho(\mathbf{r})$ rather than on its derivative as in GGA) (ADA, WDA) [74] and various hybrid approaches. The general limitation of the mentioned approaches is due to their formulation in terms of a charge or orbital density as a fundamental variable which does not reproduce the true many-body effects and thus, the spectra of strongly correlated systems. The latter demonstrate both correlated quasiparticle bands and Hubbard bands which have no analog in one-particle theory. That is why the insufficient description of correlations cannot be remedied by either

using more complicated exchange-correlation functionals in DFT or by adding a finite number of diagrams of perturbation theory. To achieve this one should go beyond DFT in order to incorporate the dynamics of the electrons in the variational functional explicitly. This is possible by choosing another variable, e.g. the localized time-dependent Green's function.

However, before to proceed with the description in terms of dynamical variables we will consider the intermediate step which have become an important precursor of the localized dynamical description. Namely, it is a localized non-local, however, static correction of the of the local one-particle Hamiltonian introduced to circumvent the difficulties experienced by the LDA in the description of strongly-correlated solids.

5.3 The LDA+ U method

The important difference of LDA from the exact Kohn-Sham density functional is that in the latter the local potential has to demonstrate a discontinuous jump when adding or subtracting the electron. This leads, e. g. to the well-known failure of LDA to describe the band gap in Mott insulators [75].

The second important aspect is that while the LDA orbital energies $\epsilon_i = \partial E_{\text{tot}}/\partial n_i$ are often obtained different from the experimental one-particle excitation spectrum, the total energy ϵ_{tot} is calculated rather accurately. However, as it was shown by Brandow [76], the non-magnetic LDA calculations combined with on-site Hartree-Fock interactions for the $3d$ -electrons leads to a rather realistic description of the various Mott-Hubbard phenomena.

These and analogous observations have led to the formulation of the so-called LDA+ U method [18, 77] which supplements the LDA potential with an orbital-dependent correction by taking approximately into account the strong localized interactions in d - or f -electron shells. The main idea of LDA+ U method is that it separates from the whole electron system the localized d -electron subsystem for which the strong Coulomb repulsion U is taken into account in the form of a model Hubbard term $\frac{1}{2} \sum_{i \neq j} n_i n_j$. The rest consisting of the delocalized conduction electrons is described by the orbital-independent one-particle

LDA potential.

The one-particle excitation spectrum of such a system is a set of many-particle states distinguished by the absence or addition of a particular d -electron. If we treat the localized electrons as having the same kinetic energy ϵ_d and experiencing the same Coulomb repulsion U the total energy of the localized subsystem with N electrons can be represented as $E_N = \epsilon_d n + UN(N-1)/2$ and the corresponding one-particle excitation spectrum as $\epsilon = E_{N+1} - E_N = \epsilon_d + UN$. The Coulomb energy of all d - d -interactions in a N -electron system is $UN(N-1)/2$. Replacing it by the Hubbard term (neglecting for a while the exchange and non-sphericity) we obtain the following functional:

$$E_{\text{tot}} = E_{\text{tot}}^{\text{LDA}} - \frac{1}{2} UN(N-1) + \frac{1}{2} U \sum_{i \neq j} n_i n_j, \quad (5.20)$$

and the corresponding orbital energies:

$$\epsilon_i = \frac{\partial E_{\text{tot}}}{\partial n_i} = \epsilon^{\text{LDA}} + U \left(\frac{1}{2} - n_i \right). \quad (5.21)$$

The last term shifts the occupied LDA orbitals ($n_i = 1$) down $-U/2$ and unoccupied ($n_i = 0$) up $+U/2$ giving the additional contribution in the band gap. Similarly one can obtain the orbital-dependent correction to the one-particle potential as a variation over the particular orbital instead of the total charge density:

$$V_i(\mathbf{r}) = V^{\text{LDA}}(\mathbf{r}) + U \left(\frac{1}{2} - n_i \right). \quad (5.22)$$

This form restores the discontinuous behavior of the one-electron potential of the exact Kohn-Sham density functional.

5.3.1 The Coulomb interaction matrix

One can treat the orbital-dependent correction more accurately by taking into account the exchange and non-sphericity of the Coulomb interaction by constructing the total energy as a functional of the full local density and the d -occupation matrix [19]:

$$E_{\text{tot}}[\rho(\mathbf{r}), n_d] = E_{\text{tot}}^{\text{LSDA}}[\rho(\mathbf{r})] + E^U[n_d] - E^{\text{DC}}[n_d], \quad (5.23)$$

where E^U is the Coulomb interaction energy of the d -shell and E^{DC} is the so-called double-counting energy which should cancel the part of the Coulomb d - d -interaction included in $E_{\text{tot}}^{\text{LSDA}}$. In general the occupation matrix n_d can contain spin-flip terms due to some source of perturbation with lower symmetry as e.g. spin-orbit coupling or non-collinear magnetic ordering. Thus, the second term in Eq. (5.23) can be written as

$$E^U = \frac{1}{2} \sum_{1234} (V_{1324} - V_{1342}) n_{12} n_{34}, \quad (5.24)$$

where the indices $i, (i = 1, 2, \dots)$ mark the localized spin-orbital basis function $\phi_{l\sigma_i}(r)Y_{lm_i}$. The matrix of the on-site rotationally-invariant Coulomb interaction V_{1234} is given in the following form [78]:

$$V_{1234} = \delta_{\sigma_1\sigma_3}\delta_{\sigma_2\sigma_4} U_{m_1m_2m_3m_4} = \delta_{\sigma_1\sigma_3}\delta_{\sigma_2\sigma_4} \sum_{k=0}^{2l} a_{m_1m_3m_2m_4}^k F^k, \quad (5.25)$$

with the radial Slater F^k and the angular a^k integrals defined with respect to the localized orbital functions $\phi_l(r)Y_{lm}(\hat{r})$ as following:

$$F^k = \int r^2 dr \int r'^2 dr' \phi^2(r)\phi^2(r') \frac{r_{<}^k}{r_{>}^{k+1}},$$

$$a_{m_1m_3m_2m_4}^k = \frac{4\pi}{2k+1} \sum_{k'=-k}^k \langle Y_{lm_1} | Y_{kk'} | Y_{lm_3} \rangle \langle Y_{lm_2} | Y_{kk'}^* | Y_{lm_4} \rangle. \quad (5.26)$$

The matrix elements V_{1212} and $V_{1212} - V_{1221}$ are related to the products of the diagonal elements of the occupation matrix and thus can be identified as pairs of direct and exchange interaction integrals. By averaging these matrices over all possible pairs of indices $\{(1, 2)\}$ within the certain spin subsystem defines the averaged Coulomb direct U and exchange J integrals used in the expression for E^{DC} . Namely, using the properties of the integrals F and a , one can obtain the following

relations

$$\begin{aligned}
U &= \frac{1}{(2l+1)^2} \sum_{mm'} U_{m_1 m_2 m_1 m_2} \\
&= F^0, \\
U - J &= \frac{1}{2l(2l+1)} \sum_{m \neq m'} (U_{m_1 m_2 m_1 m_2} - U_{m_1 m_1 m_2 m_2}) \\
&= F^0 - \frac{1}{2l} \sum_{k=2}^{2l} (C_{lkl}^{000})^2 F^k, \tag{5.27}
\end{aligned}$$

where C_{lkl}^{000} is a Clebsch-Gordon coefficient. Using these expressions for the particular cases of d - and f -electrons the exchange integrals can be written explicitly as

$$\begin{aligned}
J_{l=2} &= \frac{1}{14}(F^2 + F^4), \\
J_{l=3} &= \frac{1}{6435}(286F^2 + 195F^4 + 250F^6), \tag{5.28}
\end{aligned}$$

The meaning of U can be identified as the change in the energy of the many-body electron system when moving one d -electron between two equivalent atoms. This process is accompanied by the inverse movement of the fast p - and s -electrons which is called screening. This screening substantially lowers the energy cost needed for the replacement of the d -electron. Thus the value of U used in the LSDA+U calculations should be significantly smaller than the bare U considered in the Hubbard model.

While the intrasite exchange parameter J could be calculated rather unambiguously in *ab-initio* approaches, the estimation of the intrasite Coulomb interaction parameter U substantially scatters. The unscreened values of U are typically very large, about 15-20 eV. The electron screening substantially decreases them normally to about 3-8 eV. In real solid the screening charge is distributed over the neighboring sites which makes the estimation of U very complicated. While constrained LSDA studies give rather satisfactory agreement with experiment for Ce, U and late transition-metal oxides, in $3d$ -transition metals the values of U are largely overestimated [79, 80]. For example, in Fe the estimate leads to $U=6$ eV, while experiments indicate a value

1-2 eV. For early transition-metal oxides, e.g. VO, the theoretical U is 6 eV which is two times larger than the experimental value. Accordingly, the established procedure is to use the Coulomb and the Stoner effective interaction in the calculational scheme as input parameters which is, of course, a serious drawback from the *ab-initio* viewpoint. However, it has been found that in many cases LSDA+ U method gives a very successful description which is not too much sensitive to the small variations of the U parameter near its optimal value.

5.3.2 The double-counting term

The most serious conceptual problem of the LSDA+ U approach is the following. Since there does not exist any microscopic or diagrammatic representation of the LSDA effective one-particle potential, it is not possible to express its Coulomb interaction part rigorously in terms of U and J . Thus, in general the form of the double-counting (DC) term in Eq. (5.23) remains unknown. That is why the application of LSDA+ U is mostly restricted to systems close to particular limiting cases where the DC can be found exactly. Namely, these are the so-called atomic limit (AL) which corresponds to the case when the particular orbital is either fully occupied or fully empty and the mean-field limit (MF) which corresponds to the uniform orbital occupation [19].

In the MF-case the Coulomb interaction energy in Eq. (5.24) can be represented using Eq. (4.3) as a mean-field average over the orbitals:

$$\begin{aligned}
 E^{\text{DC}} &= \frac{1}{2} \sum_{1234} (V_{1324} - V_{1342}) \langle n_{12} n_{34} \rangle \\
 &\approx \frac{1}{2} \sum_{12} (V_{1212} - V_{1221}) \\
 &\times (n_{11} \langle n \rangle_{\sigma_2} + n_{22} \langle n \rangle_{\sigma_1} - \langle n \rangle_{\sigma_1} \langle n \rangle_{\sigma_2}), \quad (5.29)
 \end{aligned}$$

with $\langle n \rangle_{\sigma}$ being the average occupation number within a certain σ spin subsystem:

$$\langle n \rangle_{\sigma} = \frac{1}{2l+1} \sum_{m=-l}^l n_{mm}^{\sigma\sigma}. \quad (5.30)$$

The corresponding double-counting part of the one-particle potential is found as

$$\begin{aligned}
V_{12}^{\text{DC(MF)}} &= \frac{\partial \epsilon^{\text{DC}}}{\partial n_{12}} = \delta_{12} \sum_3 [V_{1313} - V_{1331}] \langle n \rangle_{\sigma_3} \\
&= \delta_{12} \sum_{m'} [U_{mm'mm'} \langle n \rangle_{-\sigma_1} + (U_{mm'mm'} - U_{mm'm'm}) \langle n \rangle_{\sigma_1}] \\
&= \delta_{12} [U(2l+1) \langle n \rangle_{-\sigma_1} + U(2l+1) \langle n \rangle_{\sigma_1} - (U+2lJ) \langle n \rangle_{\sigma_1}] \\
&= \delta_{12} [U(2l+1)(\langle n \rangle_{-\sigma_1} + \langle n \rangle_{\sigma_1}) - (U+2lJ) \langle n \rangle_{\sigma_1}] \\
&= \delta_{12} [U(N - \langle n \rangle_{\sigma_1}) - J(N_{\sigma_1} - \langle n \rangle_{\sigma_1})], \tag{5.31}
\end{aligned}$$

with $N_\sigma = (2l+1)\langle n \rangle_\sigma$ and $N = N_\sigma + N_{-\sigma}$. Subtracting V^{DC} from the corresponding potential for the total Coulomb interaction energy (5.24) we obtain the full LSDA+U one-particle effective potential:

$$\begin{aligned}
V_{12}^{\text{LSDA+U-MF}}(\mathbf{r}) &= \\
&\delta_{12} \left(V_{\sigma_1}^{\text{LSDA}}(\mathbf{r}) - V_{11}^{\text{DC(MF)}} \right) \\
&+ \sum_{34} (V_{1324} - V_{1342}) n_{34}. \tag{5.32}
\end{aligned}$$

Using the similar technique and implying $\langle n \rangle_\sigma = 1/2$, one finds the corresponding expression for the DC around the atomic limit [19]:

$$V_{12}^{\text{DC(AL)}} = \delta_{12} \left[U(N - \frac{1}{2}) - J(N_{\sigma_1} - \frac{1}{2}) \right]. \tag{5.33}$$

As one can see from Eqs. (5.24) and (5.25), the term $F^0 = U$ contained in the matrix elements $U_{m_1 m_2 m_3 m_4}$ provides the splitting of the localized states into the lower and upper Hubbard bands. The higher-order terms $F^k, k > 0$ are responsible for the angular corrections within the localized shell. When the screening is substantial and the effective term $U - J$ becomes small, the localized subsystem will be close to the MF-limit and the higher-order terms will gain the dominance. Comparing these contribution to the orbital polarization corrections to the LSDA method suggested by Brooks and coworkers [81–83] one notices that the LSDA+U includes these corrections in a more general form, namely without treating the occupation matrix as being spin-diagonal. Thus, for example the LSDA+U-MF should give similar to

the OP method improvement concerning the description of the orbital moments in $3d$ -transition metals in comparison to the LSDA.

On the other hand, for the strongly-correlated systems as Mott insulators where the strong Coulomb repulsion leads to a large band gap, the AL-limit is more appropriate. It turns out that also for many other materials where the electrons are localized by the strong Coulomb repulsion (as rare earths, impurity systems and high- T_C superconductors) LSDA+U is a rather accurate and reliable tool to calculate their electronic structure.

However, as one can see, LSDA+U only is able to emphasize a certain type of the inhomogeneities which are already induced within the LSDA but cannot induce them itself. For example, for the case when LSDA provides the same occupation for all orbitals, the LSDA+U correction will vanish. The same is true for the half-filled paramagnetic band in the Mott insulators: the LSDA+U would never give the increase of the band gap if it was not originally induced by LSDA. This is the reason why the LSDA+U fails to describe metals in the vicinity of a Mott-Hubbard insulator transition and predicts magnetic order where it is not observed [84, 85]. This happens due to the absence of the quasiparticle description which even in the limit of large Coulomb repulsion but with a non-integer occupation number leads to the metallic character realized by quasiparticles with larger effective mass. In this sense, LSDA+U can be seen as only the static Hartree-Fock approximation to the general spectral density functional theory [49] which takes into account the dynamics of correlations.

5.4 Spectral density functional theory

The practically manageable way to account for the localized dynamical correlations is the so-called dynamical mean-field theory (DMFT) [86, 87] which will be the subject of the next chapter. On the other hand, it can be viewed as a particular mean-field approximation to the more general spectral density functional theory (SDFT) recently developed by *Savrasov* and *Kotliar* [49]. Instead of the local density, the central quantity in SDFT is the one-particle Green's function of the many-body system perturbed by a certain non-local time-dependent localized

source. The latter means that this perturbation totally vanishes outside the localized area Ω_{loc} , for example:

$$\theta_{\text{loc}}(\mathbf{r}, \mathbf{r}') = \begin{cases} 1, & \text{if } \mathbf{r} - \mathbf{r}' \in \Omega_{\text{loc}} \\ 0, & \text{else} \end{cases}. \quad (5.34)$$

Thus, the function becomes local when the localization area shrinks to an infinitesimally small space domain. Although the main subject is to obtain a method accounting for the real-space localized dynamical correlations, it is worth to mention that the SDF in the same way can be formulated by considering the corresponding localized domain in reciprocal space [49].

We introduce the localized Green's function $G_{\text{loc}}(\mathbf{r}, \mathbf{r}', \epsilon)$ which coincides with the exact Green's function $G(\mathbf{r}, \mathbf{r}', \epsilon)$ inside the localization area and is zero outside:

$$G_{\text{loc}}(\mathbf{r}, \mathbf{r}', \epsilon) = G(\mathbf{r}, \mathbf{r}', \epsilon)\theta_{\text{loc}}(\mathbf{r}, \mathbf{r}'). \quad (5.35)$$

The introduction of a localized perturbation J_{loc} modifies the action of the system as follows

$$S' [J_{\text{loc}}] = S + \int d^3r dt \int d^3r' dt' J_{\text{loc}}(\mathbf{r}, t; \mathbf{r}', t') \psi^\dagger(\mathbf{r}, t) \psi(\mathbf{r}', t'), \quad (5.36)$$

where the space integration is restricted to the localization area. The field operators $\psi(\mathbf{r}, t)$ are defined as shown in Eq. (2.5). The partition function Z and the free energy F become functionals of J_{loc} :

$$Z [J_{\text{loc}}] = \exp \{-F [J_{\text{loc}}]\} = \int D [\psi^\dagger \psi] e^{-S' [J_{\text{loc}}]}. \quad (5.37)$$

The total energy as a functional of the localized Green's function (namely, the SDF) is found as the Legendre transformation of the free energy by exchanging the variable J_{loc} to G_{loc} :

$$\Gamma_{\text{SDF}} [G_{\text{loc}}] = F [J_{\text{loc}}] - \text{Tr} \{J_{\text{loc}} G_{\text{loc}}\}. \quad (5.38)$$

The invertibility of the Legendre transformation implies that the variables J_{loc} and G_{loc} are related as:

$$J_{\text{loc}} = -\frac{\delta \Gamma_{\text{SDF}}}{\delta G_{\text{loc}}}, \quad G_{\text{loc}} = \frac{\delta F}{\delta J_{\text{loc}}}. \quad (5.39)$$

Thus, representing J_{loc} in terms of G_{loc} we obtain Γ_{SDF} as a functional of G_{loc} only. Obviously, there is a close analogy to the DFT where the corresponding functional Γ_{DFT} depends on the local density which is obtained from the corresponding G_{loc} by shrinking its localization area and neglecting the time-dependence.

The existence of these functionals for the equilibrium system was studied within perturbation theory [88]. It is stated in particular [49] that the proof of the analog of the Hohenberg-Kohn theorem reduces to the proof of the invertibility of the corresponding functional and the free energy. This is, on the other hand, equivalent to the possibility to perform the Legendre transformation from $F[J_{\text{loc}}]$ to $\Gamma[G_{\text{loc}}]$.

In the next step the total energy is decomposed into the kinetic energy of the non-interacting system, external potential energy, Hartree energy and exchange-correlation energy which is done performing the expansion of Γ_{SDF} in powers of the electron charge [88, 89]. The lowest-order term is the sum of the kinetic energy and the energy of the external potential. In the Baym-Kadanoff approach this term is represented as

$$K[G] = \text{Tr} \{ \ln G \} - \text{Tr} \{ (G_0^{-1} - G^{-1}) G \} , \quad (5.40)$$

where G_0 is the non-interacting Green's function:

$$G_0(\mathbf{r}, \mathbf{r}', \epsilon) = \delta(\mathbf{r} - \mathbf{r}') [\epsilon + \nabla_{\mathbf{r}}^2 - V_{\text{ext}}(\mathbf{r})]^{-1} . \quad (5.41)$$

Analogously to the DFT, the SDFT introduces a set of auxiliary particles in some effective localized non-local and energy-dependent potential $\Sigma_{\text{eff}}(\mathbf{r}, \mathbf{r}', \epsilon)$ and the auxiliary Green's function $\mathcal{G}(\mathbf{r}, \mathbf{r}', \epsilon)$ defined in the whole space as:

$$\mathcal{G}^{-1}(\mathbf{r}, \mathbf{r}', \epsilon) = G_0^{-1}(\mathbf{r}, \mathbf{r}', \epsilon) + \Sigma_{\text{eff}}(\mathbf{r}, \mathbf{r}', \epsilon) . \quad (5.42)$$

The effective potential Σ_{eff} is adjusted in such a way that \mathcal{G} coincides with the exact Green's function G_{loc} inside the localization domain, i.e.

$$G_{\text{loc}}(\mathbf{r}, \mathbf{r}', \epsilon) = \mathcal{G}(\mathbf{r}, \mathbf{r}', \epsilon) \theta_{\text{loc}}(\mathbf{r}, \mathbf{r}') . \quad (5.43)$$

Note, that this also guarantees that \mathcal{G} delivers the exact density. These considerations are schematically illustrated by Fig. 5.1. Thus, one can

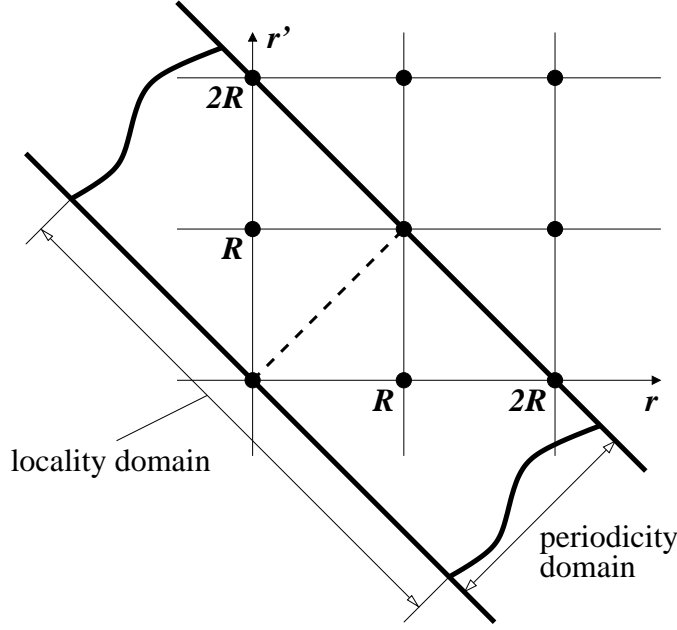


Fig. 5.1. Schematic illustration of the SDFT real-space domains. The auxiliary Green's function \mathcal{G} coincides with the exact Green's function within the locality domain area bounded by thick curves. Within the translational symmetry this picture is \mathbf{R} -periodic. In particular to deliver the exact density it is only necessary to have the information about the Green's function along the dashed line ($\mathbf{r} = \mathbf{r}'$).

represent the kinetic part of the functional in terms of \mathcal{G} :

$$K[\mathcal{G}] = \text{Tr} \{ \ln \mathcal{G} \} - \text{Tr} \{ (G_0^{-1} - \mathcal{G}^{-1}) \mathcal{G} \} \quad (5.44)$$

and the total SDF functional as:

$$\Gamma_{\text{SDF}}[\mathcal{G}] = K[\mathcal{G}] + \Phi^{\text{SDF}}[G_{\text{loc}}] = K[\mathcal{G}] + E_{\text{H}}[\rho] + \Phi_{\text{xc}}^{\text{SDF}}[G_{\text{loc}}], \quad (5.45)$$

with Φ^{SDF} being the energy of interaction with the effective potential Σ_{eff} which is separated as a sum of the Hartree energy E_{H} and the exchange-correlation part $\Phi_{\text{xc}}^{\text{SDF}}$.

The minimum of Γ_{SDF} is achieved by variation with respect to the variable \mathcal{G} : $\frac{\delta \Gamma_{\text{SDF}}[\mathcal{G}]}{\delta \mathcal{G}(\mathbf{r}, \mathbf{r}', \epsilon)} = 0$, which leads to Eq. (5.42) as well as for the definition of the effective potential Σ_{eff} :

$$\Sigma_{\text{eff}}(\mathbf{r}, \mathbf{r}', \epsilon) = \frac{\delta \Phi^{\text{SDF}}[G_{\text{loc}}]}{\delta \mathcal{G}(\mathbf{r}, \mathbf{r}', \epsilon)} = \frac{\delta \Phi^{\text{SDF}}[G_{\text{loc}}]}{\delta G_{\text{loc}}(\mathbf{r}, \mathbf{r}', \epsilon)} \theta_{\text{loc}}(\mathbf{r}, \mathbf{r}'). \quad (5.46)$$

Using the definition of G_0 in Eq. (5.41) together with Eq. (5.42) we can construct the pendant of the Kohn-Sham equation:

$$[\epsilon + \nabla^2] \mathcal{G}(\mathbf{r}, \mathbf{r}', \epsilon) + \int d^3 r'' \Sigma_{\text{eff}}(\mathbf{r}, \mathbf{r}'') \mathcal{G}(\mathbf{r}'', \mathbf{r}', \epsilon) = \delta(\mathbf{r} - \mathbf{r}'). \quad (5.47)$$

If the electron exchange-correlation interaction is not restricted by the localization domain, then the SDF turns into the Baym-Kadanoff functional which delivers the full one-particle Green's function of the system. Otherwise it can be viewed as a localized approximation to the Baym-Kadanoff theory which delivers the exact ground-state properties as far as the form of $\Phi_{\text{xc}}^{\text{SDF}}$ is known.

Summarizing, we emphasize that SDF provides the existence of the one-particle Green's function functional, that can be minimized within the self-consistent procedure sketched in Fig. 5.2 that is analogous to that one set up for the DFT.

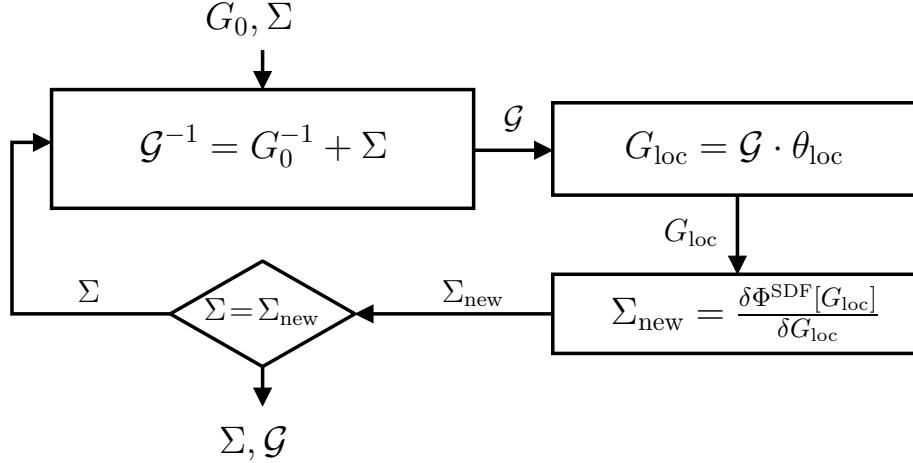


Fig. 5.2. Illustration of the self-consistent solution of the SDF problem. Starting from the non-interacting function G_0 and the initial guess for the localized self-energy Σ we obtain the auxiliary function \mathcal{G} within the whole space as $\mathcal{G}^{-1} = G_0^{-1} + \Sigma$. Then the localized part G_{loc} is extracted by $G_{\text{loc}} = \mathcal{G} \cdot \theta_{\text{loc}}$. The latter is used to derive the self-energy as a functional derivative of Φ^{SDF} . The loop is repeated until the self-consistent self-energy is found. All quantities are evaluated for fixed time (or energy) and space arguments.

5.5 The dynamical-mean field approximation

Since the dynamical mean-field theory (DMFT) have appeared earlier than the SDFT itself, it could be represented as a separate approach without reviewing the SDFT basics. However, one can trace better the analogy with the DFT-LDA if it is presented as a sort of mean-field approximation to SDFT. DMFT is based on the work of *Metzner* and *Vollhardt* [50] who derived the non-trivial limit of the Hubbard model for the large coordination number and the work of *Georges et. al* [21] who made the connection between the localized and the delocalized descriptions. Detailed overviews of DMFT can be found in Refs. [86] and [87].

First of all, similar to the LDA+U, the DMFT considers the two-particle interactions within a certain electronic subsystem, namely in the d -, or f -shell which is well-localized within the atomic site. Thus, the localization domain is site-centered instead of travelling throughout the solid as illustrated in Fig. 5.3. This leads to a certain drawback,

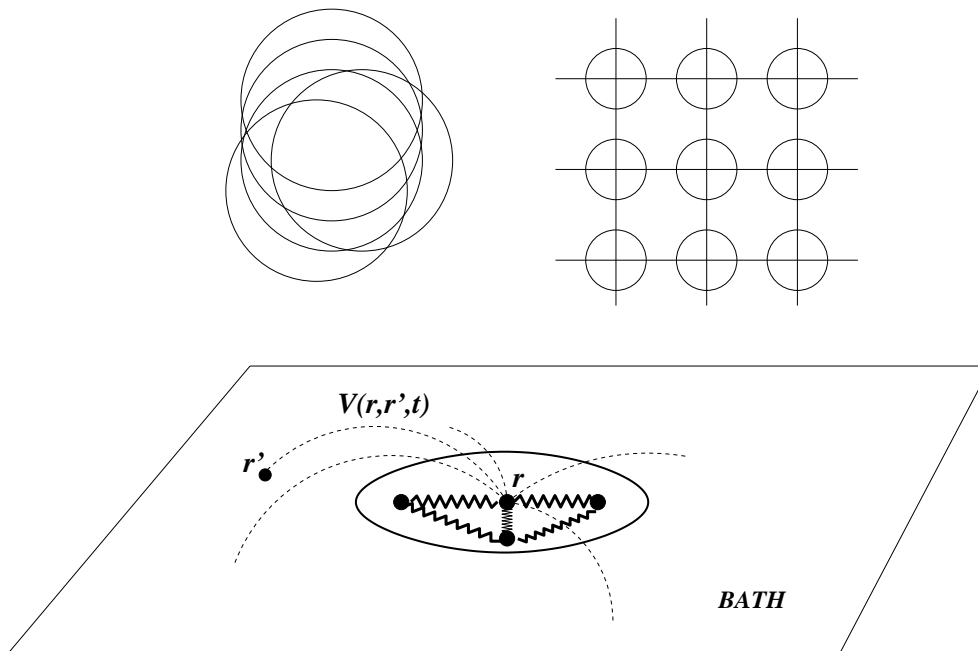


Fig. 5.3. Localization domains in SDFT (upper left side) and in the DMFT (upper right side). Lower panel: illustration of the Anderson model. Localized d -electrons coupled by the non-local time-dependent interaction $V(r, r', t)$ with the surrounding bath. The interaction within a d -shell is marked by zigzag lines.

namely, it is not possible any more to reproduce the exact density of states from G_{loc} and as a result to recover the Hartree energy directly.

On the other hand, this situation is rather close to the real systems containing $3d$ - and $5f$ -elements in which the correlated electrons are well-localized within the atomic sites. Thus, it is natural to consider the non-local correlation only for the d - or f -electron subsystem within its localization domain.

However, in real solids the situation is complicated by the additional coupling of the d -electrons with the s and p delocalized shell. In the DMFT this problem is avoided by the mean-field description of the coupling. Namely, the d -electrons feel the time-dependent non-local interaction with the delocalized shell as a sort of time-dependent but local mean-field, which is created by the spatial integration over the delocalized shell. In the literature the latter is usually referred as “bath”. To perform such an integration we have to know the many-body wave function of the bath. On the other hand, by presenting the coupling as an interaction of the randomly situated bath particles coupled to the certain space point \mathbf{r} (see Fig. 5.3), the integral influence, namely the random variable $V_{\text{bath}}(\mathbf{r}, t) = \sum_{\mathbf{r}'} V(\mathbf{r}, \mathbf{r}', t)$ will have normal (\mathbf{r}, t) -parameterized distribution that does not depend on the particular distribution of $V(\mathbf{r}, \mathbf{r}', t)$ once the number of particles in the bath increases to infinity (Central Limit theorem). As was numerically shown by *Metzner* and *Vollhardt* this sum converges very fast. For example, in the model which is equivalent to 6 bath particles it is already close to the infinite limit [86].

Having incorporated all external influence with respect to the localized electron subsystem into the local scalar potential V_{bath} , the conditions of the Baym-Kadanoff approach are satisfied and the many-body problem of the localized shell can be solved exactly using the perturbational technique discussed in Chapter 3. Since the DMFT model is equivalent to the famous *Anderson* effective impurity model (AIM) [3, 24, 90] the corresponding many-body technique solving the Baym-Kadanoff equations is referred as “impurity solver”.

Of course, the function $V_{\text{bath}}(\mathbf{r})$ is unknown. On the other hand, if the self-energy and the corresponding Green’s function of the interacting d -system are known, it is possible to find the effective one-particle Green’s function of the bath \mathcal{G}_0 from the following saddle-point equa-

tion:

$$\mathcal{G}_0^{-1}(\mathbf{r}, \mathbf{r}', \epsilon) = G_{\text{loc}}^{-1}(\mathbf{r}, \mathbf{r}', \epsilon) - \Sigma(\mathbf{r}, \mathbf{r}', \epsilon). \quad (5.48)$$

Then, it can be used as an input quantity for the Baym-Kadanoff problem of the interacting d -electrons which can be approximately solved by one of the impurity solvers which delivers the corresponding self-energy. Thus we have a closed relationship between all introduced quantities and the overall problem can be solved self-consistently as shown in Fig. 5.4. The particular feature of the DMFT is that the whole inter-

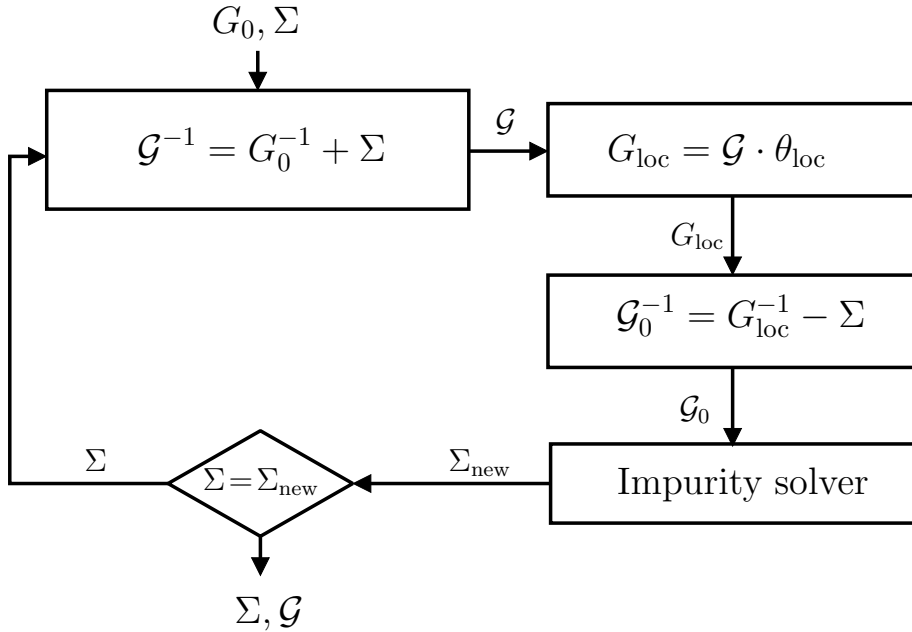


Fig. 5.4. Illustration of the self-consistent solution of the DMFT problem. Starting from the non-interacting function G_0 and the initial guess for the localized self-energy Σ we obtain the auxiliary function \mathcal{G} within the whole space as $\mathcal{G}^{-1} = G_0^{-1} + \Sigma$. Then the localized part G_{loc} is extracted by $G_{\text{loc}} = \mathcal{G}\theta_{\text{loc}}$. In the next step the Green's function \mathcal{G}_0 accounting for the interaction only between the conduction and localized systems is created; for that reason the many-body interaction Σ is extracted from G_{loc} . \mathcal{G}_0 is used as an input for the many-body problem within the localized shell. The latter is solved by applying a certain many-body technique (impurity solver) which derives the self-energy Σ_{new} . The loop is repeated until the self-consistent self-energy is found. All quantities are evaluated for fixed time (or energy) and space arguments.

acting system is split into one being treated exactly and another one treated within the mean-field approximation.

Like any mean-field theory, DMFT becomes exact in the limit of large coordination number or infinite dimensionality [50]. On the other hand, there are two particular limits, specific for SDF, where it becomes exact – the non-interacting limit ($U = 0$) and the atomic limit ($t = 0$) [21, 86]. The main constraints of the theory are inherited from the LDA+U approach, namely it is the arbitrariness in the estimation of U and the choice of the correlated orbitals.

5.6 LDA+DMFT

Since the DMFT method is not an *ab-initio* approach, it can be implemented by choosing as a reference the Kohn-Sham ground state provided by the LSDA approach. Since DMFT treats the systems on the level of model Hamiltonians and LSDA reliably describes the weakly-interacting systems, the LSDA+DMFT can provide a reasonable approximation to the exact functional. As pointed out by Savrasov [49], one can think about the LSDA as the most primitive impurity solver, which derives an extremely local self-energy with its localization radius collapsed to a single \mathbf{r} point. This allows to consider the interaction contribution Φ^{SDF} as a functional of the localized Green's function G_{loc} and the local density ρ :

$$\Phi [G_{\text{loc}}, \rho] = E_{\text{H}} [\rho] + E_{\text{xc}}^{\text{LSDA}} [\rho] + \tilde{\Phi} [G_{\text{loc}}] - \Phi^{\text{DC}} [G_{\text{loc}}], \quad (5.49)$$

where the functional $\tilde{\Phi} [G_{\text{loc}}]$ accounts for the strongly correlated localized electrons which cannot be adequately described by LSDA, while the solution of the impurity model for the itinerant electrons is well approximated by LSDA and does not need an energy resolution for their self-energies. The unseparated contributions from the localized and itinerant electrons are accounted via the corresponding double-counting term $\Phi^{\text{DC}} [G_{\text{loc}}]$. The discussion of the DC terms in principle can be extended from the LSDA+U approach. During the last few years different formulations for the double-counting for particular systems were proposed [91–95], however none of them can be considered as a rigorous method to treat the double-counting in the general case. Thus it still remains one of the shortcoming aspects of LSDA+DMFT method.

A further approximation simplifying the calculations can be made by considering the SDF as dependent only on the correlated sub-block of

the G_{loc} matrix. Indeed, within the localized orbital basis the subspace of the correlated orbitals can be well-identified. Thus all saddle-point equations (Fig. 5.4) will involve the size-reduced matrices. As an input the Green's function G_0 for the DMFT scheme the LSDA Green's function G^{LSDA} is used.

When the DMFT self-consistency is achieved one can use the converged auxiliary function \mathcal{G} to calculate the new density of states which will in turn modify the Hartree $E_{\text{H}}[\rho]$ and the exchange-correlation $E_{\text{xc}}^{\text{LSDA}}[\rho]$ energies. This leads to the doubled iterative procedure which delivers the minimum of the SDF as a functional of two variables.

Implemented in the form of the LSDA+DMFT scheme, DMFT studies have already solved many long-standing problems in the description of correlated systems. Among these results one can mention the work of *Savrasov* and *Kotliar* [84] who gave an explanation for the mechanism of the α - δ phase transition and the so-called “three-peak” structure in the photoemission spectrum of Pu. The properties of Mott insulators were studied by *Nekrasov et al.* [23] and *Laad et al.* [96]. The problem of magnetic properties and the DOS spectrum of transition metals was investigated by *Lichtenstein* and *Katsnelson* [93, 97]. The improved description of the pure Fano-effect in the valence band photoemission of ferromagnets was done by *Minár et al.* [98]. The description of angular-resolved photoemission of Ni was done by *Braun et al.* [95]. The description of optical and magneto-optical properties in transition metals was given by *Perlov et al.* [99, 100] and *Chadov et al.* [101].

As it was mentioned above, by taking into account that the notion of locality is not restricted to the single-site and could be extended to a cluster or supercell, DMFT could be applied within cluster methods which leads to the account of some \mathbf{k} -dependence of the self-energy, which is important for the proper description of any type of the non-local correlations. Since the cluster models interpolate between the single-site and the full lattice description with increasing cluster size, they assume $1/d$ corrections to the DMFT in a non-perturbative way. Depending on the form in which the “local” Green's function is derived in the particular cluster approach combined with the particular implementation of the DMFT solver it leads to different generalized cluster techniques as dynamical cluster approximation (DCA) [102, 103] and

cellular DMFT (CDMFT) [104]. A detailed overview of various cluster and cellular schemes combined with DMFT can be found in Ref. [105]. One of the complicated aspects in this methods is the proper construction of the additional inter-site components to the Coulomb interaction matrix which could be neglected for small clusters but with increasing size become essential and the effective impurity problem becomes rather complex. Thus, currently the computational most demanding methods available for the DMFT are restricted to small clusters. In this respect a particular interest gain the approach suggested by Sadovskii *et al.* [106] in which the analytical expression for the k -dependent self-energy which accounts for the dynamical non-local short-range collective spin-density wave-like antiferromagnetic spin fluctuations is derived.

Chapter 6

Numerical implementation

6.1 DMFT within the KKR method

6.1.1 Solution of the Kohn-Sham equations

For a long time the DMFT scheme was implemented using one of different band structure methods based on the LMTO formalism [107, 45, 46, 84, 49]. This gave the opportunity to calculate the electronic structure for a variety of systems with different degrees of electronic correlations. In particular, the importance of charge self-consistency first mentioned in Refs. [84] and [49] has given an important insight into the long-standing problem of the phase diagram and localization of f -electron systems and has been used to describe the correlations in half-metallic ferromagnetic materials [108]. As an alternative to the band structure methods, more accurate self-consistent methods for solving the Kohn-Sham equations based on the LSDA in terms of the Green's functions have been developed within the multiple scattering theory [109–112].

The first extension of the KKR equations including the on-site localized multi-orbital dynamical self-energy was proposed in [113]. In the framework of multiple scattering theory the solution of Eq. (5.4) is constructed in two steps. For a first step one solves the single-site scattering problem, to obtain the regular and irregular solutions of the corresponding Schrödinger equation and the scattering amplitude given in terms of the single-site t -matrix.

In terms of the four-component relativistic wave functions $\Phi(\mathbf{r}, \epsilon)$ the corresponding single-particle Kohn-Sham-Dirac equation [114, 115]

with the additional energy-dependent non-local potential Σ reads:

$$\begin{aligned} & \left[\frac{c}{i} \vec{\alpha} \cdot \vec{\nabla} + \frac{c^2}{2} (1 - \beta) + V(\mathbf{r}) - \epsilon \right] \Phi(\mathbf{r}, \epsilon) \\ & = \int d^3 r' \Sigma(\mathbf{r}, \mathbf{r}', \epsilon) \Phi(\mathbf{r}', \epsilon), \end{aligned} \quad (6.1)$$

with α_i ($i = 1, 2, 3$) and β the conventional 4×4 Dirac matrices and σ_i ($i = 1, 2, 3$) being the Pauli spin matrices in their relativistic form. The potential $V(\mathbf{r})$ is conveniently decomposed into

$$V(\mathbf{r}) = V_{\text{eff}}(\mathbf{r}) + \beta \vec{\sigma} \cdot \vec{B}(\mathbf{r}), \quad (6.2)$$

with V_{eff} the spin-averaged part of the potential including nuclear, Hartree and spin-averaged exchange-correlation contributions, and $\beta \vec{\sigma} \cdot \vec{B}$ is its spin-dependent part.

Because of the localized nature of the DMFT the non-local self-energy can be represented using an arbitrary set of localized spherically symmetric functions $\phi_\Lambda(\mathbf{r})$:

$$\Sigma(\mathbf{r}, \mathbf{r}', \epsilon) = \sum_{\Lambda\Lambda'} \Sigma_{\Lambda\Lambda'}(\epsilon) \phi_\Lambda^\dagger(\mathbf{r}) \phi_{\Lambda'}(\mathbf{r}'). \quad (6.3)$$

The right-hand part of the Eq. (6.1) can be approximately written as follows [113]:

$$\begin{aligned} \int d^3 r' \Sigma(\mathbf{r}, \mathbf{r}', \epsilon) \Phi(\mathbf{r}', \epsilon) & = \sum_{\Lambda\Lambda'} \Sigma_{\Lambda\Lambda'}(\epsilon) \phi_\Lambda^\dagger(\mathbf{r}) \int d^3 r' \phi_{\Lambda'}(\mathbf{r}') \Phi(\mathbf{r}') \\ & \approx \sum_{\Lambda\Lambda'} \Sigma_{\Lambda\Lambda'}(\epsilon) \Phi(\mathbf{r}). \end{aligned} \quad (6.4)$$

The solution of Eq. (6.1) is represented by the ansatz

$$\Phi(\mathbf{r}, \epsilon) = \sum_{\Lambda} \begin{pmatrix} g_\Lambda(r, \epsilon) \chi_\Lambda(\hat{r}) \\ i f_\Lambda(r, \epsilon) \chi_{-\Lambda}(\hat{r}) \end{pmatrix}, \quad (6.5)$$

where g and f are radial parts of the major and minor components and the spin-angular function χ_Λ is given by

$$\chi_\Lambda(\hat{r}) = \sum_{\sigma} C_{\Lambda}^{\sigma} Y_l^{\mu-\sigma}(\hat{r}) \chi_{\sigma}, \quad (6.6)$$

with $C_{\Lambda}^{\sigma} = C(l, \frac{1}{2}, j; \mu - \sigma, \sigma)$ the Clebsch-Gordon coefficients, $Y_l^{\mu-\sigma}(\hat{r})$ complex spherical harmonics and χ_{σ} the Pauli spinor functions [116]. The spin-orbit and relativistic quantum numbers κ and μ , respectively, have been combined to $\Lambda = (\kappa, \mu)$, with $-\Lambda = (-\kappa, \mu)$. Inserting Φ into Eq. (6.1) leads to a set of coupled radial equations, where the self-energy is taken into account only for the major component:

$$\begin{aligned} \frac{\partial}{\partial r} P_{\Lambda} &= -\frac{\kappa}{r} P_{\Lambda} + \left[\frac{\epsilon}{c^2} + 1 \right] Q_{\Lambda} - \frac{1}{c^2} \sum_{\Lambda'} V_{\Lambda\Lambda'}^{-} Q_{\Lambda'}, \\ \frac{\partial}{\partial r} Q_{\Lambda} &= \frac{\kappa}{r} Q_{\Lambda} - \epsilon P_{\Lambda} + \sum_{\Lambda'} [V_{\Lambda\Lambda'}^{+} + \Sigma_{\Lambda\Lambda'}(\epsilon)] P_{\Lambda'}. \end{aligned} \quad (6.7)$$

The auxiliary functions P and Q are defined as

$$\begin{aligned} P_{\Lambda}(r, \epsilon) &= r g_{\Lambda}(r, \epsilon), \\ Q_{\Lambda}(r, \epsilon) &= c r f_{\Lambda}(r, \epsilon). \end{aligned} \quad (6.8)$$

The potential matrix is defined as

$$V_{\Lambda\Lambda'}^{\pm}(r) = \langle \chi_{\pm\Lambda} | V_{\text{eff}} \pm \vec{\sigma} \vec{B} | \chi_{\pm\Lambda'} \rangle. \quad (6.9)$$

The number of coupled partial waves is restricted to $2(l_{\text{max}} + 1)^2$ by fixing an upper limit l_{max} for the angular momentum expansion of the wave function in Eq. (6.5). For example, for $l_{\text{max}} = 2$ one has up to 18 partial waves coupled; i.e., one has to solve up to 36 coupled equations for the functions P and Q . However, for a cubic system with $\hat{B} = \hat{z}$ and $l_{\text{max}} = 2$ one has at most 3 partial waves coupled due to the high symmetry of the system.

Using the above radial differential equations a set of $2(l_{\text{max}} + 1)^2$ linearly independent regular solutions can be created by initializing the outward integration with a selected spin-angular character dominating close to the nucleus; i.e., one demands that

$$\Phi_{\Lambda}(\mathbf{r}, \epsilon) = \sum_{\Lambda} \Phi_{\Lambda\Lambda'}(\mathbf{r}, \epsilon) \xrightarrow{r \rightarrow 0} \Phi_{\Lambda\Lambda}(\mathbf{r}, \epsilon). \quad (6.10)$$

After having solved the system of coupled equations for the wave functions Φ_{Λ} one gets the corresponding single-site t -matrix by introducing

the auxiliary matrices a and b :

$$\begin{aligned} a_{\Lambda\Lambda'}(\epsilon) &= -ipr^2 [h_{\Lambda}^-(\mathbf{r}, \epsilon), \Phi_{\Lambda\Lambda'}(\mathbf{r}, \epsilon)]|_{r=R}, \\ b_{\Lambda\Lambda'}(\epsilon) &= ipr^2 [h_{\Lambda}^+(\mathbf{r}, \epsilon), \Phi_{\Lambda\Lambda'}(\mathbf{r}, \epsilon)]|_{r=R}, \end{aligned} \quad (6.11)$$

with $p = \sqrt{\epsilon(1 + \epsilon/c^2)}$ the relativistic momentum [116] and [...] denotes the relativistic form of the Wronskian [117], R is the Wigner-Seitz radius. The functions h^{\pm} are the relativistic version of the Hankel functions of the first and second kind [116]:

$$h_{\Lambda}^{\pm}(\mathbf{r}, \epsilon) = \sqrt{\frac{1 + \epsilon/c^2}{c^2}} \begin{pmatrix} h_{\bar{l}}^{\pm}(pr) \chi_{\Lambda}(\hat{r}) \\ \frac{ipc \operatorname{sgn}(\kappa)}{\epsilon + c^2} h_{\bar{l}}^{\pm}(pr) \chi_{\bar{\Lambda}}(\hat{r}) \end{pmatrix}, \quad (6.12)$$

with the angular momentum $\bar{l} = l - \operatorname{sgn}(\kappa)$ for the minor component corresponding to $-\kappa$. Finally, the single-site t -matrix is obtained as

$$t(\epsilon) = \frac{i}{2p} [a(\epsilon) - b(\epsilon)] b^{-1}(\epsilon). \quad (6.13)$$

By a superposition of the wave functions according to the boundary conditions

$$Z_{\Lambda}(\mathbf{r}, \epsilon) = \sum_{\Lambda'} Z_{\Lambda'\Lambda}(\mathbf{r}, \epsilon) \xrightarrow{r \rightarrow R} \sum_{\Lambda'} j_{\Lambda'}(\mathbf{r}, \epsilon) t_{\Lambda'\Lambda}^{-1}(\epsilon) - ip h_{\Lambda}^+(\mathbf{r}, \epsilon), \quad (6.14)$$

one gets an alternative set of linearly independent regular solutions Z to the single-site Dirac equation. These functions are normalized in analogy to non-relativistic multiple-scattering theory according to the convention of *Faulkner* and *Stocks* [111] and allow us straightforwardly to set up the electronic Green's function (see below). The additionally needed irregular solutions J are fixed by the boundary condition

$$J_{\Lambda}(\mathbf{r}, \epsilon) \xrightarrow{r \rightarrow R} j_{\Lambda}(\mathbf{r}, \epsilon), \quad (6.15)$$

and are obtained by inward integration. The functions j_{Λ} are the relativistic version of the spherical Bessel functions defined in analogy to Eq. (6.12).

Having constructed the regular and irregular solutions of the single-site problem together with the t -matrix the corresponding expression

for the Green's function reads [111]:

$$\begin{aligned}
G(\mathbf{r} + \mathbf{R}_n, \mathbf{r}' + \mathbf{R}_m, \epsilon) = & \\
& \sum_{\Lambda\Lambda'} Z_{\Lambda}^n(\mathbf{r}, \epsilon) \tau_{\Lambda\Lambda'}^{nm}(\epsilon) Z_{\Lambda}^{m\times}(\mathbf{r}', \epsilon) \\
& - \delta_{mn} \sum_{\Lambda} [Z_{\Lambda}^n(\mathbf{r}, \epsilon) J_{\Lambda}^{n\times}(\mathbf{r}', \epsilon) \Theta(r' - r) \\
& + J_{\Lambda}^n(\mathbf{r}, \epsilon) Z_{\Lambda}^{n\times}(\mathbf{r}', \epsilon) \Theta(r - r')] . \tag{6.16}
\end{aligned}$$

The vectors \mathbf{r} and \mathbf{r}' are restricted to the n -th and m -th unit cell volumes, which are centered at \mathbf{R}_n and \mathbf{R}_m respectively. The superscript "×" is used to distinguish between right- and left-side solutions to Eq. (6.1). Fortunately, the latter ones are obtained from the same radial differential equations as the conventional right-hand side solutions Z and J ; i.e., from Eqs. (6.7) with the potential matrix elements $V_{\Lambda\Lambda'}$ replaced by $V_{\Lambda'\Lambda}$.

The central quantity in Eq. (6.16) is the scattering path operator τ which for the case of the periodic crystal can be obtained via the Brillouin zone (BZ) integration:

$$\tau^{nm}(\epsilon) = \frac{1}{V_{\text{BZ}}} \int_{\text{BZ}} d^3k [t^{-1}(\epsilon) - G(\mathbf{k}, \epsilon)]^{-1} e^{i\mathbf{k}\mathbf{R}_{nm}}, \tag{6.17}$$

where V_{BZ} is the volume of the first BZ and $\mathbf{R}_{nm} = \mathbf{R}_n - \mathbf{R}_m$ and $G(\mathbf{k}, \epsilon)$ is the Fourier transform of the real space KKR structure constants matrix [118] depending only on the relative positions of the scatterers.

In order to obtain the effective impurity Green's function used in the DMFT scheme, the KKR Green's function (6.16) must be projected onto the impurity site. This is achieved by performing the following

projection step using the basis functions ϕ_Λ :

$$\begin{aligned}
G_{\Lambda\Lambda'}^{mn}(\epsilon) &= \tau_{\Lambda\Lambda'}^{nn}(\epsilon) \sum_{\Lambda_1\Lambda_2} \left[\int d^3r' \phi_\Lambda^\dagger(\mathbf{r}') Z_{\Lambda_1}(\mathbf{r}', \epsilon) \right] \left[\int d^3r' Z_{\Lambda_2}^\times(\mathbf{r}', \epsilon) \phi_{\Lambda'}(\mathbf{r}') \right] \\
&- \sum_{\Lambda_1} \int d^3r' \left[\int_0^{r'} d^3r'' \phi_\Lambda^\dagger(\mathbf{r}'') Z_{\Lambda_1}(\mathbf{r}'', \epsilon) \right] J_{\Lambda_1}^\times(\mathbf{r}', \epsilon) \phi_{\Lambda'}^\times(\mathbf{r}') \\
&- \sum_{\Lambda_1} \int d^3r' \left[\int_{r'}^{r_{\text{WS}}} d^3r'' \phi_\Lambda^\dagger(\mathbf{r}'') J_{\Lambda_1}(\mathbf{r}'', \epsilon) \right] Z_{\Lambda_1}^\times(\mathbf{r}', \epsilon) \phi_{\Lambda'}^\times(\mathbf{r}'). \quad (6.18)
\end{aligned}$$

As discussed in Sec. 5.6, only the selected l -diagonal block is used in the following. For transition metals dealt with mostly here this implies that only the d -block is considered.

As a rather natural choice of the basis functions the set of Z_Λ functions could be taken. However, the numerical tests have shown that the procedure becomes unstable if the basis functions are energy dependent. To stabilize it we have fixed them at the certain reference energy corresponding to the center of mass of the correlated shell, which at each iteration is recalculated.

The scheme of the whole self-consistent LSDA+DMFT approach adapted within the KKR method is presented in Fig. 6.1. The self-consistent algorithm corresponds to the general DMFT scheme outlined in Fig. 5.4. The specific features of the scheme are the following.

The full one-particle Green's function $G_{\text{LSDA+DMFT}}$ is found by solving the Kohn-Sham-Dirac equations (6.1) which explicitly account for the localized self-energy Σ . Thus, the Green's function $G_{\text{LSDA+DMFT}}$ straightforwardly can be identified with the auxiliary Green's function \mathcal{G} that is used to extract the localized contribution G_{loc} by projecting onto the corresponding orbital basis (see Eq. (6.18)). Then the bath Green's function \mathcal{G}_0 (only the d -block of the corresponding matrix) is calculated using the saddle-point equation (5.48). These steps are summarized in Fig. 6.1 a).

Since all the quantities are built in terms of the analytical retarded Green's functions, all the corresponding saddle-point equations can be written for any complex energy in the upper semi-plane. The choice of the complex energy mesh provides a satisfactory balance between the

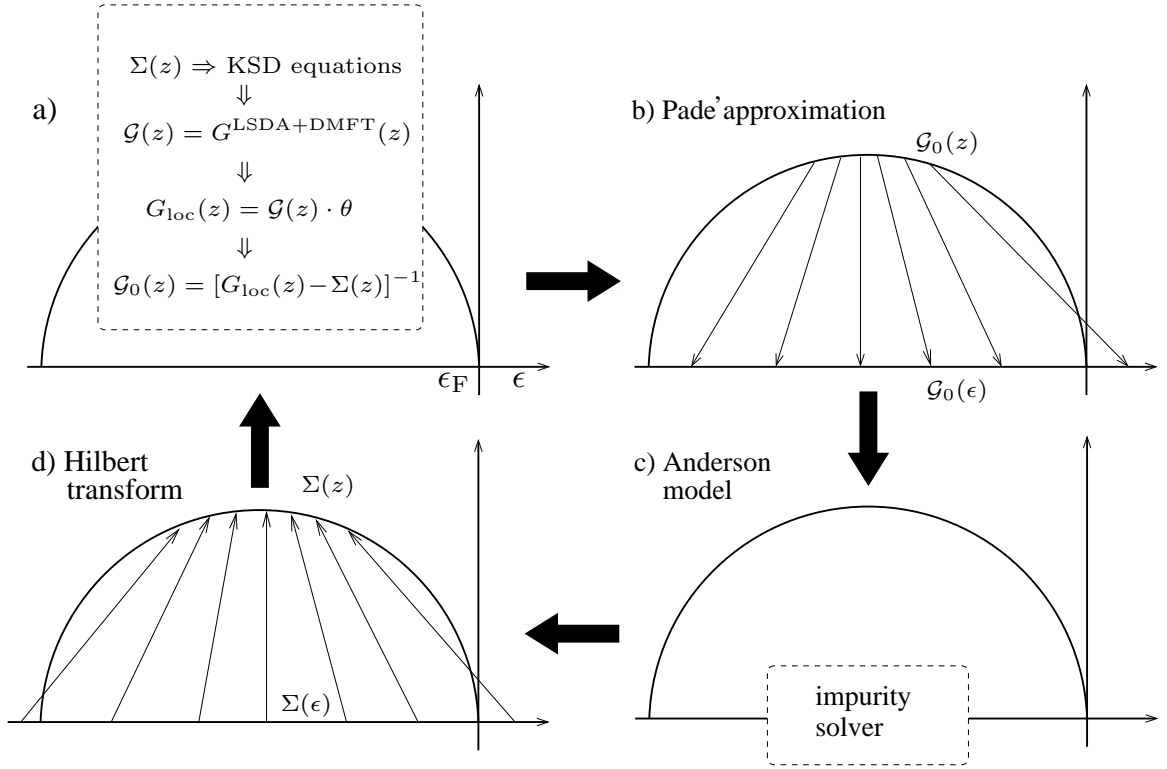


Fig. 6.1. Self-consistent KKR+DMFT scheme using the impurity solver for real energies. The horizontal line represents the real energy axis, with the vertical - imaginary axis crossing at the Fermi level ϵ_F . Panel (a): the LSDA delocalized Green's function is calculated from solutions of the Kohn-Sham-Dirac equation on the complex energy contour (semicircle). Panel (b): localized (single-site projected) Green's function is continued analytically onto the real axis via the Padé approximation. Panel (c): the real-axis impurity solver is applied to calculate the localized self-energy $\Sigma(\epsilon)$. Panel (d): the self-energy is analytically continued to the complex contour by an integral Hilbert transform.

requirements of the highest average imaginary part of energy in order to keep the number of energy points and the \mathbf{k} -points low and the total length of the curve which in turn makes an impact on the number of energy points. The currently used complex energy mesh is taken in the form of a semi-circle with the diameter equal to $\epsilon_F - \epsilon_B$ (ϵ_B : the bottom of the valence band) and turned out to be a good compromise in practical calculations.

In the current implementation two comparable solvers for the DMFT problem are used: the first one, the TMA (T -matrix approximation) utilizes the real axis formalism described in Sec. 3.3, another one [47], the so-called FLEX (T -matrix Plus Fluctuation Exchange) is

implemented for a complex energy mesh using the Matsubara poles.

In fact any DMFT solver which derives the self-energy for the corresponding impurity problem can be used. In both cases the *Padé* analytical continuation (often called Padé approximation) [119] is used to map the bath Green's function \mathcal{G}_0 onto the real axis (Fig. 6.1 b)) (or on the Matsubara poles) where the many-body problem is solved (Fig. 6.1 c)). To map back the self-energy from the real axis to the complex plane the *Hilbert* transformation (3.34) (or if the self-energy is calculated on the Matsubara poles - one more Padé approximation) is used, where the $G^{\text{LSDA+DMFT}}$ Green's function is in turn calculated by solving the Kohn-Sham-Dirac equations with the new self-energy (Fig. 6.1 a)).

This self-consistent procedure assumes the simultaneous converging of the local density ρ and the self-energy Σ .

6.1.2 Common features and comparison of the DMFT solvers

According to its construction, the self-energy follows the structure of the input Green's function in all the channels and all the orders of perturbation theory, having all the symmetry operations which the corresponding Green's function matrix has. Thus, for example, if we consider the non-relativistic case, neglecting the spin-orbit coupling, the spin-flip matrix elements of the self-energy will be zero and the matrix can be turned to diagonal form by corresponding unitary rotation. If one works within the spherical potential approximation and is not interested in the orbital polarization, a practical way is to take the average over the different elements for each spin channel. The self-energy applied even in such a simple form already leads to pronounced effects connected with the spectral properties of *3d*-transition metals which are missed within the LSDA picture. As it follows from various investigations, the most important role in the improvement of the LSDA description of DOS, angle-integrated photoemission, total energy and optical conductivity spectra in *3d*-transition metals is played by the 2nd-order (PP) channel of the self-energy, while the static (1st-order) contribution is rather small and is normally neglected by setting the self-energy to zero on the Fermi-level. The typical influence of the 2nd-order self-energy on the DOS spectrum is shown on Fig. 6.2 for hcp Co. As it follows, the DMFT leads to a noticeable renormalization of the

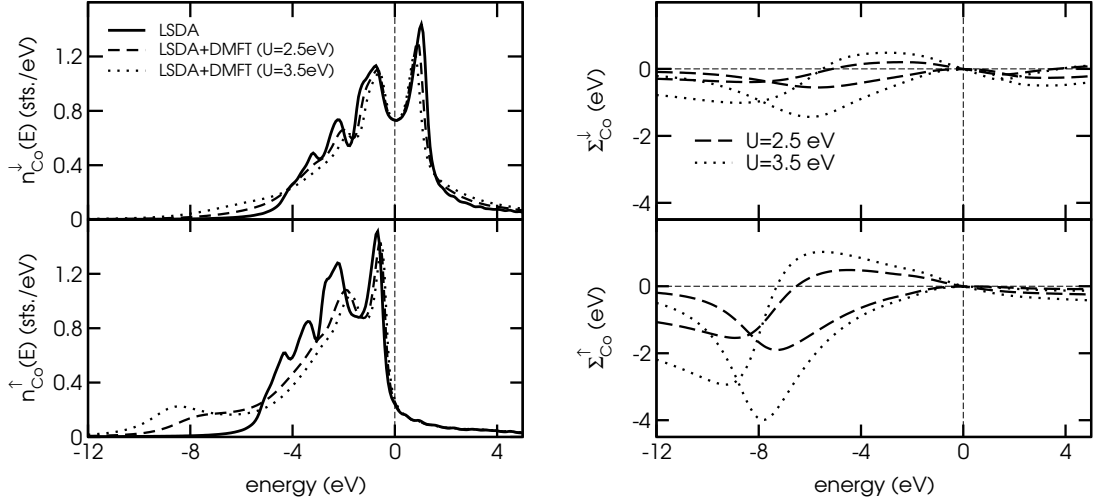


Fig. 6.2. Left panel: spin-resolved d -DOS of hcp Co calculated via the LSDA (full line) and the LSDA+DMFT (dashed line: $U=2.5$ eV, dotted line: $U=3.5$ eV) approach within the self-consistent KKR+DMFT(TMA) scheme. The corresponding spin-polarized orbital-averaged real and imaginary self-energies are presented in the right panel.

majority-spin DOS spectrum, by shifting the peaks situated near the Fermi level closer to it and making the band more narrow. Towards the Fermi level the changes of the DOS spectrum become smaller along with a correspondent behavior of the self-energy. Due to the small amplitude of the minority-spin self-energy the changes in the corresponding DOS component are small as well.

The qualitative analysis of the changes in the DOS spectrum imposed by the DMFT is given on Fig. 6.3. As it follows, in the vicinity of the Fermi level the real component of the self-energy shifts the poles of the Green's function closer to the Fermi level, without shifting them beyond. This means that the integral properties of the system, as, e. g. magnetic moments are not affected. In general one can expect some density transfer over the Fermi level due to the imaginary component of the self-energy which causes some additional broadening of the DOS peaks. However, since such DOS transfer occurs in both directions and the broadening width falls down towards the Fermi level rather fast (as $\propto \alpha(\epsilon - \epsilon_F)^2$) it should not noticeably affect the integral properties of the system. An exception can only be expected for strongly correlated systems with the large peak of the density of states at the Fermi level as e. g. in correlated impurities or heavy fermionic systems. However,

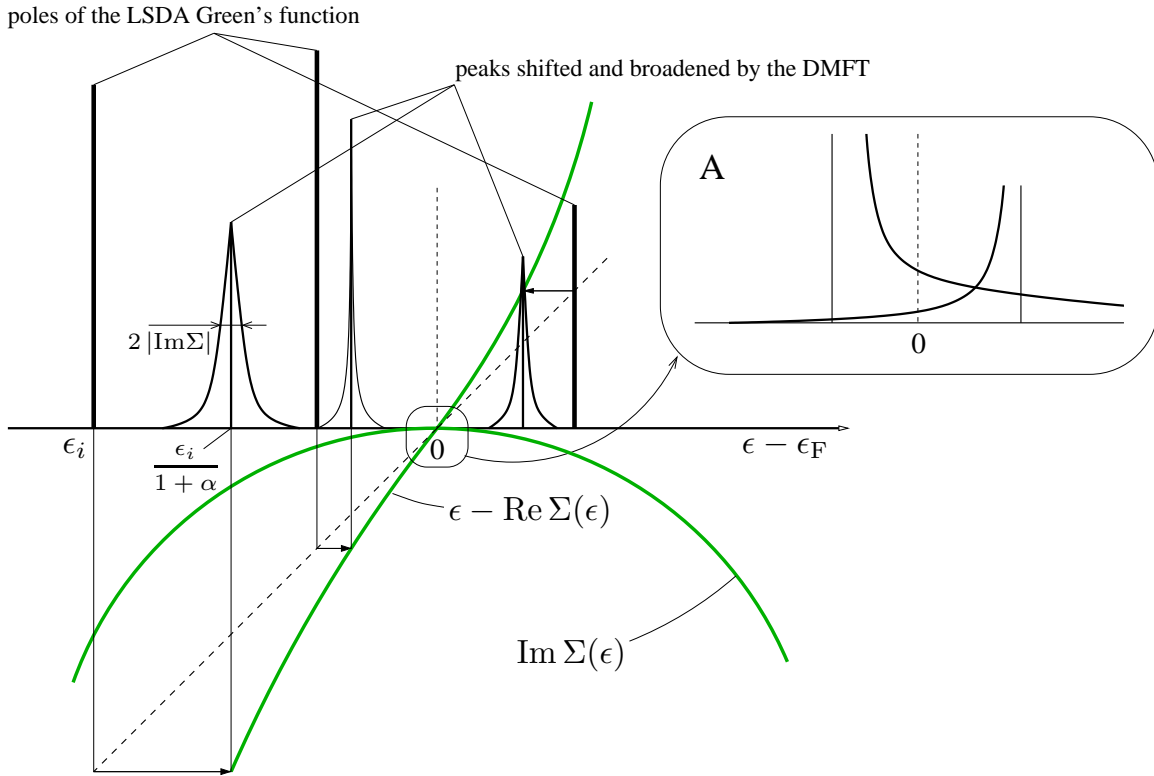


Fig. 6.3. Schematic illustration of the changes in the one-particle spectrum imposed by DMFT in the vicinity of the Fermi energy. The addition of the real self-energy $\text{Re}\Sigma(\epsilon) \approx -\alpha(\epsilon - \epsilon_F)$, $\alpha > 0$, shifts the peaks ϵ_i by $1+\alpha$ times closer to the Fermi energy. The additional broadening of the shifted peaks occurs due to the imaginary part of the self-energy, $\text{Im}\Sigma(\epsilon) \approx -\alpha(\epsilon - \epsilon_F)^2$. The broadening can lead to a change in the occupation due to the non-compensated transferring of states over the Fermi level as illustrated with a larger scale on panel A.

by turning to moderately correlated systems, the following tests for the transition metals show that there is almost no influence of the dynamical effects on their magnetic moments observed. The corresponding results for bcc Fe, hcp Co and fcc Ni are shown on Fig. 6.4. As it follows, the relative change of the magnetic moments caused by the broadening of the peaks within the LSDA+DMFT calculations with respect to the corresponding LSDA moments makes at most 2.5-3% in the case of Fe. For Co and Ni the deviations from LSDA values are much smaller. Thus, *the magnetic moments in locally correlated systems depend mostly on static correlation effects.*

Far from the Fermi level (e. g. around -7 eV in the case of Co

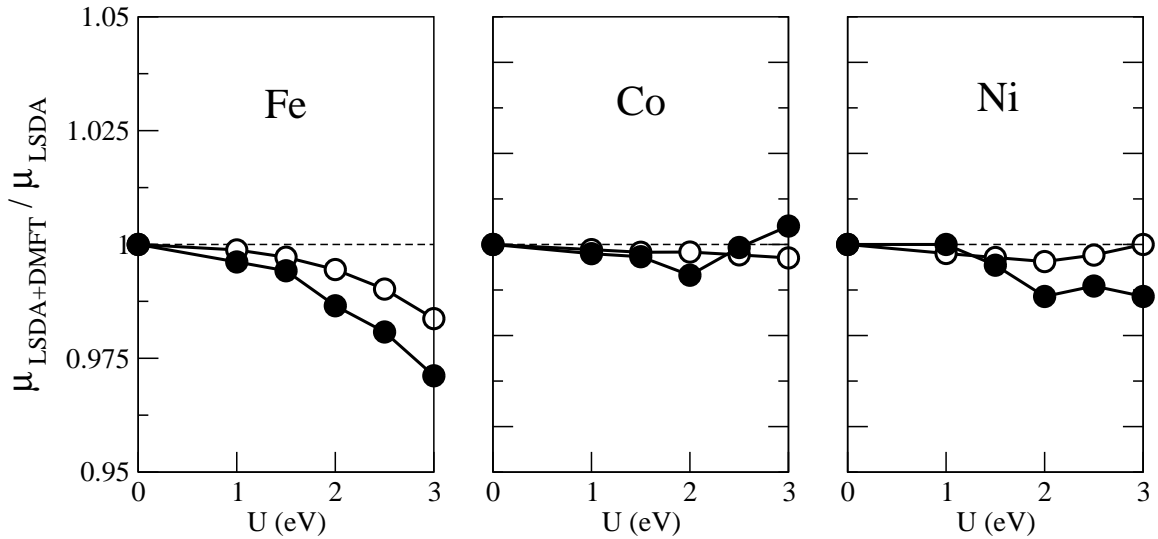


Fig. 6.4. Relative values of the spin (open circles) and orbital (filled circles) magnetic moments of bcc Fe, hcp Co and fcc Ni calculated within the self-consistent LSDA+DMFT approach as a function of U with respect to the corresponding LSDA values. The value of J parameter is fixed at 0.9 eV.

(Fig. 6.2)) the real component of the self-energy changes its sign and the DOS peaks are shifted into the opposite direction. Together with the corresponding large broadening in this energy regime it forms the so-called lower Hubbard band represented by the satellite centered approximately at 7 eV for $U=2.5$ eV and at 9 eV for $U=3.5$ eV.

When studying the influence of localized correlations on such delicate properties as orbital moments, complicated angle-resolved photoemission spectra and magneto-optical spectra, one has carefully account for the orbital polarization of the self-energy which possesses a rather complex structure within the fully-relativistic treatment: even if the spin-flip terms are neglected, the crystal symmetry is broken and we have to calculate at least 10 non-vanishing elements of the 10×10 self-energy matrix. For such a calculation a high precision within the whole LSDA+DMFT procedure is required, in particular it should be combined with an account for the non-spherical potential in order to account correctly for orbital polarization. The situation becomes more complex if we consider the $5f$ actinide metal systems. The large spin-orbit coupling results in a huge amplitude of the spin-flip elements of the Green's function and in turn, in large spin-flip matrix elements of

the self-energy. For this case one has to perform precise calculations for about 30 non-vanishing energy-dependent matrix elements (accordingly within the impurity solver one will deal with roughly 1000 energy-dependent elements). Moreover, since the dynamical many-body effects are exceptionally strong for these systems, the influence of the higher-order channels as well as of the static contributions should also be investigated. However, due to the complexity of the $5f$ actinide systems this question cannot be answered yet.

The comparison of the corresponding self-consistent self-energies and densities of states for both TMA and FLEX solvers is given in Fig. 6.5.

It is instructive to figure out the significance of the 3rd-order channel since the T -matrix approximation accounts for the 2nd-order PP-channels only. For this purpose we compare two available solvers, namely the real-axis T -matrix approximation (TMA) (Sec. 3.3) with another one, the Matsubara-based T -matrix approximation including additional 3rd-order PH-channel (FLEX) [47], both implemented in the self-consistent KKR+DMFT scheme. The additional possible difference caused by the finite-temperature entropy contribution implicitly accounted within the Matsubara formalism should be rather small for the commonly used in FLEX temperature regime $T \approx 400$ K that corresponds to 0.03 eV. Thus, the main difference between the two solvers should originate from the 3rd-order contribution.

Filling the d -shell by moving from Fe to Ni one observes more or less a noticeable difference only for the majority spin-channel in the DOS spectra caused by the larger majority-spin amplitudes of the self-energy.

To ensure that the effect of the finite temperature is indeed small we perform complementary FLEX calculations with a PH-channel switched off (Fig. 6.6). As it follows, despite of the temperature difference (400 K), the DOS calculated within the real-energy TMA and complex-energy TMA schemes both using only the 2nd-order PP-channel become nearly indistinguishable. Thus, we can conclude that although the influence of the 3rd-order channels is much smaller than that of the 2nd-order, its contribution is more pronounced than the entropy contribution in the room-temperature regime.

Since the results of both methods agree very well, we can consider the real-axis-based T -matrix approximation as a reliable technique

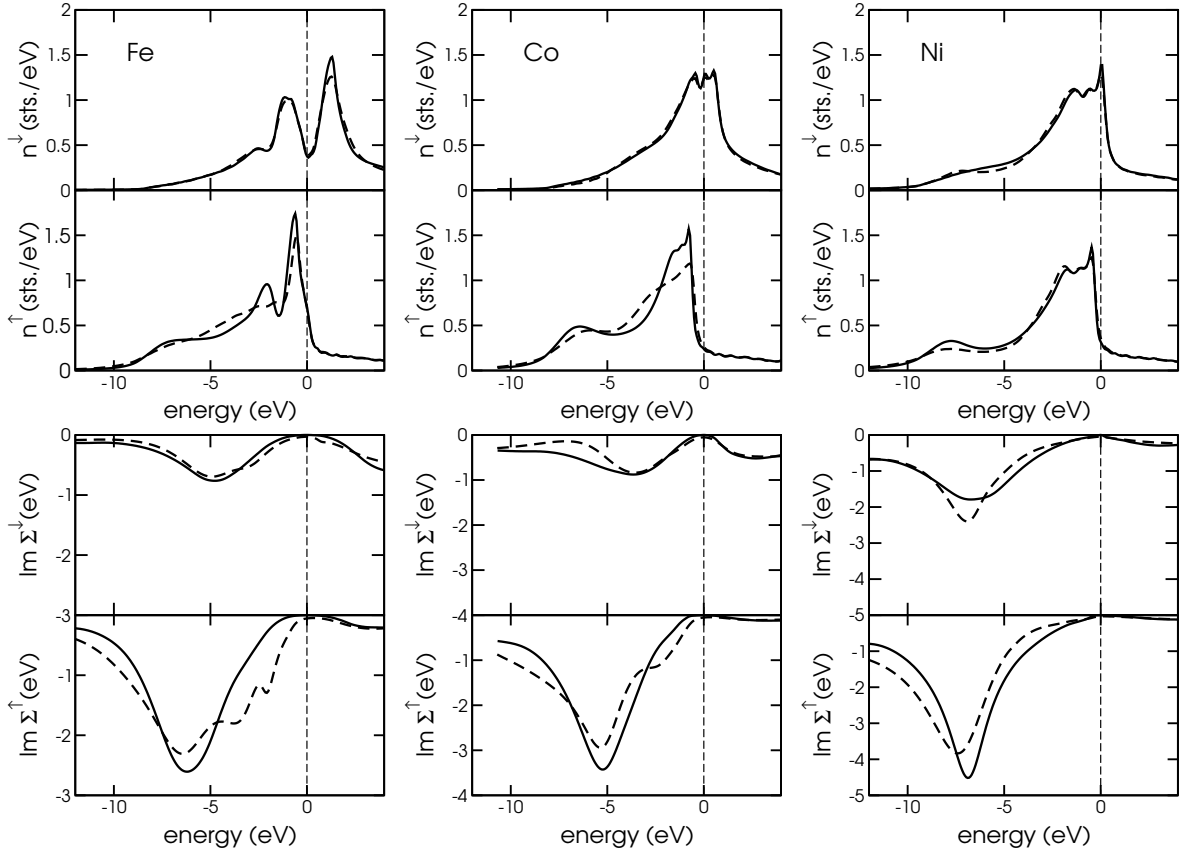


Fig. 6.5. Comparison of the two impurity solvers within the self-consistent KKR+DMFT calculation of DOS (upper panel) for bcc-Fe, fcc-Co and fcc-Ni. Solid and dashed lines correspond to the TMA and FLEX ($T=400$ K) schemes, respectively. In both schemes the Coulomb effective parameters are $U_{\text{Fe}}=2.0$ eV, $U_{\text{Co}}=2.5$ eV, $U_{\text{Ni}}=3.0$ eV. The effective exchange parameter has a value of $J=0.9$ eV for all three systems. The Fermi energy is set to zero. The lower panels represent the corresponding comparison of spin-resolved orbital-averaged imaginary self-energies.

which recovers the main features imposed by the dynamical correlations in $3d$ -transition metals.

6.2 Application to ground-state properties

6.2.1 Orbital magnetic moments

While the spin magnetic moments in $3d$ -transition metals, their alloys and impurities are described rather accurately by LSDA, the orbital moments are systematically underestimated. For example, the average

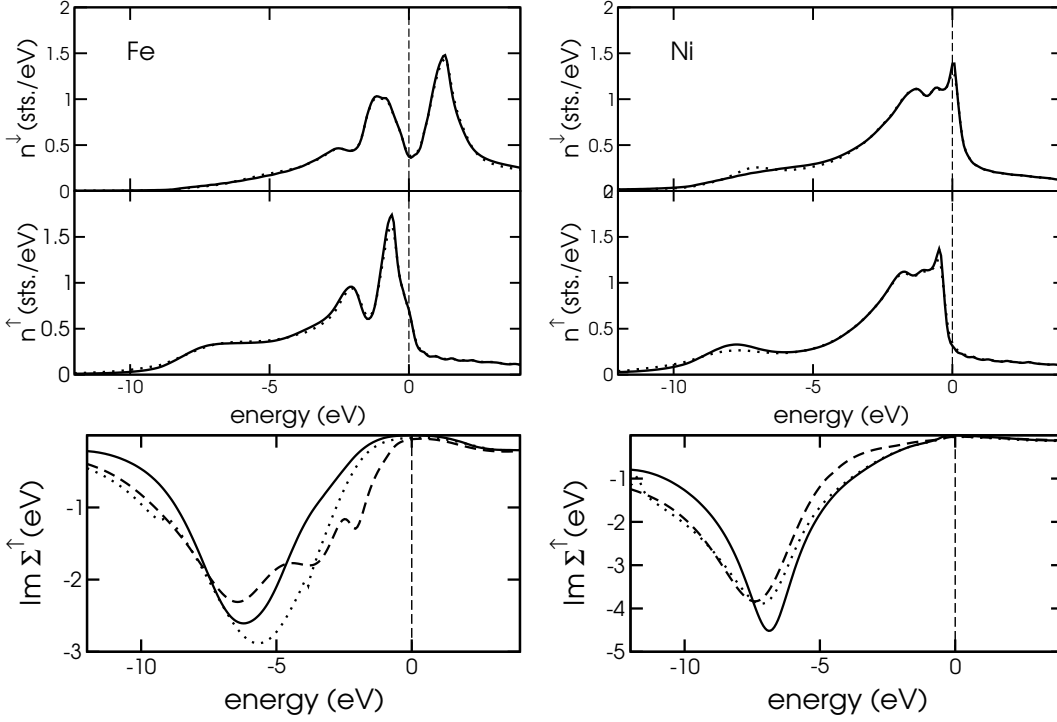


Fig. 6.6. The same comparison as in Fig. 6.5. The dotted one marks calculations using only the PP-channel in the FLEX scheme ($T=400$ K).

underestimation for Fe is about 40%, and for Co - about 50%. The reason for this is well-known: the functional variables of the LSDA potential (the charge and spin density) are defined as an average over occupied orbitals. It is natural that such an approximation gives a good description only for the quantities which are slightly dependent on the deviations of orbital occupation numbers from their average, as e.g. spin magnetic moments.

The approximate expression for the orbital moment generally used within relativistic density functional theory is the following [120]:

$$\mu_{\text{orb}} = -\frac{\mu_B}{\pi} \text{Im} \int d\epsilon \int d^3r \beta l_z G(\mathbf{r}, \mathbf{r}, \epsilon), \quad (6.19)$$

where β is one of the 4×4 Dirac matrices, l_z is the z component of the 4×4 matrix vector $l_z = I_4 \otimes (\mathbf{l})_z$ with \mathbf{l} the conventional angular momentum operator. Using perturbation theory one can also show that the most substantial contribution to μ_{orb} is connected with the differences of the m and $-m$ components of the Green's function at the

Fermi level:

$$\mu_{\text{orb}} \sim -\frac{\mu_{\text{B}}}{\pi} \text{Im} \sum_{m>0} m \left[\left(G_{mm}^{\uparrow} - G_{-m-m}^{\uparrow} \right) + \left(G_{-m-m}^{\downarrow} - G_{mm}^{\downarrow} \right) \right] \Bigg|_{\epsilon=\epsilon_{\text{F}}}. \quad (6.20)$$

Thus, the obvious way to increase the orbital moment would be to use a theoretical approach that accounts for an additional splitting of $G_{mm}^{\sigma} - G_{-m-m}^{\sigma}$ while retaining at the same time $G_{mm}^{\sigma} - G_{mm}^{-\sigma}$ in order to have the spin moment unchanged [121].

An often used approach to improve the description of orbital magnetism is the so-called *orbital polarization correction* (OP) scheme introduced by *Brooks et al.* [81–83] in a form of an additional *ad hoc* term to the Hamiltonian. As it was shown later by *Ebert et al.* [122], the OP enhancement can be partially achieved by utilizing the more general CDFT (current density functional) theory. Finally, *Eschrig et al.* [123] analyzing the CDFT have derived a systematic expression for the OP correction (for an overview and results of this approach see Ref. [124]). However, despite of the accurate description of the orbital moments in pure 3d-transition metals and their alloys [125, 126], the LSDA+OP calculations noticeably overestimate the unquenched orbital moments of the 3d-transition metal impurities in noble metal hosts [127, 121, 124]. In the case of deposited clusters *Gambardella et al.* [128] indicated the need to reduce the Racah parameter by about 50% in order to describe the experimental orbital moments correctly. However, the calculated magnetic anisotropy is still much too high [128, 129].

Among other reasons for the non-systematic results in the previous OP-based studies, could also be the insufficient account of localized many-body correlations. In particular, *Solovyev et al.* [130, 131] showed on the basis of model calculations within the random-phase approximation that the OP picture represents the limiting case of the more general LSDA+U concept. Thus, based on the discussion (see Subsec. 6.1.2) of the crucial influence of the static many-body interactions on the delicate balance of the magnetic properties (i.e. spin and orbital moments), we address the maturely developed LSDA+U technique.

As mentioned above, there are two cases when the DC can be exactly accounted for: the so-called atomic limit (AL) which corresponds to the case when the particular orbital is either fully occupied or fully

empty and the mean-field (MF) which corresponds to the uniform orbital occupation [19]. In the following test for pure bulk Fe, Co and Ni we try to figure out which one is more appropriate.

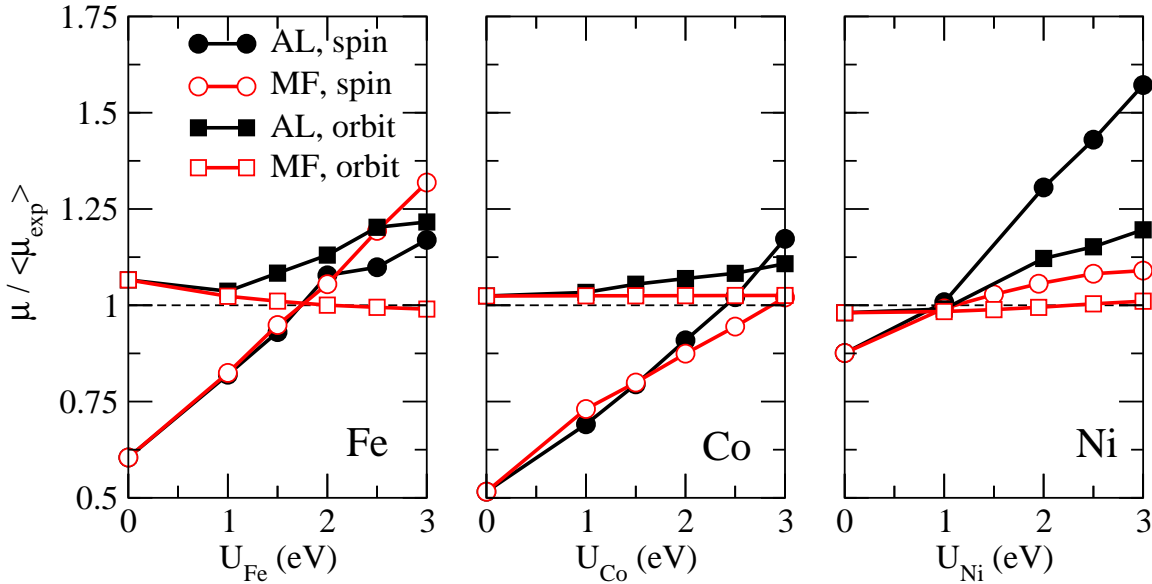


Fig. 6.7. Relative values of the spin (squares) and orbital (circles) magnetic moments of bcc Fe, hcp Co and fcc Ni calculated self-consistently within the KKR+LSDA+U approach as a function of U with respect to the corresponding averaged experimental values. The experimental averages are taken over the results given in Refs. [132–134]. Filled squares and circles correspond to the AL-type of DC, open symbols to the MF-type. The value of J parameter is fixed at 0.9 eV. The case $U=0$ corresponds to a plain LSDA calculation.

In general one observes a strong dependency of the orbital magnetic moments and a rather slight one of the spin moments on localized correlations, which is similar to the OP correction: the small orbital splittings imposed by the LSDA+U around the Fermi level have almost no effect on the spin, but enhance the orbital moment appreciably. On the other hand, the results noticeably depend on a particular type of DC. It turns out that the MF (mean-field) DC is a more appropriate choice than the AL-DC which leads to an enormously big growth of the orbital moments with increasing U parameter. This result is rather natural, since the AL-DC is more suitable for insulators with the Coulomb U much larger than the bandwidth. For Fe one finds the optimal U around 1.3 eV, for Co 1.75 eV and for Ni 1 eV. However, as it follows from the various DMFT studies as well as DMFT+GW-based estimations [135], the realistic value of U for 3d-transition metals should be

approximately 1-2 eV higher. The choice of a MF-DC substantially suppresses the growth of the orbital as well as for the spin moments and leads to optimal U values around 2 eV for bcc Fe, 2.5-3 eV for hcp Co and in the range of 1-3 eV for fcc Ni which much better agrees with the estimations mentioned above.

The final comparison with experiment for the spin and orbital magnetic moments, calculated within LSDA+U using MF-DC with the optimal values $U = 2$ eV for bcc Fe, $U = 2.5$ eV for hcp Co and $U = 3$ eV for fcc Ni is shown on Fig. 6.8.

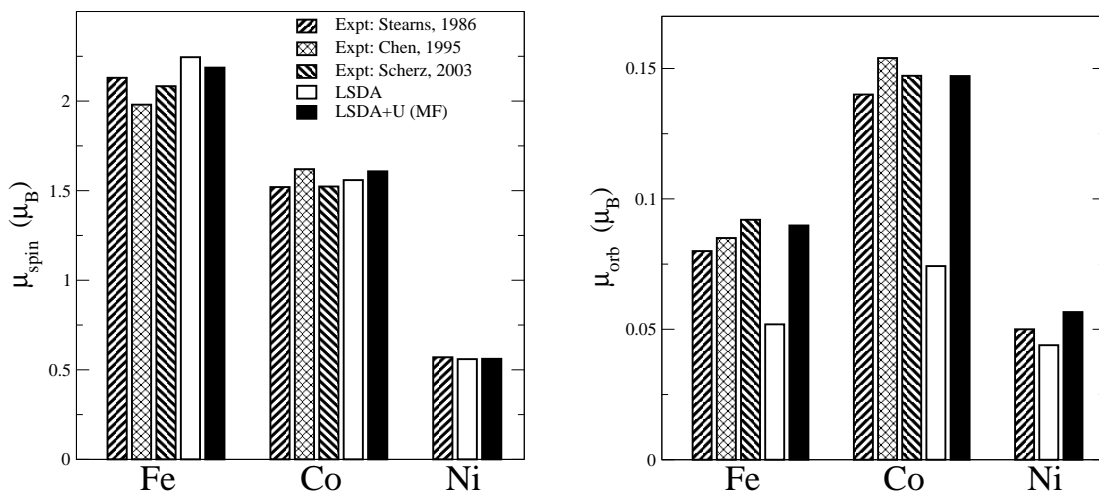


Fig. 6.8. Spin (right panel) and orbital (left panel) magnetic moments in bcc Fe, hcp Co and fcc Ni calculated using LSDA+U with MF-DC (black filled bars) compared with plain LSDA calculations (open bars) and experimental data (hatched bars) taken from [132–134]. The corresponding DMFT parameters are $U_{\text{Fe}} = 2.0$ eV, $U_{\text{Co}} = 2.5$ eV and $U_{\text{Ni}} = 3.0$ eV and $J_{\text{Fe}} = J_{\text{Co}} = J_{\text{Ni}} = 0.9$ eV.

Among other advantages, the SPR-KKR method utilized in the present work can be straightforwardly combined with the Coherent Potential Approximation (CPA) theory describing disordered alloys with the LSDA+U or/and DMFT schemes. The latter is illustrated for bcc $\text{Fe}_x\text{Co}_{1-x}$ disordered alloys. As can be seen from Fig. 6.9, while the spin magnetic moments for all approaches agree rather well, LSDA+U considerably improve the orbital moments in comparison with plain LSDA calculations in a way similar to the result obtained by *Ebert* and *Battocletti* using the LSDA+OP combined with the CPA [126].

As a further example we consider the unquenching of the orbital moment of 3d impurities embedded in the noble metal Au. In Fig. 6.10

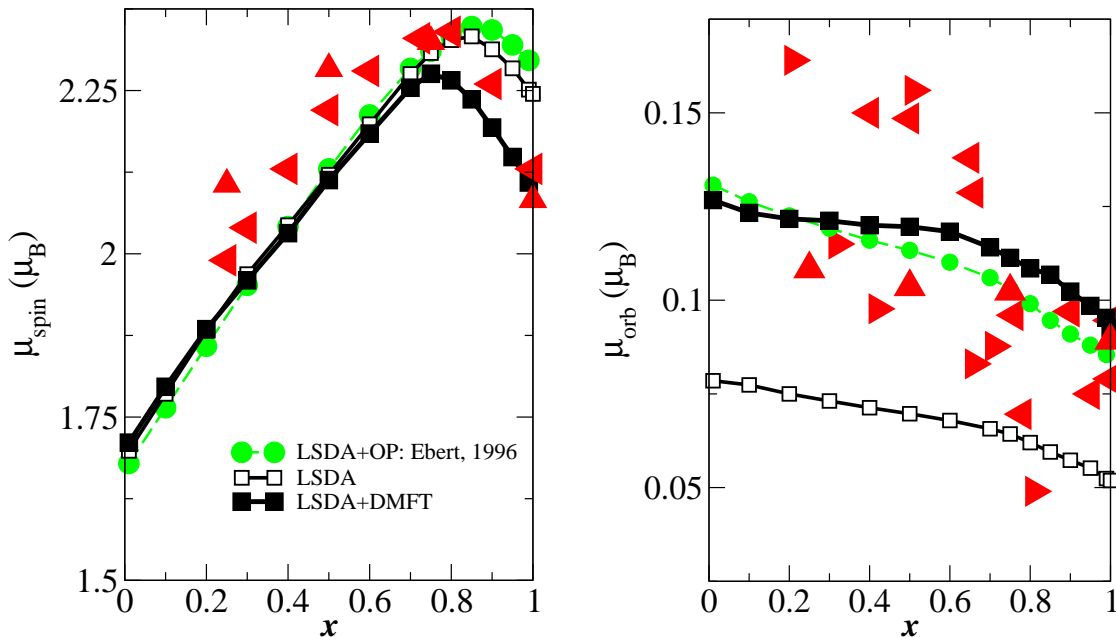


Fig. 6.9. Spin (right panel) and orbital (left panel) total magnetic moments of disordered bcc $\text{Fe}_x\text{Co}_{1-x}$ alloys calculated as a function of concentration x via the LSDA+U-MF (black squares), compared with present plain LSDA (open squares, black line) and LSDA+OP calculations (light filled circles, dashed line) [126], and experimental data (triangles) taken from Refs. [132]. The corresponding LSDA+U parameters are $U_{\text{Fe}} = 2.0$ eV, $U_{\text{Co}} = 3.0$ eV and $J_{\text{Fe}} = J_{\text{Co}} = 0.9$ eV.

the results of LSDA+U (MF) calculations are compared with the experimental orbital to spin moment ratios [127]. In light of the previous discussion (Subsec. 6.1.2) concerning the possibility of a more pronounced influence of dynamical correlations on the magnetic properties in the systems with a high DOS near the Fermi level additional calculations (LSDA+U(MF)+DMFT) accounting for static and dynamic correlations have been performed. The observed agreement for the Co impurity is very satisfying and we obtain a considerable improvement when comparing to previous OP studies [127, 121, 124]. These studies give a ratio of about 1.2 to be compared with experimental value 0.35, that agrees very well with our result. The small deviation for Fe from experiment could be attributed to the partially itinerant behavior of d -electrons in Fe which was also indicated in previous DMFT studies (e. g. in Ref. [99]). On the other hand, the absolute value of the deviation is comparable to that in the case of Co.

Both the LSDA+U and the LSDA+U+DMFT calculations give

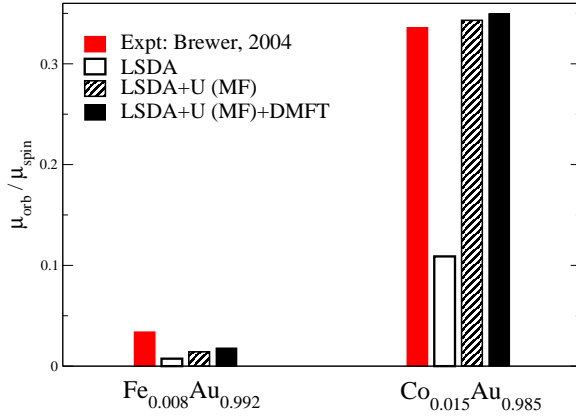


Fig. 6.10. Orbital to spin ratios of the magnetic moments of diluted Fe and Co impurities embedded in fcc Au host calculated via LSDA+U (MF) (hatched bars) and full LSDA+U(MF)+DMFT calculations (black filled bars) compared with present plain LSDA (open bars) and the experimental data (red/light bars) [127]. LSDA+U/DMFT parameters are $U_{\text{Fe}}=2.0$ eV, $U_{\text{Co}}=2.5$ eV and $J_{\text{Fe}}=J_{\text{Co}}=0.9$ eV.

nearly the same result thus one can conclude that in these type of systems there is no pronounced influence of dynamical correlations effects on their magnetic properties.

6.2.2 Calculation of the total energy

Considering the localized dynamical self-energy as a small perturbation $\Sigma(\epsilon)$ in the system described within the LSDA the approximate expression for the corresponding total energy can be derived by retaining only the terms linear with respect to the perturbation. Obviously, all the terms in Eq. (5.10) except for the band contribution are at least 2nd-order in density (or Green's function). Thus the change of the total energy is caused mainly by the band-energy change. It can be derived using the following equation for the perturbed LSDA Green's function $\mathcal{G} = G(\epsilon + \Sigma(\epsilon))$:

$$\mathcal{G}(\epsilon) = G(\epsilon) + G(\epsilon)\Sigma(\epsilon)\mathcal{G}(\epsilon). \quad (6.21)$$

Taking into account that $G(\epsilon) \sim 1/\epsilon$ the corresponding band energy will be represented as following:

$$\begin{aligned} E_{\text{band}} &= -\frac{1}{\pi} \text{Im} \int^{\epsilon_F} d\epsilon \epsilon [G(\epsilon) + G(\epsilon)\Sigma(\epsilon)\mathcal{G}(\epsilon)] \\ &\approx E_{\text{band}}^{\text{LSDA}} - \frac{1}{\pi} \text{Im} \int^{\epsilon_F} d\epsilon \Sigma(\epsilon)\mathcal{G}(\epsilon) \end{aligned} \quad (6.22)$$

The last term can be identified as the so-called *Galitsky-Migdal* energy E_{GM} [136, 137], multiplied by a factor of two:

$$E_{\text{GM}} = \frac{1}{2} \text{Tr} \{ \Sigma G \}. \quad (6.23)$$

Thus, the total energy of the perturbed system can be approximated as

$$E_{\text{tot}} \approx E_{\text{tot}}^{\text{LSDA}} - \frac{1}{\pi} \text{Im} \int^{\epsilon_{\text{F}}} d\epsilon \Sigma(\epsilon) \mathcal{G}(\epsilon). \quad (6.24)$$

Analogously, one can consider the SDFT expression for the total energy (5.45) with the interaction part given by Eq. (5.49). The kinetic contribution given by the Baym-Kadanoff theory (see Eq. (5.44)) can be represented as

$$\begin{aligned} K[\mathcal{G}] &= \text{Tr} \{ \ln \mathcal{G} \} - \text{Tr} \{ (G^{-1} - \mathcal{G}^{-1}) \mathcal{G} \} \\ &= \text{Tr} \{ \ln \mathcal{G} \} + \text{Tr} \{ \Sigma \mathcal{G} \} \end{aligned} \quad (6.25)$$

The last term can be identified with the dynamical part of the exchange-correlation energy $\tilde{\Phi}_{\text{xc}}[\mathcal{G}]$, since $\Sigma = \delta \tilde{\Phi}_{\text{xc}}[\mathcal{G}] / \delta \mathcal{G}$. Neglecting the double-counting of the dynamical contribution $\Phi^{\text{DC}} = 0$, this leads to an expression for the corresponding total energy:

$$E_{\text{tot}} = \text{Tr} \{ \ln \mathcal{G} \} + \text{Tr} \{ \Sigma \mathcal{G} \} + \text{Tr} \{ \Sigma \mathcal{G} \} + E_{\text{H}}^{\text{LSDA}}[\rho] + E_{\text{xc}}^{\text{LSDA}}[\rho]. \quad (6.26)$$

Approximating the first term as

$$\begin{aligned} \text{Tr} \{ \ln \mathcal{G} \} &= \text{Tr} \left\{ \ln (G^{-1} + \Sigma)^{-1} \right\} \\ &= -\text{Tr} \left\{ \ln (G^{-1} (1 + \Sigma G)) \right\} \\ &= \text{Tr} \{ \ln G \} - \text{Tr} \{ \ln (1 + \Sigma G) \} \\ &\approx \text{Tr} \{ \ln G \} - \text{Tr} \{ \Sigma G \} \end{aligned} \quad (6.27)$$

and retaining in $\text{Tr} \{ \Sigma \mathcal{G} \}$ only the 1st-order terms we arrive at a relation similar to Eq. (6.24):

$$\begin{aligned} E_{\text{tot}} &\approx \text{Tr} \{ \ln G \} + \text{Tr} \{ \Sigma G \} + E_{\text{H}}^{\text{LSDA}}[\rho] + E_{\text{xc}}^{\text{LSDA}}[\rho] \\ &= E_{\text{tot}}^{\text{LSDA}} + \text{Tr} \{ \Sigma G \}, \end{aligned} \quad (6.28)$$

where the trace acts as

$$\text{Tr} \{AB\} = -\frac{1}{\pi} \text{Im} \int d\epsilon \int d^3r d^3r' A(\mathbf{r}, \mathbf{r}', \epsilon) B(\mathbf{r}', \mathbf{r}, \epsilon). \quad (6.29)$$

The following test for bulk fcc Ni (Fig. 6.11) probes the precision of the approximations in Eqs. (6.26) and (6.28). As it follows, by adding

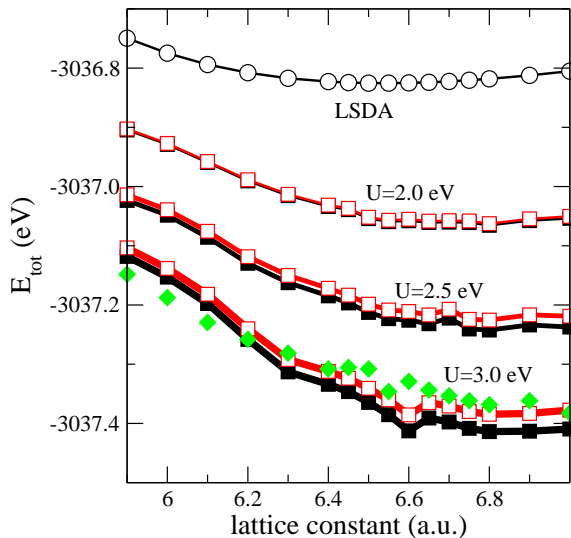


Fig. 6.11. The total energy per atom for fcc Ni as a function of the lattice constant calculated by the KKR method. The open circles mark the LSDA results, filled squares LSDA+DMFT results. The increase of the U parameter (2.0, 2.5, 3.0 eV) corresponds to the increase of the line width. Open squares mark the sum of the LSDA total energy and the doubled Galitsky-Migdal contribution $2E_{\text{GM}}$ obtained within the LSDA+DMFT scheme. The light diamonds mark the LSDA+U-MF+DMFT result for $U=3.0$ eV.

the doubled Galitsky-Migdal energy to the LSDA total energy nearly perfect agreement with the LSDA+DMFT result is obtained. This implicitly confirms that the double-counting energy for Ni can be considered as rather small, in line with the previous discussion. Thus, the change in the total energy imposed by the account of localized correlations is caused mainly by the 2nd-order dynamical effects. Indeed, the complementary LSDA+U-MF+DMFT ($U=3.0$ eV) calculations shown in Fig. 6.11 demonstrate that the static contribution to the total energy described within the LSDA+U approach is almost canceled by the MF-DC.

6.2.3 Summary

Summarizing the results discussed above it is important to emphasize the influence of localized many-body correlations in 3d-transition

metals examined for the various situations ranging from the pure bulk systems, to concentrated alloys and impurity systems.

In particular, when dealing with orbital magnetic moments, the major importance of static correlations should be stressed. As it follows from the calculations, the most important contribution comes from the 1st-order relativistic effects, i.e. primarily the orbital-resolved self-energy has to be accounted for, while the spin-flip terms can be neglected. Nevertheless, due to the small values of the orbital splittings induced by the static correlations a highly precise self-consistent calculational scheme accounting for the non-sphericity of the potential is required.

As it also follows from the calculations of the total energy, the treatment of the localized correlations can be provided more easily if one strictly separates the static and the dynamical effects which gives an opportunity to apply the DMFT methods for the latter and the LSDA+U technique for the former. Thus, the problem of the correct double-counting could be treated separately in the context of the LSDA+U. In particular, the MF-DC could be considered as a more appropriate and rather universal choice in the case of 3d-transition metals instead of the often used zero-static approximation.

6.3 Applications to photoemission

6.3.1 Introduction

Much information on the electronic structure of magnetic solids is gained by valence band photoemission, that in particular allows to monitor the dispersion of the electronic band structure. However, photoemission spectra are very difficult to interpret without accompanying theoretical calculations. For these in turn one in general has to solve a corresponding many-electron problem, which is impossible without the use of more or less severe approximations. For materials for which the kinetic energy of the electrons is more important than the Coulomb interaction, the most successful first principles method is the LSDA. For the last two decades *ab initio* calculations of the valence band photoemission of solids based on the LSDA yielded a good basis for the interpretation of experimental spectra, often leading to a quanti-

tative agreement between theoretical and experimental spectra (for an overview see Ref. [138] and references therein). The situation is very different when one considers materials showing pronounced correlation effects, since in all calculations the LSDA eigen-energies are implicitly interpreted to be the one-particle excitation energies of the system. It is well known that there are two possible sources of error connected with that approach: Firstly, the LSDA provides only an approximate expression for the (local) exchange-correlation potential. Secondly, even with the exact exchange-correlation potential at hand, one is left with the problem that there is no known correspondence between the Kohn-Sham eigen-energies and the one-particle excitation energies [139–142].

In principle for an exact description of the excitation energies the corresponding many-body problem has to be dealt with in a more satisfying way leading to a complex and non-local self-energy.

The combination of the DMFT with the multiple scattering or Korringa Kohn Rostoker (KKR) band structure method [143] in a self-consistent way (as discussed in the beginning of the present chapter) allows in a straightforward way to incorporate dynamical correlation effects into calculations of various X-ray spectroscopies among which valence band photoemission will be discussed here.

Magnetic circular dichroism in magnetically ordered systems is closely related to the Fano-effect [144] that also occurs as a consequence of the spin-orbit coupling. The term Fano-effect denotes the observation that one can have a spin-polarized photo-current from a non-magnetic sample if circularly polarized radiation is used for excitation. While for a non-magnetic sample the spin-polarization of the photo-current is reversed, this symmetry is in general broken for a magnetically ordered system leading to magnetic circular dichroism. This implies in particular that if a spin-resolved photoemission experiment is done with circularly polarized radiation coming in along the direction of the magnetization of a ferromagnetic material and spin analysis of the photo-current is done with respect to this direction, the spin-polarization of the photo-current due to spin-orbit coupling is superimposed to that due to magnetic ordering. In the following it is demonstrated by experiments on Fe and Co that the pure Fano-effect can also be observed in angle-integrated valence band X-ray photoemission spectroscopy (VB-XPS) for ferromagnets, if the circularly polarized radiation impinges

perpendicular to the magnetization and if subsequent spin analysis is done with respect to the direction of the photon beam.

High-energy angle-resolved photoemission spectroscopy (ARPES) for investigating valence-band dispersions has been challenged more than 20 years ago [145]. However, only in recent years the technical problems connected with this could be solved leading to a powerful tool to investigate the electronic structures and Fermi surfaces of solids. In contrast to the low-energy ARPES, which is a very surface sensitive technique, high-energy ARPES primarily probes bulk properties of the investigated systems. This implies in particular that it becomes possible to investigate strongly correlated systems, with a reduced influence of the surface on the measured spectra. So far high-energy ARPES has been successfully applied among others to investigate a rare-earth compounds [146, 147] and transition metal oxides [148–150]. We present here a theoretical approach to calculate high-energy ARPES spectra with dynamical correlation effects included, based on a fully-relativistic formalism.

Accompanying calculations based on local spin-density approximation (LSDA) and using a fully relativistic implementation of the one-step model of photoemission allow for a detailed discussion of the experimental spectra. In addition we show that the use of LSDA in combination with dynamical mean field theory (DMFT) leads even for Fe and Co to an improvement of the agreement of theoretical and experimental VB-XPS spectra as it will be discussed furthermore in Sec. 6.3.3. In addition, the first theoretical results for high-energy angle-resolved valence band photoemission of Ni are presented in Sec. 6.3.4. The theoretical framework for these calculations will be reviewed and introduced in Sec. 6.3.2.

6.3.2 Theoretical framework

A rather sophisticated fully relativistic description of spin and angle-resolved photoemission has been developed during the last years by several groups [151–154, 138]. This is based on the one-step-model and represents the electronic Green's function by making use of the multiple scattering or Korringa Kohn Rostoker (KKR) formalism. By dealing with the multiple scattering problem in real space, a very simple ex-

pression was derived by Ebert and Schwitalla [153] for the spin-resolved and angle-integrated valence-band photoemission spectra of ferromagnetic solids. In this section we will present a formalism to deal with two special cases discussed here. This includes a generalization of the expressions derived by Ebert and Schwitalla [153] to the spin-density matrix formalism as described for example by Ackermann and Feder [155] for the angle-integrated case. This approach is necessary to describe properly the pure Fano-effect observed in valence band X-ray photoemission (VB-XPS) for ferromagnets [98]. In this case the circularly polarized radiation impinges perpendicular to the magnetization and the subsequent spin analysis is done with respect to the direction of the photon beam. A second case discussed here is the high-energy angle-resolved VB-XPS, which in recent years has been extensively applied to different materials to probe their bulk properties in particular for strongly correlated compounds [147, 146, 148–150]. The dynamical correlation effects will be accounted within the LSDA+DMFT scheme.

To deal with the geometry of the photoemission experiment described above we adopt the spin-density matrix formalism as described by Ackermann and Feder [155] for the angle-integrated case. This approach allows to express the photo-current and its spin polarization in terms of the spin density matrix

$$\rho(\epsilon) = \sum_{m_s m'_s} |m_s\rangle \tilde{I}_{m_s m'_s} \langle m'_s| . \quad (6.30)$$

The intensity spin matrix $\tilde{I}_{m_s m'_s}(\epsilon, \mathbf{k}; \omega, \mathbf{q}, \lambda)$ of the photoelectron current observed in VB-XPS is derived by starting from Fermi's "golden rule" [156]:

$$\begin{aligned} \tilde{I}_{m_s m'_s}(\epsilon, \mathbf{k}; \omega, \mathbf{q}, \lambda) &= \text{const} \sqrt{\epsilon + \omega} \int d\mathbf{r}_1 \int d\mathbf{r}_2 \\ &\times \phi_{\mathbf{k}m_s}^\dagger(\mathbf{r}_1, \hat{R}, \epsilon + \omega) X_{\mathbf{q}}^\lambda(\mathbf{r}_1) \\ &\times G(\mathbf{r}_1, \mathbf{r}_2, \epsilon) X_{\mathbf{q}}^{\lambda\dagger}(\mathbf{r}_2) \phi_{\mathbf{k}m'_s}(\mathbf{r}_2, \hat{R}, \epsilon + \omega). \end{aligned} \quad (6.31)$$

Here the operator $X_{\mathbf{q}}^\lambda$ describes the interaction of the electrons and the radiation field with the vector potential $\vec{A}_{\mathbf{q}}^\lambda(\omega)$ representing the radiation with the energy ω , wave vector \mathbf{q} and polarization λ . The

initial valence band states at energy ϵ are represented by the single particle retarded Green's functions $G(\mathbf{r}_1, \mathbf{r}_2, \epsilon)$. The corresponding final state $\phi_{\mathbf{k}m_s}$ is identical to a time-reversed LEED state. With the spin density matrix ρ available the spin-averaged photo-current intensity \bar{I} and photo-electron spin polarization \mathbf{P} are given as $\bar{I} = \text{Tr}\{\rho\}$ and $\mathbf{P} = \text{Tr}\{\vec{\sigma}\rho\}/\bar{I}$, respectively, with $\vec{\sigma}$ the vector of spin matrices. Finally, if a spin analysis of the photo-current is performed with respect to a direction \hat{n} , the corresponding spin-projected photo-current I_σ is given by:

$$I_\sigma^\lambda = (1 + \sigma \mathbf{P} \cdot \mathbf{n}) \bar{I} / 2, \quad (6.32)$$

with $\sigma = \pm 1$ corresponding to spin-up and spin-down. In the following, the spin density matrix is defined with respect to a right-handed coordinate system with its z-axis chosen along the magnetization of the sample that in turn is oriented parallel to the surface plane. The x-axis coincides with the surface normal that specifies the direction \mathbf{n} for the spin analysis.

Using relativistic multiple scattering theory for spin-polarized systems, the final LEED states may be expressed by [157]:

$$\begin{aligned} \phi_{\mathbf{k}m_s}(\mathbf{r}_n, \epsilon') &= 4\pi \sqrt{\frac{\epsilon' + c^2}{2\epsilon' + c^2}} \sum_{\Lambda} i^{-l} C_{\Lambda}^{-m_s} Y_l^{\mu+m_s}(-\hat{k}) \\ &\sum_m e^{i\mathbf{k} \cdot \mathbf{R}_m} \sum_{\Lambda'} \tau_{\Lambda'\Lambda}^{nm*}(\epsilon') \left[\hat{T} Z_{\Lambda'}(\mathbf{r}_n, \epsilon') \right]. \end{aligned} \quad (6.33)$$

Here $\epsilon' = \epsilon + \omega$ is the energy of the detected photoelectrons, $\tau_{\Lambda'\Lambda}^{nm}$ is the scattering path operator, while Z_{Λ} is a regular solution to the single site Dirac equation. The quantities $C_{\Lambda}^{m_s}$ and $Y_l^{m_l}$ are the Clebsch-Gordon coefficients and the spherical harmonics, respectively. \hat{T} is the time reversal operator.

Inserting Eq. (6.33) and the expression for the electronic Green's function [143] into Eq. (6.31) allows one to deal with spin- and angular-resolved photoemission spectra in a fully relativistic way in complete analogy to the approach of Feder and coworkers [158]. This leads to

the following expression for the intensity spin matrix:

$$\begin{aligned}
\tilde{I}_{m_s m'_s}(\epsilon, \mathbf{k}; \omega, \mathbf{q}, \lambda) &= C \sum_{\Lambda \Lambda''} i^{l-l''} C_{\Lambda}^{-m_s} C_{\Lambda''}^{-m'_s} Y_l^{\mu+m_s^*}(-\hat{k}) \\
&\times Y_{l''}^{\mu''+m'_s}(-\hat{k}) \sum_{mm'} e^{i\mathbf{k}\cdot(\mathbf{R}_m-\mathbf{R}_{m'})} \sum_{nn'} e^{i\mathbf{q}\cdot(\mathbf{R}_n-\mathbf{R}_{n'})} \sum_{\Lambda'\Lambda'''} \tau_{\Lambda'\Lambda}^{nm}(\epsilon') \tau_{\Lambda'''\Lambda''}^{n'm'^*}(\epsilon') \\
&\times \left[\sum_{\Lambda_1 \Lambda_2} M_{\Lambda'\Lambda_1}^{\mathbf{q}\lambda} \tau_{\Lambda_1 \Lambda_2}^{nn'}(\epsilon) \bar{M}_{\Lambda_2 \Lambda'''}^{\mathbf{q}\lambda} - \delta_{nn'} \sum_{\Lambda_1} I_{\Lambda'\Lambda_1 \Lambda'''}^{\mathbf{q}\lambda} \right]. \quad (6.34)
\end{aligned}$$

The corresponding transition matrix elements $M_{\Lambda\Lambda'}^{\mathbf{q}\lambda}$, $\bar{M}_{\Lambda\Lambda'}^{\mathbf{q}\lambda}$ and $I_{\Lambda\Lambda'\Lambda''}^{\mathbf{q}\lambda}$ are given by [153]:

$$M_{\Lambda\Lambda'}^{\mathbf{q}\lambda} = \int d\mathbf{r} \left[\hat{T} Z_{\Lambda}(\mathbf{r}, \epsilon') \right]^{\times} X_{\mathbf{q}}^{\lambda}(\mathbf{r}) Z_{\Lambda'}(\mathbf{r}, \epsilon), \quad (6.35)$$

$$\bar{M}_{\Lambda\Lambda'}^{\mathbf{q}\lambda} = \int d\mathbf{r} Z_{\Lambda}^{\times}(\mathbf{r}, \epsilon) X_{\mathbf{q}}^{\lambda\times}(\mathbf{r}) \left[\hat{T} Z_{\Lambda'}(\mathbf{r}, \epsilon') \right], \quad (6.36)$$

and

$$\begin{aligned}
I_{\Lambda\Lambda'\Lambda''}^{\mathbf{q}\lambda} &= \int d\mathbf{r} \int d\mathbf{r}' [T Z_{\Lambda}(\mathbf{r}, \epsilon')]^{\times} X_{\mathbf{q}}^{\lambda}(\mathbf{r}) Z_{\Lambda'}(\mathbf{r}_{<}, \epsilon) \\
&\times J_{\Lambda'}^{\times}(\mathbf{r}_{>}, \epsilon) X_{\mathbf{q}}^{\lambda\times}(\mathbf{r}') [T Z_{\Lambda''}(\mathbf{r}', \epsilon')]. \quad (6.37)
\end{aligned}$$

Here $Z_{\Lambda}(\mathbf{r}, \epsilon)$ and $J_{\Lambda}(\mathbf{r}, \epsilon)$ are the regular and irregular solutions to the Eq. (6.1).

For the XPS regime a number of simplifications can be used. First, one can assume that XPS primarily probes bulk properties. This means that it is sufficient to deal with the excitation process for a representative unit cell at \mathbf{R}_0 . Second, arguments can be given [159, 160] that for the XPS regime the \mathbf{k} conservation does seem to hold at these energies (how well is still to be understood - see Refs. [146–150]). As a consequence, the photocurrent $I(\epsilon, \mathbf{k}, m_s; \omega, \mathbf{q}, \lambda)$ is determined only by the electronic properties within the unit cell at site \mathbf{R}_0 . Furthermore, all multiple scattering events for the final state can be ignored [160] for high energies of the exciting radiation. This single scatterer approximation amounts to restrict the sum over sites \mathbf{R}_m in Eq. (6.33) to

$\mathbf{R}_m = \mathbf{R}_n$. Accordingly, Eq. (6.34) can be rewritten:

$$\begin{aligned} \tilde{I}_{m_s m'_s}(\epsilon, \mathbf{k}; \omega, \mathbf{q}, \lambda) &= C \sum_{\Lambda \Lambda''} i^{l-l''} C_{\Lambda}^{-m_s} C_{\Lambda''}^{-m'_s} \\ &\quad \times Y_l^{\mu+m_s*}(-\hat{k}) Y_{l''}^{\mu''+m'_s}(-\hat{k}) \\ &\quad \times \left\{ \sum_{\Lambda_1 \Lambda_2} \left[\sum_{\Lambda'} t_{\Lambda'\Lambda}^0(\epsilon') M_{\Lambda'\Lambda_1}^{\mathbf{q}\lambda} \right] \tau_{\Lambda_1 \Lambda_2}^{00}(\epsilon) \left[\sum_{\Lambda'''} t_{\Lambda'''\Lambda''}^{0*}(\epsilon') \bar{M}_{\Lambda_2 \Lambda'''}^{\mathbf{q}\lambda} \right] \right. \\ &\quad \left. - \sum_{\Lambda' \Lambda'' \Lambda_1} t_{\Lambda'\Lambda}^0(\epsilon') I_{\Lambda'\Lambda_1 \Lambda''}^{\mathbf{q}\lambda} t_{\Lambda'''\Lambda''}^{0*}(\epsilon') \right\}. \quad (6.38) \end{aligned}$$

The corresponding expression gets quite simple if it is averaged with respect to \mathbf{k} to simulate an angle-integrated spectrum:

$$\begin{aligned} \tilde{I}_{m_s m'_s}(\epsilon; \omega, \mathbf{q}, \lambda) &= C \sum_{\substack{\Lambda \Lambda'' \\ l=l'' \\ \mu+m_s=\mu''+m'_s}} C_{\Lambda}^{-m_s} C_{\Lambda''}^{-m'_s} \\ &\quad \left\{ \sum_{\Lambda_1 \Lambda_2} \left[\sum_{\Lambda'} t_{\Lambda'\Lambda}^0(\epsilon') M_{\Lambda'\Lambda_1}^{\mathbf{q}\lambda} \right] \tau_{\Lambda_1 \Lambda_2}^{00}(\epsilon) \left[\sum_{\Lambda'''} t_{\Lambda'''\Lambda''}^{0*}(\epsilon') \bar{M}_{\Lambda_2 \Lambda'''}^{\mathbf{q}\lambda} \right] \right. \\ &\quad \left. - \sum_{\Lambda' \Lambda'' \Lambda_1} t_{\Lambda'\Lambda}^0(\epsilon') I_{\Lambda'\Lambda_1 \Lambda''}^{\mathbf{q}\lambda} t_{\Lambda'''\Lambda''}^{0*}(\epsilon') \right\}. \quad (6.39) \end{aligned}$$

Finally, to compare theoretical spectra based on Eq. (6.39) various broadening mechanisms are incorporated in a phenomenological way. Intrinsic life-time effects are described by a Lorentzian-broadening with an energy dependent width $\Gamma(\epsilon) = a + b(\epsilon - \epsilon_F)^2$. Instrumental broadening in turn is accounted by Gaussian broadening with a broadening parameter σ (for the spectra to be shown below the following parameters have been used: Fe: $a = 0.01$ eV, $b = 0.01$ eV⁻², $\sigma = 0.4$ eV; Co: $a = 0.01$ eV, $b = 0.01$ eV⁻², $\sigma = 0.2$ eV). In the case of high-energy angle-resolved VB-XPS the influence of finite life times has been represented by a Lorentzian broadening according to the kinetic energy of the final state ($\Gamma = 0.1$ eV, as calculated from the universal curve of electron attenuation length).

Within this approach correlation effects are represented by a complex localized self-energy $\Sigma(\epsilon)$ that enters the Kohn-Sham-Dirac equa-

tions (6.1) used to calculate the one-particle Green's function. Thus, the correlation effects are directly included into the scattering path operator $\tau_{\Lambda'\Lambda}^{nn}$ in Eq. (6.34), and therefore the correlation effects are accurately included in the VB-XPS calculations presented below. The correlation effects are treated in the framework of LSDA+DMFT using the FLEX version of the DMFT solver. Having some evidence that the LSDA+DMFT double-counting is rather small in $3d$ -transition metals, we take into account the purely dynamical correlations neglecting the static component of the self-energy.

6.3.3 Fano-effect in the VB-XPS of Fe and Co

The experimental VB-XPS intensities I and spin polarization ΔI_λ are calculated for a photon energy of 600 eV for Fe and Co, that have been normalized to have a maximum amplitude of 100, are summarized in Fig. 6.12, where the theoretical results based on the LSDA (dashed line) as well as LSDA+DMFT (straight line) are compared with experimental data [161]. The self-energy within the DMFT is calculated in terms of two parameters - averaged screened Coulomb interaction U and exchange interaction J . The screening of the exchange interaction is usually small and the value of J can be calculated directly and is approximately equal to 0.9 eV for all $3d$ elements. This value has been adopted for all our calculations presented here. For the value of U we used for Fe 2 eV and for Co 1.5 eV. As can be seen in Fig. 6.12 the theoretical results based on the LSDA (dashed line) for both metals are in fair agreement with the corresponding experimental data. This can be expected, as Fe and Co are considered to be weakly correlated systems. However, by including the corresponding self-energy calculated by means of the DMFT we obtain a considerable improvement for the spin averaged intensity I as well as the spin polarization ΔI_+ ; in particular in the case of Fe. For the total intensity I of Fe we observed essential improvement in the energy region -2 to -8 eV, where a quasi-particle satellite structure comparable to the well known 6 eV satellite of Ni is present. The observed double peak structure of the spin polarization ΔI_+ is shifted even more to lower energies. In addition a small but finite polarization is obtained in the region of high binding energy. In the case of Co the DMFT did not modify the obtained spectra as

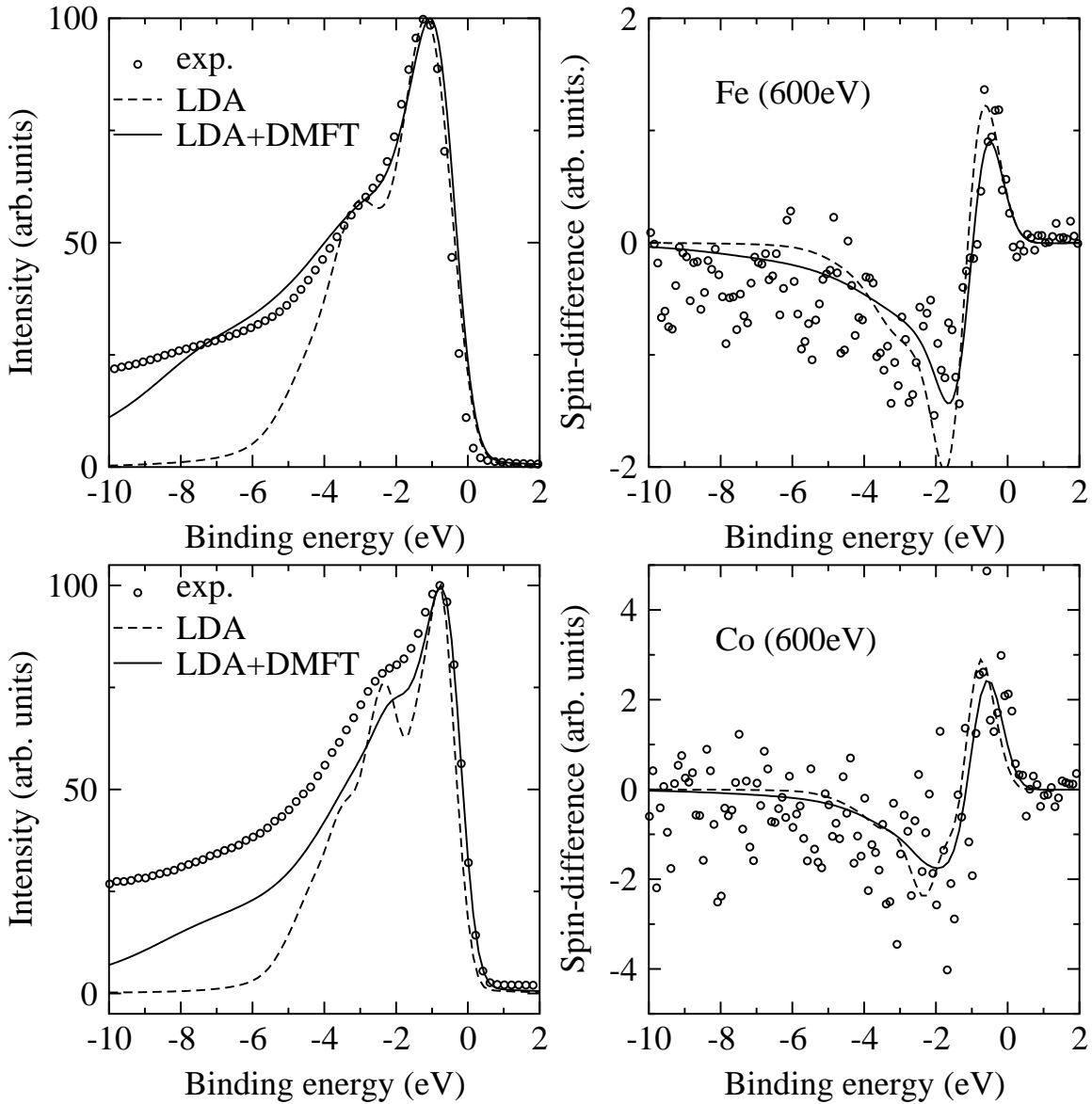


Fig. 6.12. Left: The experimental (dots) and theoretical data (LSDA - dashed line, LSDA+DMFT - full line) for spin and angle-integrated VB-XPS spectra of bcc-Fe and hcp-Co for a photon energy of 600 eV. Right: Spin-difference $\Delta I = I_{+}^{\uparrow} - I_{+}^{\downarrow}$ of the photocurrent for excitation with circularly polarized radiation. For the calculation of the electronic self-energy within DMFT we used $J=0.9$ eV and $U=2$ eV for bcc-Fe and $U=1.5$ eV for hcp-Co and the temperature $T=350$ K.

much as in the case of Fe.

6.3.4 High-energy angle-resolved VB-XPS of Ni

In the top panel of Fig. 6.13 we present the Bloch spectral functions $A(\mathbf{k}, \epsilon)$ in the $\Gamma - \Delta - X$ direction as calculated by means of the LSDA (left) and LSDA+DMFT (right), respectively. In the case of Ni there

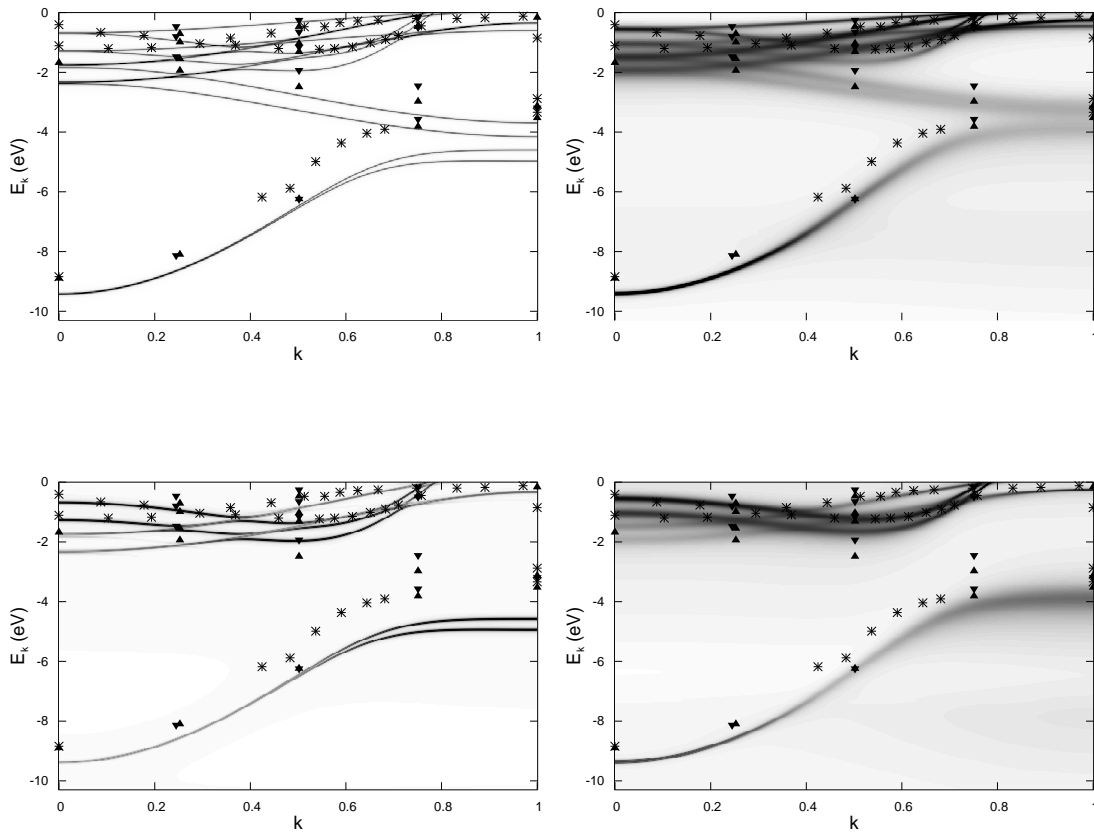


Fig. 6.13. Top: Bloch spectral functions $A(\mathbf{k}, \epsilon)$ in the $\Gamma - \Delta - X$ direction obtained within the LSDA (left) and LSDA+DMFT (right) schemes. Bottom: Angle-resolved VB-XPS spectrum of Ni for a photon energy of 600 eV, normal emission and the k -vector (in units of $2\pi/a$) oriented along the [001]-direction ($U=3.0$ eV, $J=0.9$ eV and $T=500$ K). The experimental data (marked by various symbols) are taken from Refs. [62, 162–164].

are three main correlation effects: narrowing of the occupied part of the d -band, decrease of the exchange splitting and presence of the famous 6 eV satellite compared to the LSDA calculations. The first two one

can clearly see in the corresponding theoretical data. The 6 eV satellite is clearly visible in the DOS curves (presented in Sec. 6.1.2) but obviously not in the \mathbf{k} -resolved Bloch spectral function for $\Gamma - X$ line. This reflects the anisotropy of the contributions to the 6 eV satellite in reciprocal space. The main contribution to the 6 eV satellite comes from the $\Gamma - K$ direction. However, the position of the 6 eV satellite is shifted to a slightly lower binding energies (7-8 eV). This shift and the large broadening of the resonance is normally attributed due to the perturbation approach of the DMFT solver used here.

As it follows the band structure calculated by LSDA+DMFT is in sound agreement with previous experimental data [62, 162–164]. The lower panel of Fig. 6.13 shows corresponding angle resolved VB-XPS spectra for a photon energy of 600 eV, normal emission and the \mathbf{k} vector oriented along the [001]-direction. One can clearly see the shift of the majority bands towards the Fermi level as a direct consequence of the real part of the self-energy. The imaginary part of the self-energy provides a noticeable broadening of the states. Because of the matrix elements (see Eq. 6.34) and the resulting selection rules, some bands are not observed in the theoretical spectrum. On the other hand, in comparison with Bloch spectral functions, the intensity is weighted by these matrix element.

6.3.5 High-energy angle-integrated VB-XPS of NiMnSb

Local correlation effects also substantially influence the formation of the peculiar two-peak structure of the high-energy angle-integrated VB-XPS spectrum of the half-metallic Heusler alloy NiMnSb which is not reproducible within the LSDA picture.

Indeed, as it follows from Fig. 6.14, the LSDA calculations for the photon energy 500 eV lead to three distinct peaks in the VB-XPS spectrum. On the other hand, as indicated by different studies on NiMnSb [166–168] this two-peak structure is always visible in the high-energy photoemission spectrum depending slightly on the film thickness, orientation of the surface and the account for the attenuation of x-rays within the solid.

Our calculations presented on Fig. 6.14 (left panel) show that the account of local correlations for the d -shell of Mn noticeably reduces

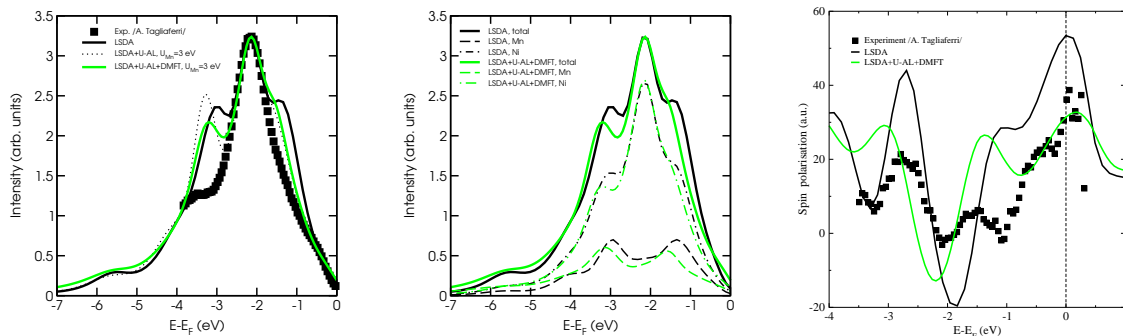


Fig. 6.14. Left panel: comparison of the VB-XPS spectrum calculated via the full-potential SPR-KKR method with experimental data (marked with black squares) measured at the photon energy $E_{\text{phot}}=500$ eV [165]. Solid black line corresponds to the plain LSDA result, dotted - LSDA+U-AL, solid light (green) - LSDA+U-AL+DMFT ($U_{\text{Mn}} = 3$ eV, $J_{\text{Mn}} = 0.9$ eV). Middle panel: decomposition of the calculated total VB-XPS spectra into Mn- (dashed line) and Ni-contributions (dot-dashed line). Right panel: comparison of the spin polarization.

the false high-energy peak introduced by LSDA in the VB-XPS spectrum at about 1.5 eV below the Fermi level. First of all it is reflected already in the LSDA+U result indicating the importance of static correlations. As we are interested in the shift of the total d -band of Mn we adopt the so-called atomic limit form (LSDA+U-AL) as was suggested before [168]. For the d -shell of Ni the account of correlations is not so important as it is mostly fully occupied. As it follows from Fig. 6.14, the further account of the dynamical correlations via the DMFT reduces the intensity of the low-energy peak in a proper way, however, its amplitude still remains relatively high compared to experiment.

As it follows from the middle panel of Fig. 6.14, the shift of the high-energy LSDA peak occurs mainly due to the shift of the Mn states away from the Fermi energy. At the same time a slight modification of the Ni states in comparison with the LSDA spectrum also takes place due to the hybridization with the Mn d -states which are affected by the account for correlations. Finally, the importance of self-consistency of the calculations should be stressed.

The right panel of Fig. 6.14 shows the comparison of the calculated spin polarization with experiment. As it follows, the account of correlations reduces the spin polarization value at the Fermi level calculated with LSDA bringing it to a very close agreement with experiment.

Chapter 7

Application to linear response theory

In this chapter we will consider the derivation of the linear response coefficients in terms of the one-particle Green's function. The derivation of the generalized response coefficients for the non-interacting electron gas within the Green's function approach can be found in [169].

7.1 Time-dependent perturbation theory

We consider the non-interacting electronic system described by the Hamiltonian H_0 and the density matrix ρ_0 . If we switch on a time dependent external perturbation $V(t)$, the Hamiltonian of the perturbed system is:

$$H(t) = H_0 + V(t). \quad (7.1)$$

Turning to the interaction picture which is best suited for time dependent perturbation theory, we have for the density matrix:

$$\rho^I(t) = e^{\frac{i}{\hbar}H_0t} \rho(t) e^{-\frac{i}{\hbar}H_0t} \quad (7.2)$$

together with the following equation of motion:

$$\frac{\partial}{\partial t} \rho^I(t) = -\frac{i}{\hbar} [V^I(t), \rho^I(t)] \quad (7.3)$$

which follows from the definition of ρ and the Schrödinger or Dirac equation [170]. If we switch on $V(t)$ adiabatically and integrate the resulting equation of motion (7.3) with respect to time imposing the

boundary condition $\rho^I(t)|_{t \rightarrow -\infty} = \rho_0$, we obtain, keeping the terms linear with respect to the perturbation:

$$\begin{aligned} \rho^I(t) &= \rho_0 - \frac{i}{\hbar} \int_{-\infty}^t dt_1 [V^I(t_1), \rho^I(t_1)] \\ &\approx \rho_0 - \frac{i}{\hbar} \int_{-\infty}^t dt_1 [V^I(t_1), \rho_0]. \end{aligned} \quad (7.4)$$

The time dependent expectation value for any local operator O which does not possess an explicit time dependency is calculated as follows:

$$\begin{aligned} \langle O \rangle(t) &= \text{Tr} \{ \rho^I(t) O^I(t) \} \\ &= \text{Tr} \{ \rho_0 O^I(t) \} - \frac{i}{\hbar} \int_{-\infty}^t dt_1 \text{Tr} \{ \rho_0 [O^I(t), V^I(t_1)] \}. \end{aligned} \quad (7.5)$$

Evaluating of the last term we have implicitly applied the cyclic invariance of the trace for each term. In general the perturbative potential dealt in response theory has the form:

$$V^I(t) = \sum_{\beta} B_{\beta}^I(t) F_{\beta}(t), \quad (7.6)$$

with \vec{F} the generalized vector force and \vec{B} the vector coupling operator. In the Schrödinger representation \vec{B} is not time dependent, while \vec{F} depends on time explicitly.

Considering the orthonormal single-particle basis $|n\rangle$ of electronic orbitals and the fermion creation and annihilation operators in the interaction representation

$$c_n^{I\dagger}(t) = c_n^{\dagger} e^{\frac{i}{\hbar}(\epsilon_n - \mu)t}, \quad c_n^I(t) = c_n e^{-\frac{i}{\hbar}(\epsilon_n - \mu)t}, \quad (7.7)$$

with μ the chemical potential, we obtain the following representation for O^I (and an analogous one for B_{β}^I):

$$O^I(t) = \sum_{nn'} O_{nn'} c_n^{I\dagger}(t) c_{n'}^I(t) = \sum_{nn'} O_{nn'} c_n^{\dagger} c_{n'} e^{i\omega_{nn'}t}, \quad (7.8)$$

with $O_{nn'} = \langle n | O | n' \rangle$ the matrix element in the basis of some suitable single-particle orbitals and $\omega_{nn'} = (\epsilon_n - \epsilon_{n'})/\hbar$. Also representing the F_β term using its Fourier transform

$$F_\beta(t_1) = \frac{1}{2\pi} \int_{-\infty}^{\infty} d\omega_1 F_\beta(\omega_1) e^{-i\omega_1 t_1} e^{0^+ t_1}, \quad (7.9)$$

where $e^{0^+ t_1}$ accounts for the adiabatic switching of the perturbation, we can rewrite the last term in Eq. (7.5) as:

$$\begin{aligned} \langle O \rangle^{(1)}(t) &= -\frac{i}{2\pi\hbar} \sum_{\beta, nn', mm'} O_{nn'} B_{\beta mm'} \text{Tr} \{ \rho_0 [c_n^\dagger c_{n'}, c_m^\dagger c_{m'}] \} \\ &\quad \times \int_{-\infty}^{\infty} d\omega_1 F_\beta(\omega_1) \int_{-\infty}^t dt_1 e^{i\omega_{nn'} t} e^{i\omega_{mm'} t_1} e^{-i\omega_1 t_1} e^{0^+ t_1}. \end{aligned} \quad (7.10)$$

To apply the Fourier transformation with respect to the time variable, we evaluate the Fourier transform of the second integral in Eq. (7.10) as

$$\begin{aligned} &\frac{1}{2\pi} \int_{-\infty}^{\infty} dt e^{i\omega t} \int_{-\infty}^t dt_1 e^{i\omega_{nn'} t} e^{i\omega_{mm'} t_1} e^{-i\omega_1 t_1} e^{0^+ t_1} \\ &= \frac{1}{2\pi} \int_{-\infty}^{\infty} dt e^{i\omega t} e^{i\omega_{nn'} t} \int_{-\infty}^0 dt_1 e^{i\omega_{mm'}(t_1+t)} e^{-i\omega_1(t_1+t)} e^{0^+(t_1+t)} \\ &= \frac{1}{2\pi} \int_{-\infty}^{\infty} dt e^{i(\omega + \omega_{nn'} + \omega_{mm'} - \omega_1 - i0^+)t} \int_{-\infty}^0 dt_1 e^{i(\omega_{mm'} - \omega_1 - i0^+)t_1} \\ &= \delta(\omega - \omega_1 + \omega_{nn'} + \omega_{mm'}) \frac{1}{\omega_{mm'} - \omega_1 - i0^+}. \end{aligned} \quad (7.11)$$

The expression for the trace operation in Eq. (7.10) we evaluate as follows:

$$\begin{aligned} &\text{Tr} \{ \rho_0 [c_n^\dagger c_{n'}, c_m^\dagger c_{m'}] \} \\ &= \text{Tr} \{ \rho_0 c_n^\dagger c_{m'} \} \delta_{mn'} - \text{Tr} \{ \rho_0 c_m^\dagger c_{n'} \} \delta_{nm'} \\ &= [\Theta_T(\epsilon_n - \mu) - \Theta_T(\epsilon_m - \mu)] \delta_{mn'} \delta_{m'n}, \end{aligned} \quad (7.12)$$

with $\Theta_T(\epsilon - \mu) = 1/(e^{\frac{\epsilon - \mu}{T}} + 1)$ being the Fermi function. Inserting Eqs. (7.11) and (7.12) into Eq. (7.10) we obtain the following expression for the expectation value:

$$\langle O \rangle^{(1)}(\omega) = \sum_{\beta} \int_{-\infty}^{\infty} d\omega_1 \sigma_{\beta}(\omega, \omega_1) F_{\beta}(\omega_1), \quad (7.13)$$

with σ_{β} the linear response coefficient defined as:

$$\begin{aligned} \sigma_{\beta}(\omega, \omega_1) = & \\ & \frac{i}{\hbar} \delta(\omega - \omega_1) \sum_{nm} [\Theta_T(\epsilon_n - \mu) - \Theta_T(\epsilon_m - \mu)] \\ & \times \frac{O_{nm} B_{\beta mn}}{\omega_1 - \omega_{mn} + i0^+}. \end{aligned} \quad (7.14)$$

The delta function $\delta(\omega - \omega_1)$ ensures that the linear component of the response $O^{(1)}$ has the same frequency as the perturbation. Thus we can consider $\sigma(\omega, \omega_1 = \omega)$ as a single-variable function:

$$\sigma_{\beta}(\omega) = i \sum_{nm} \frac{\Theta_T(\epsilon_n - \mu) - \Theta_T(\epsilon_m - \mu)}{\hbar\omega + \epsilon_n - \epsilon_m + i0^+} O_{nm} B_{\beta mn}. \quad (7.15)$$

Further we will be interested in the zero-temperature limit:

$$\Theta_{T=0}(\epsilon) = \begin{cases} 1, \epsilon \geq 0 \\ 0, \epsilon < 0 \end{cases}, \quad \mu_{T=0} = \epsilon_F, \quad (7.16)$$

which means, in particular, that the Θ function at $T = 0$ K does not have poles in the upper (and lower) complex semi-plane. Taking this into account we make use of the residue theorem applying it for the real axis path:

$$\begin{aligned} \frac{i\Theta(\epsilon_n - \epsilon_F)}{\epsilon_n - \epsilon_m + \hbar\omega + i0^+} &= -\frac{1}{\pi} \int_{-\infty}^{\infty} d\epsilon \frac{\Theta(\epsilon - \epsilon_F)}{(\epsilon - \epsilon_n)(\epsilon - \epsilon_m + \hbar\omega + i0^+)}, \\ \frac{i\Theta(\epsilon_m - \epsilon_F)}{\epsilon_n - \epsilon_m + \hbar\omega + i0^+} &= \frac{1}{\pi} \int_{-\infty}^{\infty} d\epsilon \frac{\Theta(\epsilon - \epsilon_F)}{(\epsilon - \epsilon_m)(\epsilon - \epsilon_n - \hbar\omega - i0^+)}. \end{aligned} \quad (7.17)$$

Inserting this in Eq. (7.15) we have:

$$\sigma_{\beta}(\omega) = -\frac{1}{\pi} \int_{-\infty}^{\infty} d\epsilon \Theta(\epsilon - \epsilon_{\text{F}}) \sum_{nm} O_{nm} B_{mn} \times \left[\frac{1}{(\epsilon - \epsilon_n)(\epsilon - \epsilon_m + \hbar\omega + i0^+)} + \frac{1}{(\epsilon - \epsilon_m)(\epsilon - \epsilon_n - \hbar\omega - i0^+)} \right]. \quad (7.18)$$

It is now straightforward to replace the manifold of initial and final states by the one-particle Green's function:

$$G(\epsilon) = \sum_n \frac{|n\rangle \langle n|}{\epsilon - \epsilon_n}. \quad (7.19)$$

Inserting Eq. (7.19) into Eq. (7.18) and implying $0^+ = 0$ we obtain:

$$\sigma_{\beta}(\omega) = -\frac{1}{\pi} \int_{-\infty}^{\epsilon_{\text{F}}} d\epsilon [\text{Tr} \{OG(\epsilon + \hbar\omega)B_{\beta}G(\epsilon)\} + \text{Tr} \{OG(\epsilon)B_{\beta}G(\epsilon - \hbar\omega)\}], \quad (7.20)$$

with $\text{Tr} \{ \}$ the trace over the single particle basis states $|n\rangle$.

7.2 Optical conductivity

In the presence of an external vector potential $\vec{A}(\mathbf{r}, t)$ the time dependent perturbation of the electronic system is given as:

$$V(t) = -\frac{1}{c} \int d^3r \vec{J}(\mathbf{r}) \vec{A}(\mathbf{r}, t), \quad (7.21)$$

with $\vec{J}(\mathbf{r})$ the current density. According to Eq. (7.6) we identify \vec{A} with the generalized vector force and \vec{J} with the vector coupling operator. Applying this to calculate the time dependent expectation value of the current density operator $\langle \vec{J}(\mathbf{r}) \rangle(\omega)$ using Eqs. (7.13) and (7.20), we obtain the following expression for the corresponding linear response

coefficient:

$$\begin{aligned} \sigma_{\alpha\beta}(\mathbf{r}, \mathbf{r}', \omega) &= \frac{1}{\pi c} \int_{-\infty}^{\epsilon_F} d\epsilon \\ &\times [\text{Tr} \{J_\alpha(\mathbf{r})G(\epsilon + \hbar\omega)J_\beta(\mathbf{r}')G(\epsilon)\} \\ &+ \text{Tr} \{J_\beta(\mathbf{r}')G(\epsilon)J_\alpha(\mathbf{r})G(\epsilon - \hbar\omega)\}]. \end{aligned} \quad (7.22)$$

Considering the Coulomb interaction as instantaneous, we use the Coulomb gauge for $\vec{A}(\mathbf{r}, t)$: $\vec{E}(\mathbf{r}, t) = -(1/c)\frac{\partial}{\partial t}\vec{A}(\mathbf{r}, t)$ with \vec{E} the external electric field. This leads to

$$\vec{A}(\mathbf{r}, \omega) = \frac{c}{i\omega}\vec{E}(\mathbf{r}, \omega). \quad (7.23)$$

Identifying now \vec{E} with the vector force, we renormalize accordingly the coefficient in Eq. (7.22) as

$$\begin{aligned} \sigma_{\alpha\beta}(\mathbf{r}, \mathbf{r}', \omega) &= -\frac{i}{\pi\omega} \int_{-\infty}^{\epsilon_F} d\epsilon \\ &\times [\text{Tr} \{J_\alpha(\mathbf{r})G(\epsilon + \hbar\omega)J_\beta(\mathbf{r}')G(\epsilon)\} \\ &+ \text{Tr} \{J_\beta(\mathbf{r}')G(\epsilon)J_\alpha(\mathbf{r})G(\epsilon - \hbar\omega)\}]. \end{aligned} \quad (7.24)$$

which is called the non-local optical conductivity. As it follows, for $\omega = 0$, i.e. in the static case, it diverges for pure ordered systems. As an analytical function it can be partitioned into hermitian or *absorptive* and antihermitian or *dispersive* components, which are connected with each other by Kramers-Kronig relations (3.35). For example, the absorptive part $\sigma_{\alpha\beta}^{(1)}$ of $\sigma_{\alpha\beta}$ in Eq. (7.24) is given by:

$$\sigma_{\alpha\beta}^{(1)}(\mathbf{r}, \mathbf{r}', \omega) = \frac{1}{\pi\omega} \int_{-\infty}^{\epsilon_F} d\epsilon \text{Tr} \{J_\alpha(\mathbf{r})\text{Im} G(\epsilon)J_\beta(\mathbf{r}')\text{Im} G(\epsilon + \hbar\omega)\}, \quad (7.25)$$

where $\text{Im} G$ stands for the antihermitian component of the Green's function.

As we will restrict ourselves in the following to the bulk systems with translational symmetry, we will be interested in the spatially averaged

optical conductivity, since the spatial variations of \vec{A} are rather small compared to the unit cell dimension:

$$\sigma_{\alpha\beta}^{(1)}(\omega) = \frac{1}{V} \int d^3r \int d^3r' \sigma(\mathbf{r}, \mathbf{r}', \omega) \quad (7.26)$$

Since the expression (7.26) is derived in terms of the one-particle Green's function, the assumption of non-interacting electrons made above can be ignored by applying Eq. (7.26) using the interacting one-particle Green's function derived as a solution of the corresponding Dyson equation (3.11).

The optical conductivity tensor can be considered as the central quantity which being determined once, can be used to obtain all the other optical and magneto-optical properties of the system. In particular, for the small complex Kerr angle, which combines the Kerr rotation θ_K and ellipticity ε_K , the following approximate expression can be used [171]:

$$\theta_K(\omega) + i\varepsilon_K \approx -\frac{\sigma_{xy}(\omega)}{\sigma_{xx}(\omega) \sqrt{1 + \frac{4\pi i}{\omega} \sigma_{xx}(\omega)}}. \quad (7.27)$$

Being the real and imaginary parts of a complex analytical function, the quantities θ_K and ε_K are in turn, connected by Kramers-Kronig relations (see Eq. (3.35)). In the analysis of the complex Kerr rotation spectrum it is sufficient to consider in details only the real part of the MOKE spectrum, i.e. the rotation, as the Kerr ellipticity is a related quantity.

In the calculations presented below for the magneto-optical Kerr effect (MOKE) the spin-orbit coupling which is together with exchange splitting the actual source of MOKE is taken into account via the second-variation technique.

7.3 Green's function within the variational basis formalism: implementation in the LMTO method

Despite the straightforward way to calculate the one-particle Green's function with the so-called Korringa-Kohn-Rostoker (KKR) Green's

function method, in the present work we utilize the wave function basis formalism [99] which with respect to the optical calculations has several advantages as it will be clear in the following.

Within this approach the one-particle basis functions we use to represent the Green's function are *energy-independent*. Taking into account the translational symmetry explicitly, the corresponding expression for the absorptive part of optical conductivity (7.26) reads:

$$\sigma_{\alpha\beta}^{(1)}(\omega) = \frac{1}{\pi\omega} \int d^3k \int_{-\infty}^{\hbar\omega} d\epsilon \sum_{nn'} M_{nn'}^{\alpha}(\mathbf{k}, \epsilon) M_{n'n}^{\beta}(\mathbf{k}, \epsilon + \hbar\omega), \quad (7.28)$$

with the corresponding spectral weighted matrix element:

$$M_{nn'}^{\alpha}(\mathbf{k}, \epsilon) = \sum_m G_{nm}(\mathbf{k}, \epsilon) \langle m_{\mathbf{k}} | J^{\alpha} | n'_{\mathbf{k}} \rangle, \quad (7.29)$$

where G_{nm} is the Green's function matrix represented in the energy-independent single-orbital basis:

$$\begin{aligned} G(\epsilon) &= \sum_{\mathbf{k}, nm} |n_{\mathbf{k}}\rangle G_{nm}(\mathbf{k}, \epsilon) \langle m_{\mathbf{k}}| \\ &= \sum_{\mathbf{k}, nm} |n_{\mathbf{k}}\rangle \langle n_{\mathbf{k}}| (\epsilon + \Sigma(\epsilon) - H_0)^{-1} |m_{\mathbf{k}}\rangle \langle m_{\mathbf{k}}|. \end{aligned} \quad (7.30)$$

The advantage of the expression (7.28) is that it implies that for each pair of energies ϵ and $\epsilon + \hbar\omega$ just the traces have to be calculated.

The efficiency and accuracy of the calculations is determined by the choice of the basis functions $|n\rangle$. One of the computationally most efficient variational methods developed to be applied to the solid state is the so-called Linear Muffin-Tin Orbitals (LMTO) method [172, 173] which allows one to get a rather accurate description of the valence/conduction band in the range of about 1 Ry, which is enough for the calculations of the optical spectra ($\hbar\omega < 6 - 8$ eV).

A test of the scheme presented is represented on Fig. 7.1 which shows results for different modes of calculation. The optical conductivity spectra calculated via Eq. (7.28) is compared with that obtained using the standard wave function scheme:

$$\sigma_{\alpha\beta}(\omega) = \frac{1}{\pi} \int d^3k \sum_{nm} \delta(\epsilon_n - \epsilon_m - \hbar\omega) \langle n_{\mathbf{k}} | J_{\alpha} | m_{\mathbf{k}} \rangle \langle m_{\mathbf{k}} | J_{\beta} | n_{\mathbf{k}} \rangle. \quad (7.31)$$

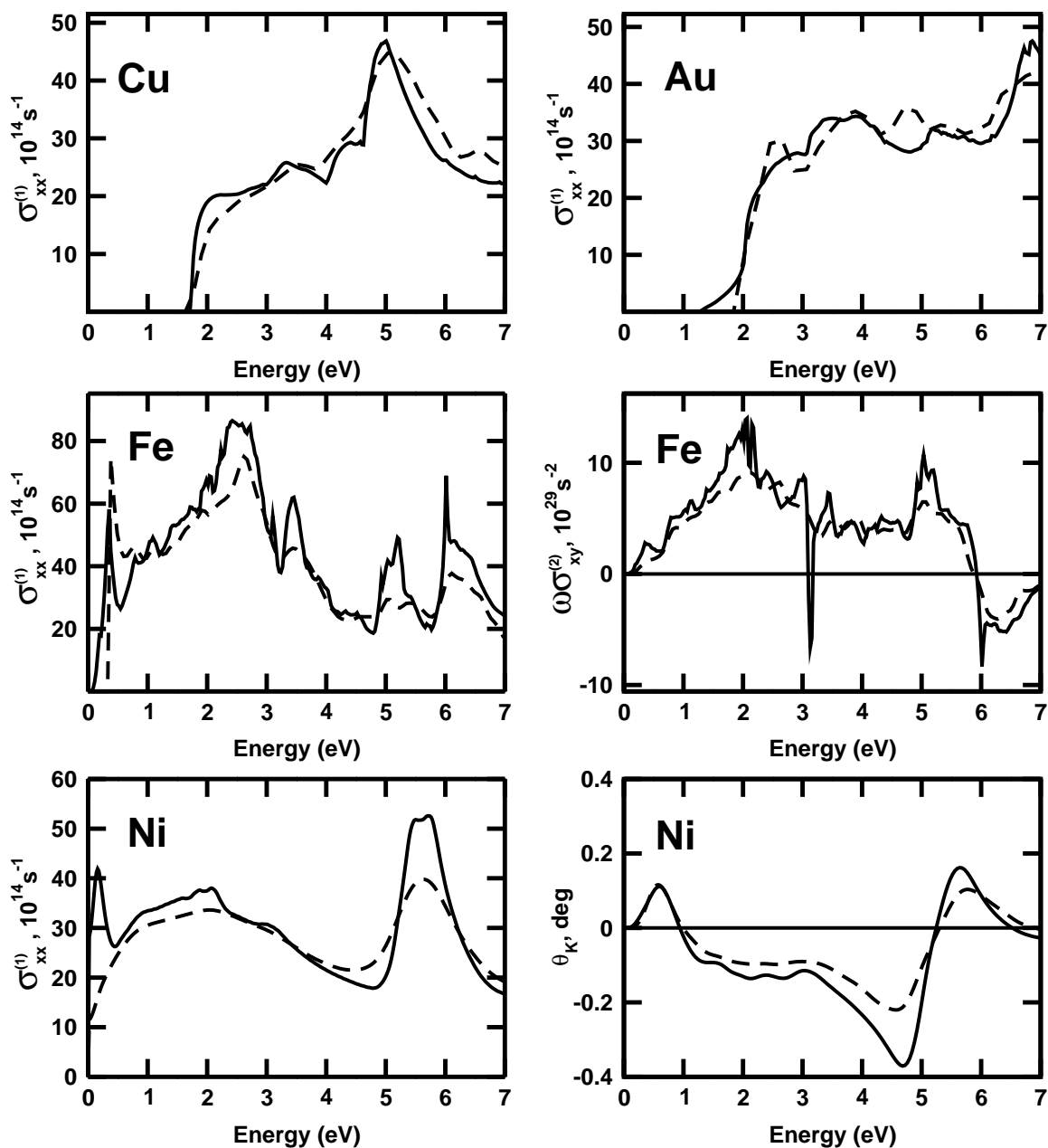


Fig. 7.1. Absorptive part of the optical conductivity calculated via the standard wave function approach (WF) (Eq. (7.31)) (solid line) and via the Green's function (GF) (Eq. (7.28)) (dashed line) with $\text{Im } \Sigma = 0.01 \text{ Ry}$ for different systems. Cu: non-spin-polarized semi-relativistic, Au: non-spin-polarized fully relativistic, Fe, Ni: spin-polarized fully-relativistic. In addition, the off-diagonal component of the optical conductivity for Fe and the Kerr rotation spectrum for Ni are shown.

For a zero self-energy both approaches are equivalent though for the present scheme it is impossible to carry out the calculations exactly on the real axis because of the divergence of the expression in the second line of Eq. (7.28). However the introduction of the small imaginary offset $i0^+$ leads to a mixing of an interband and intraband contributions to the optical conductivity. Thus to compare the results we subtract from Eq. (7.28) a Drude-like term which can be expressed as

$$\sigma(\omega) = \sigma(0) \frac{\gamma^2}{\omega^2 + \gamma^2}, \quad (7.32)$$

with $\gamma = 2i0^+$ and

$$\sigma(0) = \frac{1}{\pi} \int d^3k \sum_{mn} M_{nm}^\alpha(\mathbf{k}, \epsilon_F) M_{mn}^\beta(\mathbf{k}, \epsilon_F). \quad (7.33)$$

As it follows for all the systems there is a very satisfying agreement between these two approaches. In particular the results for Fe and Ni ensure the applicability of the approach to deal with spin-orbit induced magneto-optical properties.

7.4 Accounting for localized correlations

The next step concerning the implementation of the DMFT is to use the available data for the localized non-local self-energy and to investigate its influence on the results for the optical conductivity and magneto-optical spectra. The simplest non-local self-energy appears in the LSDA+U formalism, where the corresponding matrix elements are real and energy independent. Such a simple form allows one again to use directly the standard wave-function formalism to calculate the optical conductivity on the basis of the self-consistent potential including the 1st-order electron correlation corrections. The corresponding calculations are performed for the rather simple case of hcp Gd for which is found a very satisfying agreement between the approaches based on Eqs. (7.31) and (7.28) [99].

In order to include the full perturbation series, i.e. the dynamical self-energy, all what we need is the energy dependence of the non-local

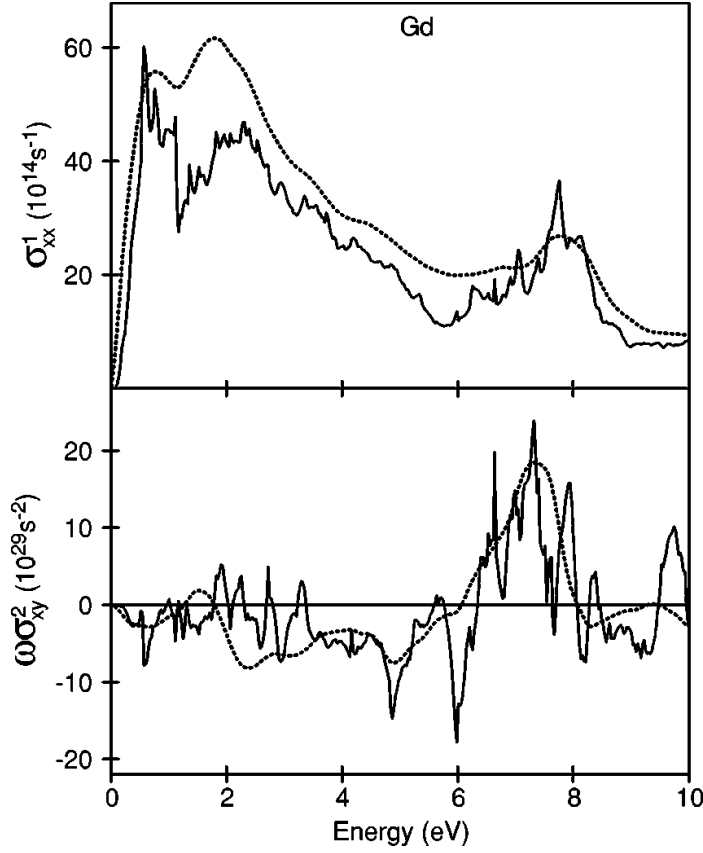


Fig.7.2. The diagonal (upper panel) and the off-diagonal (lower panel) components of the absorptive part of the optical conductivity for Gd calculated within the LSDA+U approach. Solid line: using the standard LMTO wave function scheme (Eq. (7.31)), dashed line: via the LMTO-Green's function approach (Eq. (7.28)) with $\text{Im} \Sigma = 0.01 \text{ Ry}$.

self-energy $\Sigma_{\Lambda\Lambda'}(\mathbf{r}_{\mathbf{R}}, \mathbf{r}'_{\mathbf{R}}, \epsilon)$, $\Lambda = \{\sigma lm\}$ which implies the special form similar to that given in Eq. (6.3):

$$\Sigma_{\Lambda\Lambda'}(\mathbf{r}_{\mathbf{R}}, \mathbf{r}'_{\mathbf{R}}, \epsilon) = \phi_{\Lambda}(\mathbf{r}_{\mathbf{R}}, \epsilon) \Sigma_{\Lambda\Lambda'}^{\mathbf{R}}(\epsilon) \phi_{\Lambda'}(\mathbf{r}'_{\mathbf{R}}, \epsilon), \quad (7.34)$$

where $\phi_{\Lambda}(\mathbf{r}, \epsilon)$ stands for the solution of the Schrödinger equation with the \mathbf{R} -centered LSDA potential, normalized to unity within an atomic cell.

The handling of the expression (7.34) can substantially be simplified in the framework of the LMTO method by making use of the energy-independent basis functions

$$\phi_{\Lambda\mathbf{R}}^{\mathbf{k}}(\mathbf{r}) = \Phi_{\Lambda}^{\mathbf{h}}(\mathbf{r} - \mathbf{R}) + \sum_{\Lambda'\mathbf{R}'} h_{\Lambda\mathbf{R},\Lambda'\mathbf{R}'}^{\mathbf{k}} \Phi_{\Lambda'}^{\mathbf{t}}(\mathbf{r} - \mathbf{R}'), \quad (7.35)$$

which perfectly fits to any single-site approximation of the self-energy. The superscripts "h" and "t" stand for the so-called "head" and "tail" parts of the basis functions.

In the framework of the DMFT one can formally introduce the self-energy operator which is expressed in the form:

$$\begin{aligned} \Sigma(\mathbf{r}, \mathbf{r}', \epsilon) &= \sum_{\mathbf{R}\mathbf{R}'} \delta_{\mathbf{R}\mathbf{R}'} \sum_{\Lambda\Lambda'} \Theta(|\mathbf{r} - \mathbf{R}|) Y_{\Lambda}^*(\mathbf{r} - \mathbf{R}) \\ &\times \Sigma_{\Lambda\Lambda'}^{\mathbf{R}}(\mathbf{r}, \mathbf{r}', \epsilon) \Theta(|\mathbf{r}' - \mathbf{R}'|) Y_{\Lambda'}(\mathbf{r}' - \mathbf{R}'), \end{aligned} \quad (7.36)$$

where $\Theta(r) = 1$ if \mathbf{r} is inside the atomic sphere and zero otherwise. Due to the special construction of the LMTO basis functions (7.35) only the "head" component will give a significant contribution being projected on the localized area restricted to the single-site. Thus, in terms of the "head" functions the matrix elements of the self-energy operator (7.36) get an extremely simple \mathbf{k} -independent representation:

$$\begin{aligned} \langle \phi_{\Lambda\mathbf{R}}^{\mathbf{k}} | \Sigma(\epsilon) | \phi_{\Lambda'\mathbf{R}'}^{\mathbf{k}} \rangle &\approx \int d^3r \int d^3r' \\ &\times \Phi_{\Lambda}^{\mathbf{h}*}(\mathbf{r} - \mathbf{R}) \Sigma_{\Lambda\Lambda'}^{\mathbf{R}}(\mathbf{r}, \mathbf{r}', \epsilon) \Phi_{\Lambda'}^{\mathbf{h}}(\mathbf{r}' - \mathbf{R}). \end{aligned} \quad (7.37)$$

The self-energy (7.37) is used to calculate the interacting Green's function via the Dyson equation (3.11) which is treated within the variational formalism as:

$$G_{\Lambda\Lambda'}^{\mathbf{k}}(\epsilon) = [O^{\mathbf{k}} \cdot \epsilon - H_0^{\mathbf{k}} + \Sigma(\epsilon)]_{\Lambda\Lambda'}^{-1}, \quad (7.38)$$

where H_0 and O are the LSDA Hamiltonian and overlap matrices represented within the energy-independent basis functions $\phi_{\Lambda}^{\mathbf{k}}(\mathbf{r})$.

The accuracy of this approach is restricted to the discussion given above to Figs. 7.1 and 7.2 ensuring that the error in determining of the corresponding Green's function is substantially smaller than the approximations made for the estimation of the self-energy itself [99].

The presented so-called LMTO-Green's function (LMTO-GF) approach does not include charge self-consistency in the way discussed earlier self-consistent for the KKR+DMFT scheme or the other variational-based one, presented in Ref. [174]. The reason is that due to a construction of the energy-dependent quantities as the Green's function and the self-energy on each iteration, the main advantage of the LMTO method, namely the speed of calculations, would be substantially reduced. On the other hand, this scheme can be combined with the fully self-consistent KKR+DMFT calculation which accurately

delivers the corresponding self-energy that in turn can be used to construct the LMTO Green's function.

Thus, within the present approach, the influence of the localized effects on the optical conductivity tensor occurs due to the change of the Green's function matrix elements (Eq. (7.30)) only, while the current-density elements will not be affected. Another possible source of the influence could be the change of the occupation numbers, and also the change of the Fermi energy. However, due to the Fermi-liquid properties of the dynamical self-energy these changes are expected to be of minor importance and the changes in the optical conductivity tensor can be straightforwardly attributed to the corresponding modifications in the one-particle spectrum. This leads in particular to the conclusion that the account of localized correlations modifies only the interband part of the optical conductivity, while the intraband contribution (Eq. (7.32)) determined by the Green's function at the Fermi level, remains unchanged.

7.5 Applications to 3d-transition metal systems

A first example demonstrating the applicability of the presented approach is bulk fcc Ni. The corresponding calculated optical conductivity, Kerr rotation and Kerr ellipticity spectra are shown in Fig. 7.3. As it is obvious, in spite of the various approximations discussed above the results are drastically improved by the inclusion of the dynamical self-energy, demonstrating the surprisingly good agreement with experiment both for the optical conductivity and the MOKE spectra.

Kerr-rotation spectra have received in particular broad interest because of the discovery of the giant magneto-optical Kerr effect (MOKE) in PtMnSb [178]. Thus, the magneto-optical properties of the Mn-based family of Heusler alloys became an important technological issue [175, 179–186]. However, despite of their similar structure, the group of iso-electronic alloys PtMnSb, NiMnSb and PdMnSb show quite different maximum amplitudes in their MOKE spectra [178, 175]. A theoretical description of the observed difference of the MOKE spectra became possible within *ab-initio* band-structure calculations [187, 184, 186]. However, although the various calculated MOKE spectra give reasonable

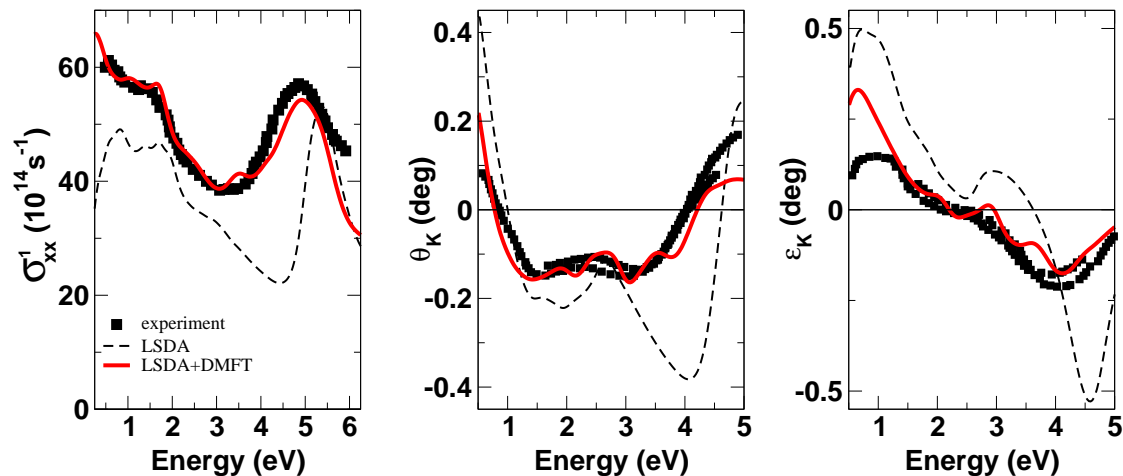


Fig. 7.3. Optical and magneto-optical properties of fcc Ni calculated using the LMTO–Green’s function approach. Right panel: absorptive part of the optical conductivity, middle: Kerr rotation, left: Kerr ellipticity. The black dashed line marks the LSDA, the red (light) solid line the LSDA+DMFT calculations. Black squares stand for the experimental data found in [175–177]. The self-energy was taken from the self-consistent KKR+DMFT calculations with $U = 3$ eV, $J = 0.9$ eV.

qualitative agreement with experiment, one can notice that there exist several systematic discrepancies generally ascribed to the use of LSDA. The following example of the NiMnSb Heusler alloy demonstrates that a much better description can be obtained by improving the treatment of the localized many-body correlations.

In the case of NiMnSb the main contribution to the optical transitions comes from the d -shell of Mn which supplies the unoccupied part of the density of states (DOS). At the same time d -electrons of Mn should be treated as locally-correlated [188]. Based on this supposition one can expect an improvement for the MO spectra in NiMnSb by an appropriate account of localized correlation effects for the Mn d -shell in band-structure calculations.

The comparison between the MO spectra of NiMnSb calculated within LSDA, LSDA+DMFT and the experimental results is shown in Fig. 7.4. As it follows, the account of localized correlations is very important to describe correctly the positions as well as the magnitudes of both low- and high-energy Kerr rotation peaks (situated at 1.4 eV and 4 eV). Again as in the previous example for pure Ni the modifications of the Kerr spectrum are related to the corresponding modifications in

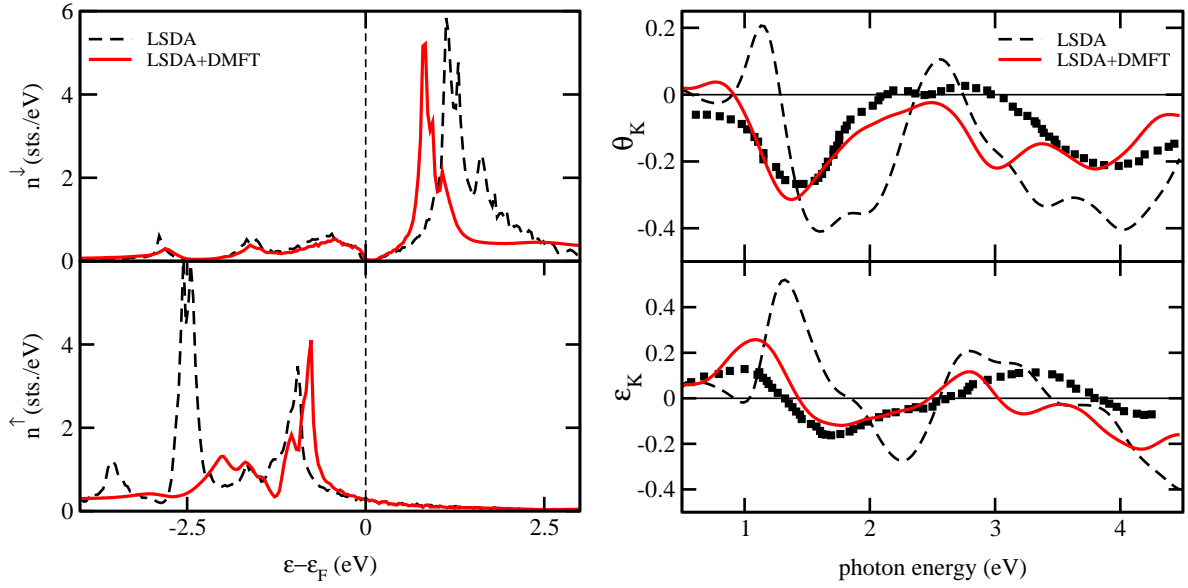


Fig. 7.4. DOS and magneto-optical spectra of NiMnSb calculated using LMTO-Green's function approach. Right panel shows the d-DOS of Mn, left panel: the complex Kerr rotation spectra: upper - Kerr rotation, lower - Kerr ellipticity. Black dashed line marks the LSDA, red (light) solid line - the LSDA+DMFT calculations. Black squares stand for the experimental data found in [175, 178]. The self-energy was taken from the self-consistent KKR+DMFT calculations with $U = 3$ eV, $J = 1$ eV.

the DOS of Mn (right panel on Fig. 7.4) which is in turn related to the dynamical self-energy spectrum shown on Fig. 7.5. One can see, that the Mn d -shell indeed experiences noticeable dynamical correlations as indicated by the amplitudes up to 4 eV of the imaginary self-energy component. For the Ni shell it is not so important to account for correlations as it is almost fully occupied. The effective Coulomb interaction is parameterized for these calculations by $U = 3$ eV and $J = 0.9$ eV. Numerical tests show that approximately the same results are obtained within the range of $U = 3 \pm 0.5$ eV.

Finally, one can conclude, that the correct description of the magneto-optical properties of both systems Ni and NiMnSb can be given only within the proper account of the 2nd-order dynamical correlations, while the 1st-order contributions and the DC can be completely neglected. The spin-flip blocks of the self-energy and the localized Green's function matrices also can be neglected due to the relatively small spin-orbit coupling.

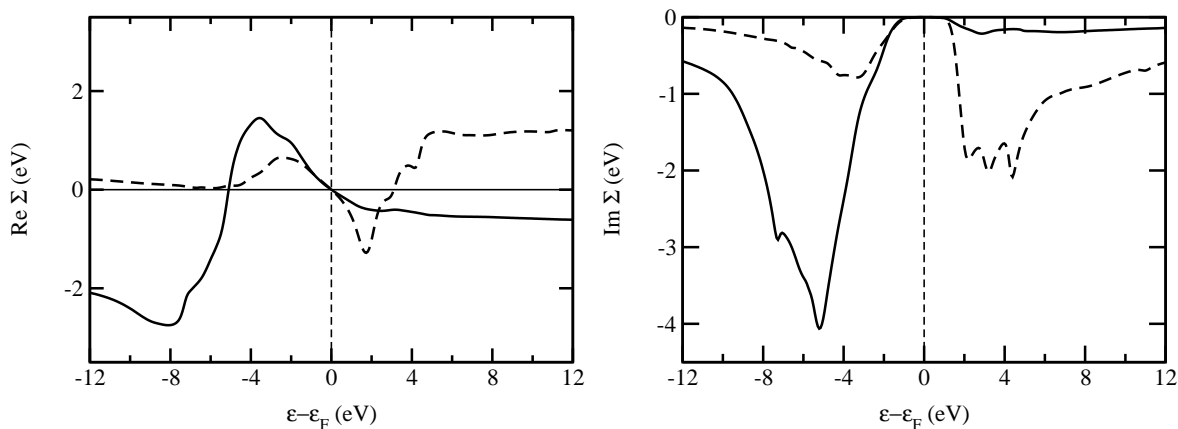


Fig. 7.5. Spin-resolved dynamical self-energy for the Mn atom within bulk NiMnSb obtained from self-consistent KKR+DMFT calculations. Right panel: real component, left panel: imaginary component. Solid and broken lines correspond to majority and minority spin components.

7.6 Application to heavy-fermion systems

It is well known that $5f$ electrons are to be made responsible for the variety of unusual physical properties in actinide compounds [189–196]. Particularly, this shows up in the magneto-optical properties of U monochalcogenides and monoptictides which have unusually large Kerr rotation spectra. One of the most difficult cases are US [190] and UN [196] which are commonly classified to be itinerant with strong localized correlations. Whereas LSDA+U calculations substantially improve the optical conductivity spectrum, they are still far from giving an appropriate result for the MOKE. As was indicated by Kraft *et al.* [190], the reason could be in the dynamical nature of the optical excitations. Here we are going to examine the optical conductivity and MOKE spectra of US metal by applying our dynamical perturbational scheme as complementary to the LSDA+U approach with AL-DC as suggested in Ref. [193]. Of course, the perturbative approach is not the best way to treat strong correlations in metals, since the high-order channels possess a significant importance and the result can substantially deviate depending on where one makes a truncation. However the qualitative information delivered by perturbational treatment may in turn, provide a more or less well defined basis concerning further studies.

The plain LSDA+U-AL results accounting for the 1st-order corre-

lations for the f -shell are shown in Fig. 7.6. As it follows, the account

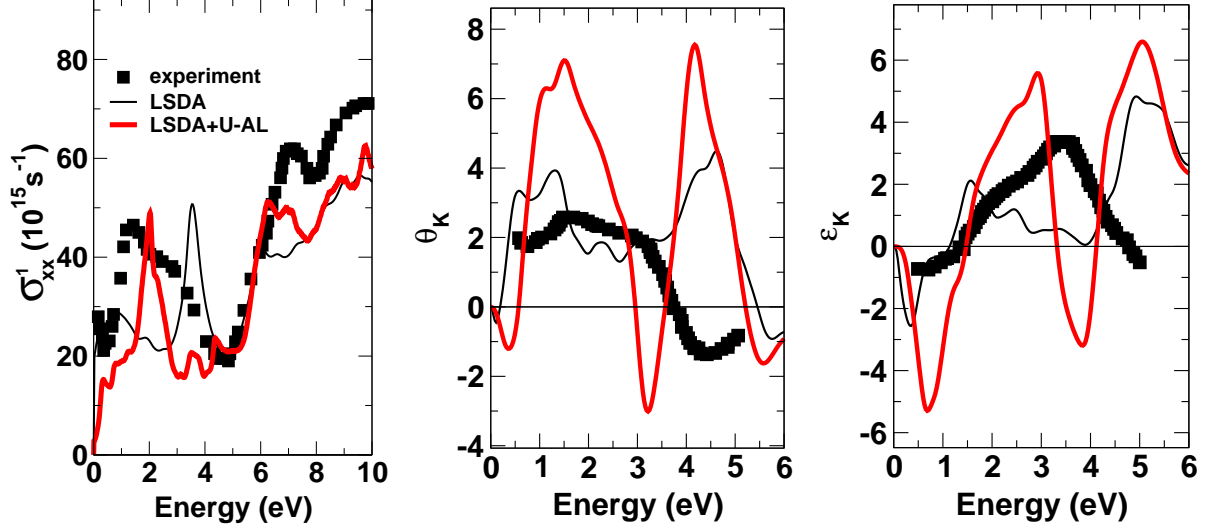


Fig. 7.6. Optical and magneto-optical spectra of US calculated using the LMTO-Green's function approach within the LSDA+U-AL approach with $U=2$ eV, $J=0.9$ eV. Right panel: absorptive part of the optical conductivity, middle: Kerr rotation, left: Kerr ellipticity. The black full line marks the LSDA, red (light) LSDA+U-AL. The black squares mark the experimental data given in Ref. [197].

of static contributions already lead to substantial modifications of both the optical conductivity and the Kerr spectra. In particular, one notices that the 3 eV peak falsely positioned due to the LSDA in the optical spectrum is shifted to the proper position with respect to the experimental one. On the other hand, the large overestimation of the MOKE amplitudes indicates the possible importance of higher-order contributions.

Indeed, as it follows from Fig. 7.7 the account of the 2nd-order channels noticeably reduces the amplitudes of the MOKE and also improves the high- and low-energy regimes in the optical conductivity spectra in comparison with the LSDA+U-AL results.

It is instructive in addition to figure out the influence of the spin-flip elements of the self-energy on the optical and MOKE spectra which are expected to be large due to the strong spin-orbit coupling. Fig. 7.8 demonstrate the comparison of the results obtained with and without account of the spin-flip self-energy matrix elements. As it follows, when the spin-flip terms are not taken into account the result possesses in-

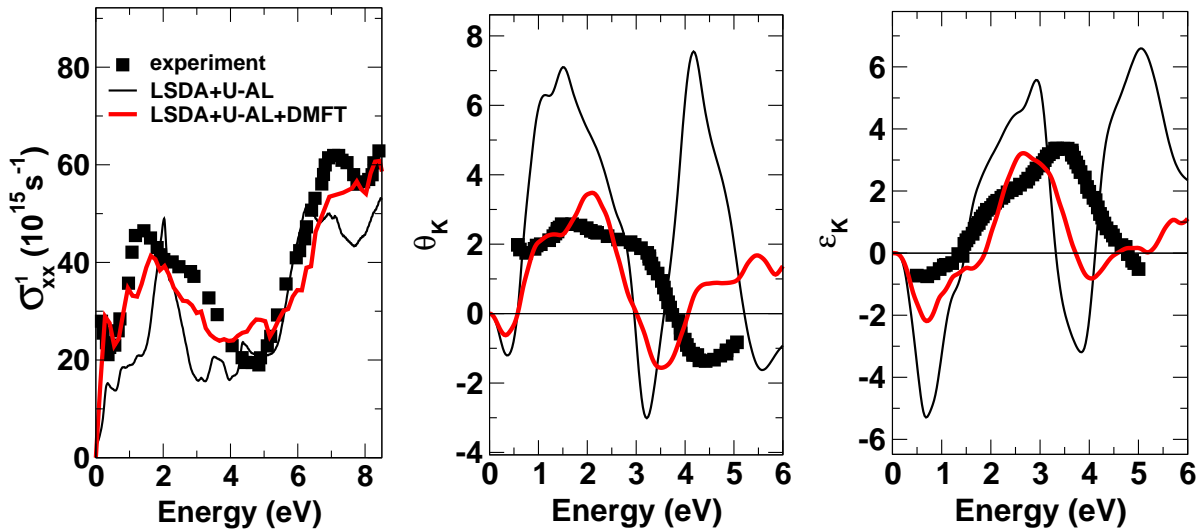


Fig. 7.7. Optical and magneto-optical spectra of US calculated using LMTO-Green's function approach within the LSDA+U-AL+DMFT approach with $U=2$ eV, $J=0.9$ eV. Right panel: absorptive part of the optical conductivity, middle: Kerr rotation, left: Kerr ellipticity. The black full line marks the LSDA+U, red (light) - LSDA+U-AL+DMFT. The black squares mark the experimental data given in Ref. [197].

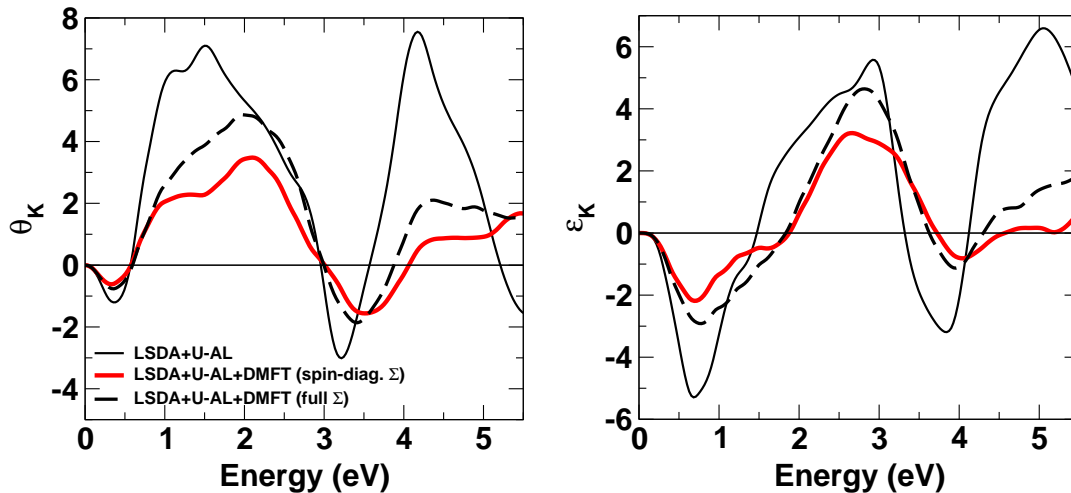


Fig. 7.8. MOKE spectra for US (right panel: Kerr rotation, left: Kerr ellipticity) calculated by the LMTO-Green's function approach. The full black line marks LSDA+U-AL results, filled red (light) - LSDA+U-AL+DMFT and the dashed line - LSDA+U-AL+DMFT with spin-flip self-energy elements set to zero. For all types of calculations $U=2$ eV, $J=0.9$ eV has been used.

interpolative behavior between LSDA+U and the full LSDA+U+DMFT spectra, noticeably deviating from both. Thus, in contrast to the $3d$ transition metals, the account of the full self-energy matrix is important for correlated actinide systems.

Despite of the general quantitative improvement, the proper description of the optical properties in the U compounds obviously requires a more accurate treatment of correlations as well as the re-examining of all the approximations made in the calculational scheme, since each of them may become a significant factor in case of a strongly correlated metal. Since the optical spectra are determined by the relative positions and widths of the p - d - and f -shells the need of the self-consistency in order to account for all the necessary hybridization effects has to be stressed. For example, the oscillator model analysis of the UN optical spectra delivers the $2p$ -shell of N as centered at -6 eV below the Fermi energy [196], whereas in the LSDA (LSDA+U) calculations it corresponds roughly to -3 eV. The analogous situation holds for US compound. Studying these aspects in details is believed to close the remaining gap between experiment and theory.

Chapter 8

Summary

According to the main goal of the present thesis, an efficient computational LSDA+DMFT toolbox for the description of correlated materials has been established. As it could be demonstrated, the method developed in this work provides an appropriate description of $3d$ -transition metal correlated bulk systems, concerning their ground-state properties (magnetic moments, total energies) as well as the high- and low-energy spectroscopies (valence-band angular-resolved photoemission, Fano-effect, optical and magneto-optical properties).

As it was demonstrated the incorporation of the perturbational impurity solvers within the spin-polarized relativistic Korringa-Kohn-Rostoker (SPR-KKR) Green's function method gives rise to a fully self-consistent procedure with respect both to the DFT (charge) and the DMFT (localized dynamical self-energy) self-consistency requirements. To our knowledge this approach is one of the first and very few fully self-consistent LSDA+DMFT implementations. Thus, the solution of the many-electron problem can be achieved with a high precision. In turn this opens a possibility to investigate very delicate properties, as was demonstrated for the example of the orbital magnetic moments of Fe, Co and Ni.

Moreover, the SPR-KKR method allows to investigate the disordered systems on the basis of the so-called Coherent Potential Approximation (CPA). This in turn was used to improve the LSDA description of the orbital magnetic moments in the disordered $\text{Co}_x\text{Fe}_{1-x}$ alloys and Fe- and Co-impurities in Au host.

Being based on the multiple-scattering formalism, the SPR-KKR

method have direct access to a description of high-energy spectroscopies. As it was shown in this work, the self-consistent account of localized correlation effects within the SPR-KKR explains the features of the angle-resolved valence-band photoemission spectra for Ni as well as of the angle-integrated photoemission spectra and the Fano-effect for Fe and Co, inaccessible to a plain LSDA treatment.

To develop a relatively fast and accurate approach for the low-energy spectroscopies, the DMFT was implemented within the wave function formalism in the framework of the Linearized Muffin-Tin Orbitals method (LMTO) which reliably describes the band structure in the range of 1 Ry around the linearization point. To retain the speed of calculations several approximations have been made in this scheme. Namely, the calculations are performed in a one-shot run, that does not allow to get the charge-self-consistent solution. In such a way all effects of the localized correlations are encapsulated in the Green's function constructed as a resolvent to the LMTO one-particle Hamiltonian and accounting for the corresponding self-energy via the Dyson equation. The self-energy could be either calculated on the basis of the LSDA LMTO Green's function (in this way it does not account for the self-consistency of the DMFT) or, if better precision is required it could be taken from a separate self-consistent calculation, as for example, from the KKR+DMFT.

As it was demonstrated for pure bulk Ni, the optical and Kerr-rotation and ellipticity spectra calculated within the LMTO+DMFT approach are in excellent agreement with experiment. On the other hand, due to the high speed of the calculations, the scheme can be applied to a much more complex systems containing many atoms per unit cell. As it follows from the presented work, the LMTO+DMFT scheme gives in comparison to a plain LSDA a significantly improved description of the magneto-optics (Kerr rotation and ellipticity spectra) in the half-metallic Heusler ferromagnet NiMnSb, which due to the large amplitude of the Kerr effect is considered as an important technological material.

In addition, the LMTO+DMFT approach was applied to the description of the optical conductivity and magneto-optical spectra in the heavy-fermion US compound. US and similar compounds are well known for a variety of their unusual physical properties which are com-

pletely inaccessible within an LSDA description. That is why, in particular the study of their optical and magneto-optical spectra, for a long time remains an issue of broad scientific interest. The qualitative agreement with the corresponding experimental spectra gives justification for the applicability of the perturbational impurity solvers even for such a strongly-correlated material. However, the reason for a noticeable deviations from experimental data cannot be uniquely distinguished yet. Nevertheless, it is demonstrated that the additional account of the localized dynamical correlations leads to a noticeable improvement of the magneto-optical as well as of the optical spectra in comparison to the LSDA+U approach which accounts for the static correlations only. Another interesting feature of these calculations is that they show the importance to account for the full dynamical self-energy matrix including the spin-flip elements, due to a large spin-orbit coupling in this material.

The developments presented in this work in principle can be exploited and developed in a several directions. First of all this concerns the fully self-consistent KKR+DMFT scheme. As we have mentioned above, any other impurity solver accounting for a specific type of the many-electron interaction can be used. One can think as well about the combination of different solvers, such as e.g. perturbational one and the QMC. Second, as we also have mentioned, the whole DMFT scheme could be extended by expanding the localization area to the cluster of atoms which gives an opportunity to account for \mathbf{k} -dependent dynamical correlations.

The LMTO+DMFT scheme also can be extended to account for \mathbf{k} -dependent dynamical correlations retaining the speed of calculations. This is possible by simply utilizing the corresponding self-energy calculated separately within the cluster version of the DMFT, GWA or some other approach. In particular, a description of the optical properties of high- T_C superconductor cuprates could be given by applying the \mathbf{k} -dependent self-energy describing the non-local dynamical correlations induced by short-ranged collective antiferromagnetic spin fluctuations [106].

Bibliography

- [1] J. Hubbard, Proc. Roy. Soc. A **276**, 238 (1963).
- [2] N. F. Mott, *Metal-insulator transitions* (Taylor & Francis Ltd, London, 1990).
- [3] P. W. Anderson, Phys. Rev. **124**, 41 (1961).
- [4] S. Caprara, M. Avington, and O. Navarro, Phys. Rev. B **61**, 15667 (2000).
- [5] R. Micnas, J. Ranniger, and S. Robaszkiewicz, Rev. Mod. Phys. **62**, 113 (1990).
- [6] A. S. Blaer, H. C. Ren, and O. Tchernyshyov, Phys. Rev. B **55**, 6035 (1997).
- [7] E. H. Lieb, Phys. Rev. Letters **62**, 1201 (1989).
- [8] M. C. Gutzwiller, Phys. Rev. Letters **10**, 159 (1963).
- [9] L. M. Roth, Phys. Rev. **184**, 451 (1969).
- [10] W. Noltig and W. Borguel, Phys. Rev. B **39**, 6962 (1989).
- [11] F. Mancini, S. Marra, and H. Matsumoto, Physica C **244**, 49 (1995).
- [12] L. P. Kadanoff and G. Baym, *Quantum Statistical Mechanichs* (Benjamin, New York, 1962).
- [13] P. Hohenberg and W. Kohn, Phys. Rev. **136**, B 864 (1964).
- [14] W. Kohn and L. J. Sham, Phys. Rev. **140**, A 1133 (1965).

-
- [15] L. J. Sham and W. Kohn, Phys. Rev. **145**, 561 (1966).
- [16] L. Hedin, Phys. Rev. **139**, A796 (1965).
- [17] M. S. Hybertsen and S. G. Louie, Phys. Rev. B **34**, 5390 (1986).
- [18] V. I. Anisimov, J. Zaanen, and O. K. Andersen, Phys. Rev. B **44**, 943 (1991).
- [19] M. T. Czyzyk and G. A. Sawatzky, PRB **49**, 14211 (1994).
- [20] A. Georges and G. Kotliar, Rev. Mod. Phys. **68**, 13 (1996).
- [21] A. Georges, G. Kotliar, W. Krauth, and M. J. Rozenberg, Rev. Mod. Phys. **68**, 13 (1996).
- [22] V. I. Anisimov, A. I. Poteryaev, M. A. Korotin, A. O. Anokhin, and G. Kotliar, J. Phys.: Condensed Matter **9**, 7359 (1997).
- [23] I. A. Nekrasov, K. Held, N. Blumer, A. I. Poteryaev, V. I. Anisimov, and D. Vollhardt, European Physical Journal B **18**, 55 (2000).
- [24] P. W. Anderson, Nobel Lecture (1977).
- [25] J. E. Hirsch and R. M. Fye, Phys. Rev. Letters **56**, 2521 (1986).
- [26] M. Jarrel, Phys. Rev. Letters **69**, 168 (1992).
- [27] V. Drchal, V. Janis, J. Kudrnovsky, V. S. Oudovenko, X. Dai, K. Haule, and G. Kotliar, J. Phys.: Condensed Matter **17**, 61 (2005).
- [28] G. H. Wannier, Phys. Rev. **52**, 191 (1937).
- [29] W. Kohn, Phys. Rev. **115**, 809 (1959).
- [30] G. Laughlin, M. R. Woodward, and A. T. Amos, Intern. J. Quantum. Chem. **8**, 491 (1974).
- [31] N. Nagaosa, *Quantum field theory in strongly correlated solids* (Springer-Verlag, Berlin, 1999).
- [32] L. D. Landau, Sov. Phys.–JETP **30**, 1058 (1956).

-
- [33] L. Landau, Sov. Phys.–JETP **32**, 59 (1957).
- [34] H. Bruus and K. Flensberg, *Many-body quantum theory in condensed matter physics* (Copenhagen, 2002).
- [35] D. H. Kobe, Annals of Physics **75**, 9 (1973).
- [36] A. L. Fetter and J. D. Walecka, *Quantum theory of many-particle systems* (McGraw-Hill, New York, 1971).
- [37] G. D. Mahan, *Many-Particle Physics* (Plenum, New York, 1990).
- [38] D. J. Scalapino and R. L. Sugar, Phys. Rev. Letters **46**, 519 (1981).
- [39] A. N. Rubtsov and A. I. Lichtenstein, JETP Letters **80**, 61 (2004).
- [40] G. Baym and L. P. Kadanoff, Phys. Rev. **124**, 287 (1961).
- [41] G. Baym, Phys. Rev. **127**, 1391 (1962).
- [42] J. M. Luttinger and J. C. Ward, Phys. Rev. **118**, 1417 (1960).
- [43] J. Schwitalla, *Einfluß der Elektron-Loch-Wechselwirkung auf die Röntgenabsorption in 3d-Metallen*, Ph.D. thesis, University of München (1997).
- [44] N. E. Bickers and D. J. Scalapino, Ann. Phys. (NY) **193**, 206 (1989).
- [45] A. I. Lichtenstein and M. I. Katsnelson, Phys. Rev. B **57**, 6884 (1998).
- [46] M. Katsnelson and A. Lichtenstein, Journal of Physics: Condensed Matter **11**, 1037 (1999).
- [47] L. V. Pourovskii, M. I. Katsnelson, and A. I. Lichtenstein, Phys. Rev. B **72**, 115106 (2005).
- [48] A. D. Poularikas, ed., *The Transforms and Applications Handbook* (CRC Press LLC, USA, 2000).
- [49] S. Y. Savrasov and G. Kotliar, Phys. Rev. B **69**, 245101 (2004).

-
- [50] W. Metzner and D. Vollhardt, Phys. Rev. Letters **62**, 324 (1989).
- [51] M. Potthoff and W. Nolting, Z. Physik B **104**, 265 (1997).
- [52] A. Georges, *Strongly correlated fermions and bosons in low-dimensional disordered systems* (Kluwer Academic Publishers, Dodrecht, 2002), vol. 72 of *NATO Science Series-II: Mathematics, Physics and Chemistry*.
- [53] O. Gunnarsson and R. O. Jones, Physica Scripta **21**, 394 (1980).
- [54] R. M. Dreizler and E. K. U. Gross, *Density Functional Theory* (Springer-Verlag, Heidelberg, 1990).
- [55] R. G. Parr and W. Yang, *Density-Functional Theory of Atoms and Molecules* (University Press, Oxford, 1989).
- [56] U. von Barth and L. Hedin, J. Phys. C: Solid State Phys. **5**, 1629 (1972).
- [57] O. Gunnarsson and B. I. Lundqvist, Phys. Rev. B **13**, 4274 (1976).
- [58] D. Ceperley and B. J. Alder, Phys. Rev. Letters **45**, 566 (1980).
- [59] S. H. Vosko, L. Wilk, and M. Nusair, Can. J. Phys. **58**, 1200 (1980).
- [60] J. P. Perdew and A. Zunger, Phys. Rev. B **23**, 5048 (1981).
- [61] J. P. Perdew and Y. Wang, Phys. Rev. B **45**, 13244 (1993).
- [62] V. L. Moruzzi, J. F. Janak, and A. R. Williams, *Calculated Electronic Properties of Metals* (Pergamon, New York, 1978).
- [63] J. P. Perdew and Y. Wang, Phys. Rev. B **33**, 8800 (1986).
- [64] J. P. Perdew, K. Burke, and M. Ernzerhof, Phys. Rev. Letters **78**, 1396(E) (1997).
- [65] J. B. Krieger, Y. Li, and G. F. Iafrate, Phys. Rev. A **47**, 165 (1993).
- [66] E. Engel and S. H. Vosko, Phys. Rev. A **47**, 2800 (1993).

-
- [67] T. Grabo and E. K. U. Gross, *Int. J. Quant. Chem.* **64**, 95 (1997).
- [68] T. Kotani, *Phys. Rev. Letters* **74**, 2989 (1995).
- [69] Y. Kim, M. Städele, and R. Martin, *Phys. Rev. A* **60**, 3633 (1999).
- [70] A. Svane and O. Gunnarsson, *Phys. Rev. Letters* **72**, 1248 (1994).
- [71] Z. Szotek, W. M. Temmerman, and H. Winter, *Phys. Rev. Letters* **72**, 1244 (1994).
- [72] M. Arai and T. Fujiwara, *Phys. Rev. B* **51**, 1477 (1995).
- [73] P. Strange, A. Svane, W. M. Temmermann, Z. Szotek, and H. Winter, *Nature* **399**, 756 (1999).
- [74] O. Gunnarsson, M. Jonson, and B. I. Lundqvist, *Phys. Rev. B* **20**, 3136 (1979).
- [75] O. Gunnarsson and K. Schönhammer, *Phys. Rev. Letters* **56**, 1968 (1986).
- [76] B. Brandow, *Adv. Phys.* **26**, 651 (1977).
- [77] K. Attenkofer, S. Stähler, M. Knülle, P. Fischer, G. Schütz, G. Wiesinger, and B. Scholz, *J. Appl. Physics* **73**, 6910 (1993).
- [78] A. Liechtenstein, V. Anisimov, and J. Zaanen, *Phys. Rev. B* **52**, R5467 (1995).
- [79] V. I. Anisimov and O. Gunnarsson, *Phys. Rev. B* **43**, 7570 (1991).
- [80] V. Drchal, O. Gunnarson, and O. Jepsen, *Phys. Rev. B* **44**, 3518 (1991).
- [81] M. S. S. Brooks, *Physica B* **130**, 6 (1985).
- [82] O. Eriksson, B. Johansson, and M. S. S. Brooks, *J. Phys.: Condensed Matter* **1**, 4005 (1989).
- [83] O. Eriksson, M. S. S. Brooks, and B. Johansson, *Phys. Rev. B* **41**, 7311 (1990).

-
- [84] S. Y. Savrasov, G. Kotliar, and E. Abrahams, *Nature* **410**, 793 (2001).
- [85] J. Bouchet, B. Siberchicot, F. Jollet, and A. Pasturel, *J. Phys.: Condensed Matter* **12**, 1723 (2000).
- [86] G. Kotliar and D. Vollhardt, *Physics Today* **57**, 53 (2004).
- [87] G. Kotliar, S. Y. Savrasov, K. Haule, V. S. Oudovenko, O. Parcollett, and C. A. Marianetti, *Rev. Mod. Phys.* **78**, 865 (2006).
- [88] R. Fukuda, T. Kotani, Y. Suzuki, and S. Yokojima, *Prog. Theor. Phys.* **92**, 833 (1994).
- [89] R. Chitra and G. Kotliar, *Phys. Rev. B* **62**, 12715 (2000).
- [90] T. Moriya, *Spin fluctuations in itinerant electron magnetism* (Springer-Verlag, Berlin, 1985).
- [91] K. Held, A. K. McMahan, and R. T. Scalettar, *Phys. Rev. Letters* **87**, 276404 (2001).
- [92] M. Katsnelson and A. Lichtenstein, *Phys. Rev. B* **61**, 8906 (2000).
- [93] A. I. Lichtenstein and M. I. Katsnelson, *Phys. Rev. Letters* **87**, 067205 (2001).
- [94] A. Petukhov, I. Mazin, L. Chioncel, and A. I. Lichtenstein, *Phys. Rev. B* **67**, 153106 (2003).
- [95] J. Braun, J. Minár, H. Ebert, M. I. Katsnelson, and A. I. Lichtenstein, *Phys. Rev. Letters* **97**, 227601 (2006).
- [96] M. S. Laad, L. Craco, and E. Müller-Hartmann, *Phys. Rev. Letters* **91**, 156402 (2003).
- [97] M. I. Katsnelson and A. I. Lichtenstein, *European Physics Journal B* **30**, 9 (2002).
- [98] J. Minár, H. Ebert, C. de Nadaï, N. B. Brookes, F. Venturini, G. Ghiringhelli, L. Chioncel, A. I. Lichtenstein, and M. I. Katsnelson, *Phys. Rev. Letters* **95**, 166401 (2005).

-
- [99] A. Perlov, S. Chadov, and H. Ebert, *Phys. Rev. B* **68**, 245112 (2003).
- [100] A. Perlov, S. Chadov, H. Ebert, L. Chioncel, A. Lichtenstein, and M. Katsnelson, *Ab initio calculations of the optical and magneto-optical properties of moderately correlated systems: accounting for correlation effects* (Kluwer Academic, Dordrecht, Boston, London, 2004), p. 161, Mathematics, Physics and Chemistry.
- [101] S. Chadov, J. Minár, H. Ebert, A. Perlov, L. Chioncel, M. I. Katsnelson, and A. I. Lichtenstein, *Phys. Rev. B* **74**, 140411(R) (2006).
- [102] M. H. Hettler, M. Mukherjee, M. Jarrell, and H. R. Krishnamurty, *Phys. Rev. B* **61**, 12739 (2000).
- [103] T. Maier, M. Jarrell, T. Pruschke, and J. Keller, *European Journal of Physics B* **13**, 613 (2000).
- [104] G. Kotliar, *Open problems in strongly correlated electron systems* (Kluwer Academic Publishers, Dordrecht, 2001), vol. 72 of *NATO Science Series-II: Mathematics, Physics and Chemistry*, pp. 325–336.
- [105] T. Maier, M. Jarrell, T. Pruschke, and M. H. Hettler, *Rev. Mod. Phys.* **77**, 1027 (2005).
- [106] M. V. Sadovskii, I. A. Nekrasov, E. Z. Kuchinskii, T. Pruschke, and V. I. Anisimov, *Phys. Rev. B* **72**, 155105 (2005).
- [107] V. Anisimov, F. Aryasetiawan, and A. Lichtenstein, *J. Phys.: Condensed Matter* **9**, 767 (1997).
- [108] L. Chioncel, M. Katsnelson, R. A. de Groot, and A. Lichtenstein, *Phys. Rev. B* **68**, 144425 (2003).
- [109] B. L. Györfy, *Phys. Rev. B* **5**, 2382 (1972).
- [110] G. Rickayzen, *Green's functions and condensed matter* (Academic Press, London, 1984), p. xxx.
- [111] J. S. Faulkner and G. M. Stocks, *Phys. Rev. B* **21**, 3222 (1980).

-
- [112] P. Weinberger, *Electron Scattering Theory for Ordered and Disordered Matter* (Oxford University Press, Oxford, 1990).
- [113] J. Minár, L. Chioncel, A. Perlov, H. Ebert, M. I. Katsnelson, and A. I. Lichtenstein, *Phys. Rev. B* **72**, 45125 (2005).
- [114] A. H. MacDonald and S. H. Vosko, *J. Phys. C: Solid State Phys.* **12**, 2977 (1979).
- [115] M. V. Ramana and A. K. Rajagopal, *J. Phys. C: Solid State Phys.* **12**, L845 (1979).
- [116] M. E. Rose, *Relativistic Electron Theory* (Wiley, New York, 1961).
- [117] H. Ebert and B. L. Györffy, *J. Phys. F: Met. Phys.* **18**, 451 (1988).
- [118] X. Wang, X.-G. Zhang, W. H. Butler, G. M. Stocks, and B. N. Harmon, *Phys. Rev. B* **46**, 9352 (1992).
- [119] H. J. Vidberg and J. W. Serene, *J. Low Temp. Phys.* **29**, 179 (1977).
- [120] H. Ebert, P. Strange, and B. L. Györffy, *J. Phys. (Paris)* **49**, 31 (1988).
- [121] S. Frotta-Pessôa, *Phys. Rev. B* **69**, 104401 (2004).
- [122] H. Ebert, M. Battocletti, and E. K. U. Gross, *Europhys. Lett.* **40**, 545 (1997).
- [123] H. Eschrig, M. Sargolzaei, K. Koepernik, and M. Richter, *Europhysics Letters* **72**, 611 (2005).
- [124] M. Sargolzaei, *Orbital Polarization in Relativistic Density Functional Theory*, Ph.D. thesis, Fakultät Mathematik und Naturwissenschaften der Technischen Universität Dresden (2006).
- [125] P. Söderlind, O. Eriksson, B. Johansson, R. C. Albers, and A. M. Boring, *Phys. Rev. B* **45**, 12911 (1992).
- [126] H. Ebert and M. Battocletti, *Solid State Commun.* **98**, 785 (1996).

-
- [127] W. D. Brewer, A. Scherz, C. Sorg, H. Wende, K. Baberschke, P. Bencok, and S. Frotta-Pessôa, *Phys. Rev. Letters* **93**, 077205 (2004).
- [128] P. Gambardella, S. Rusponi, M. Veronese, S. S. Dhesi, C. Grazioli, A. Dallmeyer, I. Cabria, R. Zeller, P. H. Dederichs, K. Kern, C. Carbone, and H. Brune, *Science* **300**, 1130 (2003).
- [129] B. Nonas, I. Cabria, R. Zeller, P. H. Dederichs, T. Huhne, and H. Ebert, *Phys. Rev. Letters* **86**, 2146 (2001).
- [130] I. V. Solovyev, A. I. Liechtenstein, and K. Terakura, *Phys. Rev. Letters* **80**, 5758 (1998).
- [131] I. V. Solovyev, *Phys. Rev. Letters* **95**, 267205 (2005).
- [132] M. B. Stearns, *Magnetic properties of 3d, 4d and 5d Elements, Alloys and Compounds* (Landolt-Börnstein, Berlin, 1984), vol. III/19a of *New Series*.
- [133] A. Scherz, *Spin-dependent X-ray Absorption Spectroscopy of 3d Transition Metals: Systematics and Applications*, Ph.D. thesis, University of Berlin (2003).
- [134] C. T. Chen, Y. U. Idzerda, H. J. Lin, N. V. Smith, G. Meigs, E. Chaban, G. H. Ho, E. Pellegrin, and F. Sette, *Phys. Rev. Letters* **75**, 152 (1995).
- [135] S. Biermann, F. Aryasetiawan, and A. Georges, *Phys. Rev. Letters* **90**, 086402 (2003).
- [136] N. E. Dahlen and U. von Barth, *J. Chem. Phys.* **120**, 6826 (2004).
- [137] N. E. Dahlen, R. van Leeven, and U. von Barth, *Phys. Rev. A* **73**, 012511 (2006).
- [138] J. Braun, *New developments in UP- and XP-spectroscopy from ferromagnetic materials, in Band-Ferromagnetism* (Springer Verlag, xxx, 2001), p. 341, *Lecture Notes in Physics*.
- [139] R. O. Jones and O. Gunnarson, *Rev. Mod. Phys.* **61**, 689 (1989).

-
- [140] W. Kohn and P. Vashishta (Plenum, New York, 1983), p. 79.
- [141] C. O. Almbladh and U. von Barth (Plenum, New York, 1985), p. 209.
- [142] G. Borstel, *Appl. Physics A* **38**, 193 (1985).
- [143] H. Ebert, in *Electronic Structure and Physical Properties of Solids*, edited by H. Dreyssé (Springer, Berlin, 2000), vol. 535 of *Lecture Notes in Physics*, p. 191.
- [144] U. Fano, *Phys. Rev.* **184**, 250 (1969).
- [145] Z. Hussain, E. Umbach, J. J. Barton, J. G. Tobin, and D. A. Shirley, *Phys. Rev. B* **25**, 672 (1982).
- [146] A. Sekiyama and S. Suga, *J. Electron. Spectrosc. Relat. Phenom.* **137-140**, 681 (2004).
- [147] T. Claesson, M. Mansson, C. Dallera, F. Venturini, C. D. Nadai, N. B. Brookes, and O. Tjernberg, *Phys. Rev. Letters* **93**, 136402 (2004).
- [148] A. Sekiyama, H. Fujiwara, S. Imada, S. Suga, H. Eisaki, S. I. Uchida, K. Takegahara, H. Harima, Y. Saitoh, I. A. Nekrasov, G. Keller, D. E. Kondakov, *et al.*, *Phys. Rev. Letters* **93**, 156402 (2004).
- [149] S.-K. Mo, H.-D. Kim, J. W. Allen, G.-H. Gweon, J. D. Denlinger, J.-H. Park, A. Sekiyama, A. Yamasaki, S. Suga, P. Metcalf, and K. Held, *Phys. Rev. Letters* **93**, 076404 (2004).
- [150] S. Suga, A. Shigemoto, A. Sekiyama, S. Imada, A. Yamasaki, A. Irizawa, S. Kasai, Y. Saitoh, T. Muro, N. Tomita, K. Nasu, H. Eisaki, *et al.*, *Phys. Rev. B* **70**, 155106 (2004).
- [151] B. Ackermann and R. Feder, *J. Phys. C: Solid State Phys.* **18**, 1093 (1985).
- [152] B. Ginatempo, P. J. Durham, B. L. Györfy, and W. M. Temmerman, *Phys. Rev. Letters* **54**, 1581 (1985).

-
- [153] H. Ebert and J. Schwitalla, Phys. Rev. B **55**, 3100 (1997).
- [154] P. Strange, J. Phys.: Condensed Matter **6**, L491 (1994).
- [155] B. Ackermann and R. Feder, Solid State Commun. **54**, 1077 (1985).
- [156] P. J. Feibelman and D. E. Eastman, Phys. Rev. B **10**, 4932 (1974).
- [157] H. Ebert and G. Y. Guo, J. Magn. Magn. Materials **148**, 174 (1995).
- [158] T. Scheunemann, S. V. Halilov, J. Henk, and R. Feder, Solid State Commun. **91**, 487 (1994).
- [159] T. Jarlborg and P. O. Nilson, J. Phys. C: Solid State Phys. **12**, 265 (1979).
- [160] H. Winter, P. J. Durham, and G. M. Stocks, J. Phys. F: Met. Phys. **14**, 1047 (1984).
- [161] J. Minár, S. Chadov, H. Ebert, L. Chioncel, A. Lichtenstein, C. de Nadaï, and N. B. Brookes, Nucl. Inst. Meth. Phys. Res. A **547**, 151 (2005).
- [162] F. J. Himpsel, J. A. Knapp, and D. E. Eastman, Phys. Rev. B **19**, 2919 (1979).
- [163] H. Møartensson and P. O. Nilsson, Phys. Rev. B **30**, 3047 (1984).
- [164] J. Büneemann, F. Gebhard, T. Ohm, R. Umstätter, S. Weiser, W. Weber, R. Claessen, D. Ehm, A. Harasawa, A. Kakizaki, A. Kimura, G. Nikolay, *et al.*, Europhys. Lett. **61**, 667 (2003).
- [165] A. Tagliaferri, unpublished .
- [166] J. S. Kang, J. H. Hong, S. W. Jung, Y. P. Lee, J. G. Park, C. G. Olson, S. J. Youn, and B. I. Min, Solid State Commun. **88**, 653 (1993).
- [167] J. S. Correa, C. Eibl, G. Rangelov, J. Braun, and M. Donath, Phys. Rev. B **73**, 125316 (2006).

-
- [168] M. I. Katsnelson, V. Y. Irkhin, L. Chioncel, A. I. Lichtenstein, and R. A. de Groot, *cond-mat* (2007).
- [169] T. Huhne, *Magneto-optical Kerr effect of multilayer and surface layer systems*, Ph.D. thesis, University of Munich (2001).
- [170] F. Schwabl, *Quantenmechanik* (Springer, Berlin, 1993).
- [171] J. L. Erskine and E. A. Stern, *Phys. Rev. B* **12**, 5016 (1975).
- [172] O. K. Andersen, *Phys. Rev. B* **12**, 3060 (1975).
- [173] H. L. Skriver, *The LMTO-method* (Springer, Berlin, 1983).
- [174] F. Lechermann, A. Georges, A. Poteryaev, S. Biermann, M. Posternak, A. Yamasaki, and O. K. Andersen, *Phys. Rev. B* **74**, 125120 (2006).
- [175] P. G. van Engen, Ph.D. thesis, Technical Univ. of Delft (1983).
- [176] M. Shiga and G. P. Pells, *J. Phys. C: Solid State Phys.* **2**, 1847 (1969).
- [177] K. Nakajima, H. Sawada, T. Katayama, and T. Miyazaki, *Phys. Rev. B* **54**, 15950 (1996).
- [178] P. G. van Engen, K. H. J. Buschow, R. Jongebreur, and M. Erman, *Appl. Physics Lett.* **42**, 202 (1983).
- [179] R. Ohyama, T. Koyanagi, and K. Matsubara, *J. Appl. Physics* **61**, 2347 (1987).
- [180] P. P. J. van Engelen, D. B. de Mooij, J. H. Wijngaard, and K. H. J. Buschow, *J. Magn. Magn. Materials* **130**, 247 (1994).
- [181] J. van Ek and J. M. Maclaren, *Phys. Rev. B* **56**, R2924 (1997).
- [182] M. C. Kautzky and B. M. Clemens, *Appl. Physics Lett.* **66**, 1279 (1995).
- [183] P. M. Oppeneer, V. N. Antonov, T. Kraft, H. Eschrig, A. N. Yaresko, and A. Y. Perlov, *Solid State Commun.* **94**, 255 (1995).

-
- [184] V. N. Antonov, P. M. Oppeneer, A. N. Yaresko, A. Y. Perlov, and T. Kraft, Phys. Rev. B **56**, 13012 (1997).
- [185] X. Gao, J. A. Woolam, R. D. Kirby, D. J. Sellmyer, C. T. Tanaka, J. Nowak, and J. S. Moodera, Phys. Rev. B **59**, 9965 (1999).
- [186] S. Picozzi, A. Continenza, and A. J. Freeman, J. Phys. D: Appl. Phys. **39**, 851 (2006).
- [187] Y. A. Uspenskii, E. T. Kulatov, and S. V. Khalilov, JETP **80**, 952 (1995).
- [188] L. Chioncel, M. I. Katsnelson, R. A. de Groot, and A. I. Lichtenstein, Phys. Rev. B **68**, 144425 (2003).
- [189] J. Schoenes, B. Frick, and O. Vogt, Phys. Rev. B **30**, 6578 (1984).
- [190] T. Kraft, P. M. Oppeneer, V. N. Antonov, and H. Eschrig, Phys. Rev. B **52**, 3561 (1995).
- [191] M. S. S. Brooks, T. Gasche, and B. Johansson, J. Phys. Chem. Solids **56**, 1491 (1995).
- [192] K. Knöpfle, L. M. Sandratskii, and J. Kübler, J. Phys.: Condensed Matter **9**, 7095 (1997).
- [193] T. Shishidou, T. Oguchi, and T. Jo, Phys. Rev. B **59**, 6813 (1999).
- [194] T. Durakiewicz, C. D. Batista, J. D. Thompson, C. G. Olson, J. J. Joyce, G. H. Lander, J. E. Gubernatis, E. Guziewicz, M. T. Butterfield, A. J. Arko, J. Bonca, K. Mattenberger, *et al.*, Phys. Rev. Letters **93**, 267205 (2004).
- [195] T. Durakiewicz, J. J. Joyce, G. H. Lander, Olson, M. T. Butterfield, E. Guziewicz, A. J. Arko, L. Morales, J. Rebizant, K. Mattenberger, and O. Vogt, Phys. Rev. B **70**, 205103 (2004).
- [196] M. Marutzky, U. Barkow, J. Schoenes, and R. Troć, J. Magn. Magn. Materials **299**, 225 (2006).
- [197] J. Schoenes, *Handbook on the Physics and Chemistry of the Actinides* (Amsterdam, 1984), vol. 1, p. 341.

Acknowledgements

Here I want thank to all people who explicitly or implicitly, this or that way helped me during my graduate studies.

I am especially indebted to Prof. Hubert Ebert, my scientific advisor, for proposing this interesting research topic and for his guidance and support he provided during all my research activity in Munich.

For the pleasant time we shared together I would warmly greet my colleagues and friends: Svitlana Polesya, Dr. Michal Kosuth, Dr. Diana Benea, Marianne Kardinal, Dr. Diemo Ködderitzsch, Sven Bornemann, Stephan Löwitzer, our secretary Rita Römling and all my friends outside the scientific work whom I met in Munich.

I express my best wishes and gratitude to Prof. Helen Homonai, my former teacher at the University in Kiew, for giving me a basic motivation to become interested in the solid state physics.

The sincere gratitude I address to Dr. Alexander Perlov who was my first-hand teacher during few years since my arrival in Munich and a very good friend.

My special thanks I express to my colleague Dr. Sergey Mankovsky for his permanent support and time he spent kindly answering my questions and clarifying my strange ideas.

I want also separately to thank my college Dr. Voicu Popescu for his patience and useful advises.

This dissertation could not be completed without the help of Dr. Jan Minár. I'm much grateful for his inevitable help with incorporation of the DMFT code into the SPR-KKR program package.

I'm indebted to Prof. A. Lichtenstein and Prof. M. Katsnelson for their fruitful ideas and many helpful discussions.

Finally, I want to thank my dear parents, my younger sister

Christina, and, of course, my beloved wife and daughter, Alexandra and Vasilisa, for their support, their patience and permanent belief. To them I would like to dedicate this work.

Financial support from the BMBF Projects 05KS4WMB2 and 05KS7WMA is gratefully acknowledged.

Curriculum vitae – Lebenslauf

PERSÖNLICHE ANGABEN

- Name: Stanislav Chadov
- Geburtsdatum: 20. August 1977
- Geburtsort: Kiew, Ukraine
- Nationalität: der Ukrainer
- Familienstand: verheiratet, 1 Kind

SCHULBILDUNG

- 1984 – 1994: Schule in Kiew, Ukraine

STUDIUM

- 1995 – 2001: Studium der Physik an der Nationalen Technischen Universität, Kiew, Ukraine. Diplomarbeit in theoretischer Festkörperphysik. Titel: "Accounting for the spin-orbit coupling in ab-initio calculations of the magnetic anisotropy in thin films"
- Juni 2001: Diplomprüfung mit Note 5 (ausgezeichnet).

BERUF

- August 2001 – Januar 2002: wissenschaftlicher Angestellter am Institut für Metallphysik, Kiew, Ukraine.
- seit Februar 2002: wissenschaftlicher Angestellter und Doktorand am Institut für Physikalische Chemie an der Ludwig–Maximilians–Universität München.

List of Publications (2002-2007)

To a large extent, the original work of this thesis has been previously published in various scientific journals or presented at conferences and workshops. A comprehensive list of the publications is given below:

1. *Green function approach for the ab initio calculation of the optical and magneto-optical properties of solids: Accounting for dynamical many-body effects*
A. Perlov, S. Chadov, H. Ebert – Phys. Rev. B **68**, 245112 (2003)
2. *Ab initio calculation of the optical and magneto-optical properties of moderately correlated magnetic solids*
A. Perlov, S. Chadov, H. Ebert, L. Chioncel, A. Lichtenstein, M. Katsnelson – J. of Magn. and Magn. Mat. **272-276**, 523-524 (2004)
3. *Ab initio calculation of the optical and magneto-optical properties of moderately correlated systems: accounting for correlation effects*
A. Perlov, S. Chadov, H. Ebert, L. Chioncel, A. Lichtenstein, M. Katsnelson – in *NATO Science Series II. Mathematics, Physics and Chemistry - Kluwer Acad. Publications, Netherlands, 2004*, edited by S. Halilov, vol. **156**, p. 161
4. *Accounting for many-body correlation effects in the calculation of the valence-band photoelectron emission spectra of ferromagnets*
J. Minár, S. Chadov, H. Ebert, L. Chioncel, A. Lichtenstein, C. de Nadai, N. B. Brookes – Nuc. Inst. and Met. in Phys. Res. A **574**, 151-162 (2005)
5. *Influence of correlation effects on the magneto-optical properties of the half-metallic ferromagnet NiMnSb*

- S. Chadov, J. Minár, H. Ebert, A. Perlov, L. Chioncel, M. Katsnelson, A. Lichtenstein – Phys. Rev. B **74**, 140411(R) (2006)
6. *Detailed fine structure of x-ray magnetic circular dichroism spectra: Systematics for heavy rare-earth magnets*
C. Sorg, A. Scherz, K. Baberschke, H. Wende, F. Wilhelm, A. Rogalev, S. Chadov, J. Minár, and H. Ebert – Phys. Rev. B **75**, 064428 (2007)
7. *Orbital magnetism in transition metal systems: The role of local correlation effects*
S. Chadov, J. Minár, M. Katsnelson, H. Ebert, D. Ködderizsch and A. Lichtenstein – *submitted to Eur. Phys. Lett.*

List of Presentations:

1. *LMTO Green's function approach for the ab-initio calculation of the optical and magneto-optical properties of solids*
Poster
2nd Annual Meeting of the Research Training Network "Computational Magnetoelectronics", Oléron, France, 05. - 09. 10. 2002
2. *LMTO Green's Function approach for the ab-initio calculation of the optical and magneto-optical properties of solids*
Talk
DPG-Frühjahrstagung, Dresden, 24. - 28.3. 2003
3. *Influence of dynamical correlation effects on magneto-optical properties of 3d-metals*
Talk
DPG-Frühjahrstagung, Regensburg, 08. - 12.3. 2004
4. *Accounting for many-body correlation effects in the calculations of the x-ray photoemission and magneto-optical properties of transition metals*
Talk
DPG-Frühjahrstagung, Berlin, 04. - 09.3. 2005
5. *Magneto-optical properties of systems with localized electronic correlations*

Poster

Workshop "First-principles approaches to optical and photoelectron spectra", München, 09. - 12.3. 2006

6. *Accounting for correlation effects in the calculation of the spin-orbit induced properties*

Talk

DPG-Frühjahrstagung, Dresden, 26. - 31.3. 2006

7. *Treatment of correlation effects within calculation of photoemission and magneto-optical spectra of solids*

Poster

Deutsche Tagung für Forschung mit Synchrotronstrahlung, Neutronen und Ionenstrahlen an Großgeräten "SNI 2006", Hamburg, 04. - 06.10. 2006

8. *Influence of correlation effects on spin-orbit induced magnetic properties of disordered systems*

Talk

DPG-Frühjahrstagung, Regensburg, 26. - 30.3. 2007

9. *LSDA+DMFT: account for the localized correlations within many-body perturbation theory*

Poster

2nd Summer School "Theory of the Electronic Structure of Materials", Schwarzwald, Königfeld, 16. - 21.9. 2007

